BULLETIN DE L'ASSOCIATION MINÉRALOGIQUE DU CANADA

THE CANADIAN MINERALOGIST

JOURNAL OF THE MINERALOGICAL ASSOCIATION OF CANADA

Volume 40 October 2002 Part 5

*The Canadian Mineralogist*
Vol. 40, pp. 1249-1286 (2002)

# A PETROLOGICAL, GEOCHEMICAL, ISOTOPIC AND FLUID-INCLUSION STUDY OF 370 Ma PEGMATITE–APLITE SHEETS, PEGGYS COVE, NOVA SCOTIA, CANADA

DANIEL J. KONTAK[§]

*Nova Scotia Department of Natural Resources, P.O. Box 698, Halifax, Nova Scotia B3J 2T9, Canada*

JAROSLAV DOSTAL

*Department of Geology, St. Mary's University, Halifax, Nova Scotia B3H 3C3, Canada*

T. KURT KYSER AND DOUGLAS A. ARCHIBALD

*Department of Geological Sciences and Geological Engineering, Queen's University, Kingston, Ontario K7L 3N6, Canada*

## ABSTRACT

The Peggys Cove area of southern Nova Scotia contains abundant, flat-lying, zoned, tourmaline-bearing aplite–pegmatite sheets cutting leucomonzogranite of the peraluminous, 372 Ma South Mountain Batholith, locally enriched in metasedimentary xenoliths. Muscovite extracted from aplite, pegmatite and quartz – muscovite – tourmaline pocket zones give flat $^{40}Ar/^{39}Ar$ age spectra with 370 Ma plateau ages. Petrographic observations indicate rapid post-crystallization cooling and minimal deuteric alteration, although erratic Al/Si ordering in feldspar suggests heterogeneous strain, also indicated by undulose textures in quartz; hence, pegmatite formation occurred in a dynamic setting. Whole-rock and mineral compositions indicate that the aplite–pegmatites are not chemically evolved compared to global geochemical databases for such rocks. Rather, they may reflect locally generated volatile-rich melts extracted from the leucomonzogranitic magma. Whole-rock REE data show that the aplite cannot be derivatives of the leucomonzogranitic magma by simple fractional crystallization. Whole-rock (WR) and mineral $\delta^{18}O$ data (WR: +11.7 to +14.7‰) are high compared to data for the SMB (WR: +8.5 to +12.5‰) and reflect equilibration of the pegmatite-forming melt with a metasedimentary source-material. Fluid-inclusion studies indicate pegmatite crystallization from a melt that exsolved a moderately saline (20–25 wt.% equiv. NaCl) fluid and constrain pegmatite formation to *ca.* 600–650°C at 3–3.5 kbar pressure. Abundant decrepitation-induced textures for the inclusions indicate pegmatite formation in an environment undergoing rapid changes in pressure, consistent with undulose extinction in quartz and Al–Si ordering in K-feldspar. The observations and data support a model of pegmatite–aplite formation *via* devolatilization of the metasedimentary xenoliths, abundant in the host rocks, and local generation of melts enriched in B during periods of cycling fluid pressure, in part related to regional stresses. Thus these tourmaline-bearing pegmatites are not related to conventional processes of late-stage fractionation of granitic magmas. Textural features of the pegmatites (*e.g.*, comb-textured K-feldspar) and aplites indicate a single period of dilatancy and infilling to form the sheets.

*Keywords*: granitic pegmatite, tourmaline, granite, geochemistry, fluid inclusions, stable isotopes, Peggys Cove, Nova Scotia.

§ *E-mail address*: kontakdj@gov.ns.ca

## Sommaire

Dans la région de Peggys Cove, dans le sud de la Nouvelle-Ecosse, on trouve une abondance de couches sub-horizontales zonées contenant aplite et pegmatite granitiques à tourmaline recoupant le leucomonzogranite du batholite hyperalumineux de South Mountain (372 Ma), enrichi localement en xénolites métasédimentaires. La muscovite extraite de l'aplite, la pegmatite, et des assemblages à quartz – muscovite – tourmaline des poches miarolitiques produit des spectres $^{40}Ar/^{39}Ar$ plats indiquant un âge de 370 Ma. Les observations pétrographiques concordent avec l'hypothèse d'un refroidissement rapide suite à la cristallisation et une altération deutérique minimale, quoiqu'un degré d'ordre Al/Si erratique du feldspath fait penser à une déformation hétérogène, tout comme une extinction roulante dans le quartz; il semble donc que la formation de la pegmatite se soit faite dans un milieu dynamique. Les compositions des roches globales et des minéraux indiquent que les échantillons d'aplite et de pegmatite ne sont pas géochimiquement évolués par rapport aux exemples dans les banques globales de données géochimiques pour de telles roches. Les données à propos des terres rares sur roches globales montrent que les aplites ne pourraient pas être dérivées d'un magma leucomonzogranitique par simple cristallisation fractionnée. Les valeurs de $\delta^{18}O$ pour les roches globales, entre +11.7 et +14.7‰, et les minéraux, sont élevées par rapport aux données sur les roches du batholite de South Mountain (entre +8.5 et +12.5‰), et montrent que le bain fondu qui a généré la pegmatite avait atteint l'équilibre avec un matériau métasédimentaire à la source. Les études des inclusions fluides indiquent une cristallisation d'un magma qui a exsolvé une phase fluide modérément saline (20–25% en poids de NaCl ou équivalent), et limitent la formation de la pegmatite à environ 600–650°C à 3–3.5 kbar. Des signes abondants d'une décrépitation des inclusions indiquent que le milieu de formation subissait d'importants changements en pression, ce qui concorde avec l'extinction roulante du quartz et la mise en ordre du feldspath potassique. D'après les observations et les données, nous proposons une modèle de dévolatilisation des xénolithes métasédimentaires, abondants dans les roches hôtes, pour expliquer la génération locale de magma enrichi en bore au cours de périodes de variations en pression de la phase fluide, en partie liées aux contraintes régionales. Ces pegmatites à tourmaline ne résultent donc pas de processus conventionnels de fractionnement à un stade tardif d'évolution d'un magma granitique. Les textures des pegmatites, par exemple le développement de cristaux de feldspath potassique en peigne, et des aplites concordent avec une seule période de dilatation et de mise en place en couches du magma.

(Traduit par la Rédaction)


*Mots-clés*: pegmatite granitique, tourmaline, granite, géochimie, inclusions fluides, isotopes stables, Peggys Cove, Nouvelle-Ecosse.

## Introduction

According to maps of the large (7200 km$^2$), 370 Ma peraluminous South Mountain Batholith (SMB) in Nova Scotia, pegmatites and aplites occur in various units of the intrusion (O'Reilly *et al*. 1982, MacDonald *et al.* 1992). Locally, euhedra of quartz and tourmaline many cm across occur in late-stage pockets. Previous investigators of the pegmatites indicate that these bodies may represent the end product of extreme fractionation, whereas others refer to local segregation from a less fractionated melt (*e.g.,* Kontak & Martin 1997). In places, the pegmatites host a variety of granophile-element mineralization (*e.g.,* New Ross area; Logothetis 1985, O'Reilly *et al*. 1982, Carruzzo *et al.* 2001). Although there have been some petrological studies of the mineralized pegmatites, no detailed integrated studies focusing on the nature and origin of tourmaline-bearing pegmatites, so prevalent in parts of the eastern SMB, have been undertaken. In this paper are presented the results of an integrated field and geochemical investigation of tourmaline-bearing sheeted aplite–pegmatite occurring along coastal exposures at Peggys Cove (Fig. 1). The occurrence of these tourmaline pegmatites not only relate to the geochemical evolution of the SMB, but their origin also has implications for the nature of tourmaline in similar geological settings globally.

## Geological Setting

The study area is underlain by peraluminous granitic rocks of the 370 Ma SMB (Fig. 1) that intrude metasedimentary rocks of the Lower Paleozoic Meguma Group, which were folded and metamorphosed during the *ca.* 395 Ma Acadian Orogenic event (Hicks *et al.* 1999). The SMB is subdivided into two intrusive phases, an early (stage 1) biotite granodiorite and biotite monzogranite, and a more evolved (stage 2) monzogranite (Fig. 1; MacDonald *et al*. 1992). Although the SMB intruded toward the end of the Acadian Orogeny, some evidence points to a syntectonic intrusion. For example, using anisotropic magnetic susceptibility (AMS), Benn *et al*. (1997, 1999) have shown that the batholith has a weak, but distinct Acadian fabric. In addition, Horne *et al*. (1988, 1992) have shown that the orientation of quartz veins and aplite–pegmatite sheets reflect NW-directed compression during SMB emplacement. A study of the contact aureole of the SMB indicates pressures of 3.2 to 3.8 kbars for batholith emplacement (Raeside & Mahoney 1996). Concordant U–Pb (zircon, monazite) and Ar–Ar (mica) ages of *ca.* 372 Ma for the SMB and satellite plutons in southern Nova Scotia indicate rapid post-crystallization cooling of granites to ≤300°C (summary in Clarke *et al*. 1997).

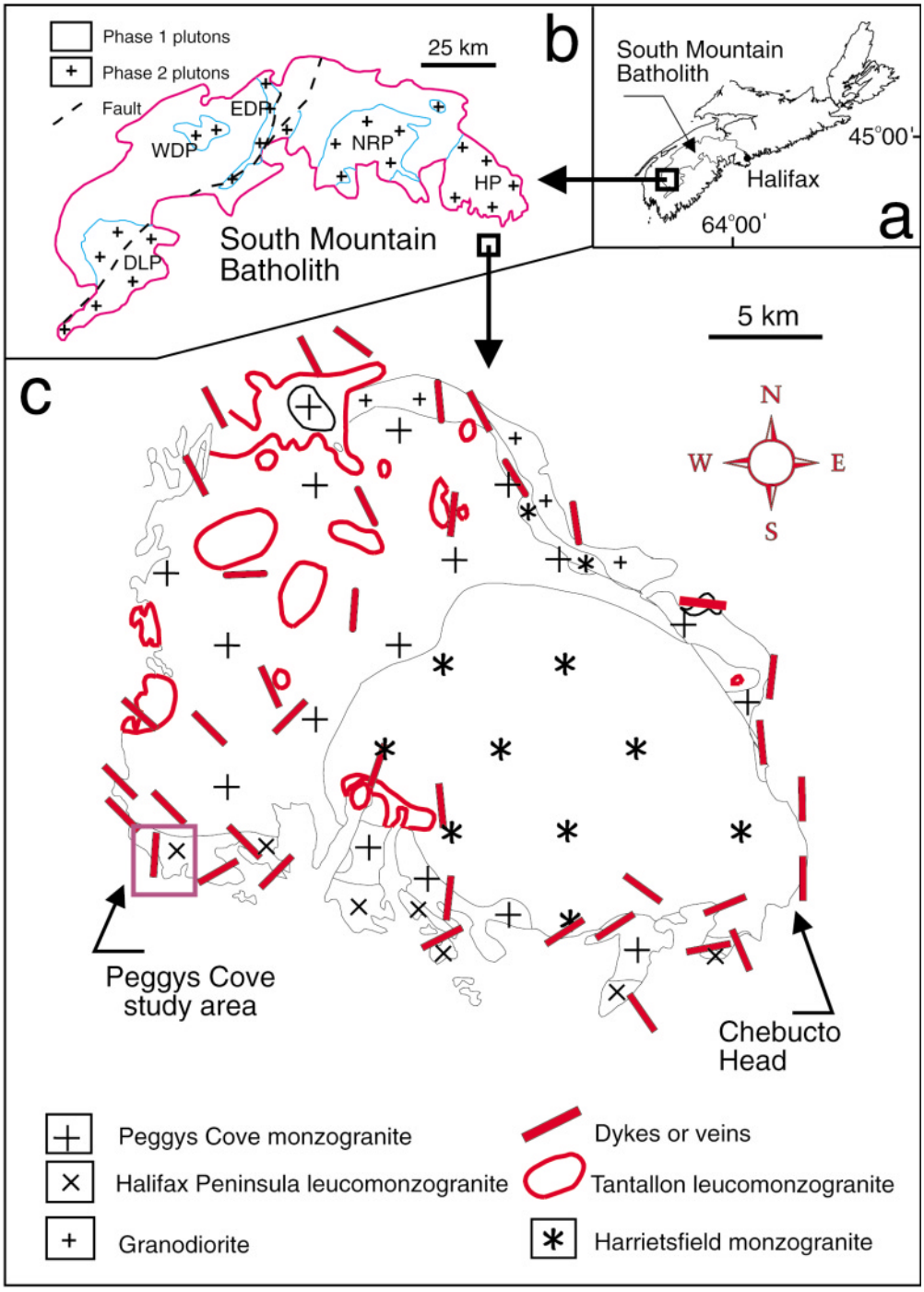


FIG. 1. (a) Location of the study area in southern Nova Scotia, Canada, showing the outline of the South Mountain Batholith. (b) Distribution of early phase-1 plutons and later phase-2 plutons (HP: Halifax pluton, NRP: New Ross pluton, EDP: East Dalhousie pluton, WDP: West Dalhousie pluton, DLP: Davis Lake pluton) in the South Mountain Batholith. (c) Geology of the zoned Halifax pluton showing the distribution of dykes and quartz veins, and location of the study area at Peggys Cove. Geology after MacDonald & Horne (1988).

Mapping of the Halifax Peninsula indicates that the area contains a single, zoned pluton referred to as the Halifax Pluton (HP; MacDonald & Horne 1988).The rocks comprising the HP (Fig. 1) are subdivided into: (1) a zoned sequence of biotite granodiorite to biotite monzogranite (*i.e.*, stage 1), including peraluminous cordierite- and muscovite-bearing phases, and (2) muscovite–biotite leucomonzogranite (stage 2). Field relationships indicate that the first sequence, which is coarser grained and characterized by K-feldspar megacrysts, is intruded by the later, finer-grained and porphyritic leucomonzogranites. Petrologically, the second-stage units are more evolved, carry minor lithophile-element mineralization (F, Sn, W), and have geochemical signatures reflecting fluid–rock interaction (MacDonald & Clarke 1991). Cutting all units of the HP are steeply dipping, NW- and NE-trending dykes and pegmatites along with quartz veins (Horne *et al.* 1988) that are generally associated with the more evolved phases of the HP (Fig. 1).

## Geology of the Peggys Cove Area

### *Host biotite monzogranite rock*

At Peggys Cove, the dominant granitic phase is a medium- to coarse-grained, K-feldspar megacrystic biotite–muscovite leucomonzogranite (Fig. 2a) that hosts variable amounts of pegmatites and aplites defining sheeted structures. Variations in the texture and modal percentages of the host granite occur on various scales, the most notable being the size and abundance of the K-feldspar (Kf) megacrysts, overall grain-size, and percentage of biotite. In one locality, exceptional layering of biotite defines a magmatic foliation (Fig. 2b) similar to that described at nearby Chebucto Head (Fig. 1; Smith 1975, Clarke & Clarke 1998). Other notable features of the granite include: (1) an abundance of melanocratic xenoliths of various shapes and sizes (≤1–2 m; Fig. 2c); these xenoliths resemble metasedimentary rocks, in some cases similar to the Meguma Group, but others may have different origins; (2) local occurrence of ovoid zones of coarse quartz–feldspar pegmatite enveloping corroded melanocratic xenoliths (Fig. 2d).

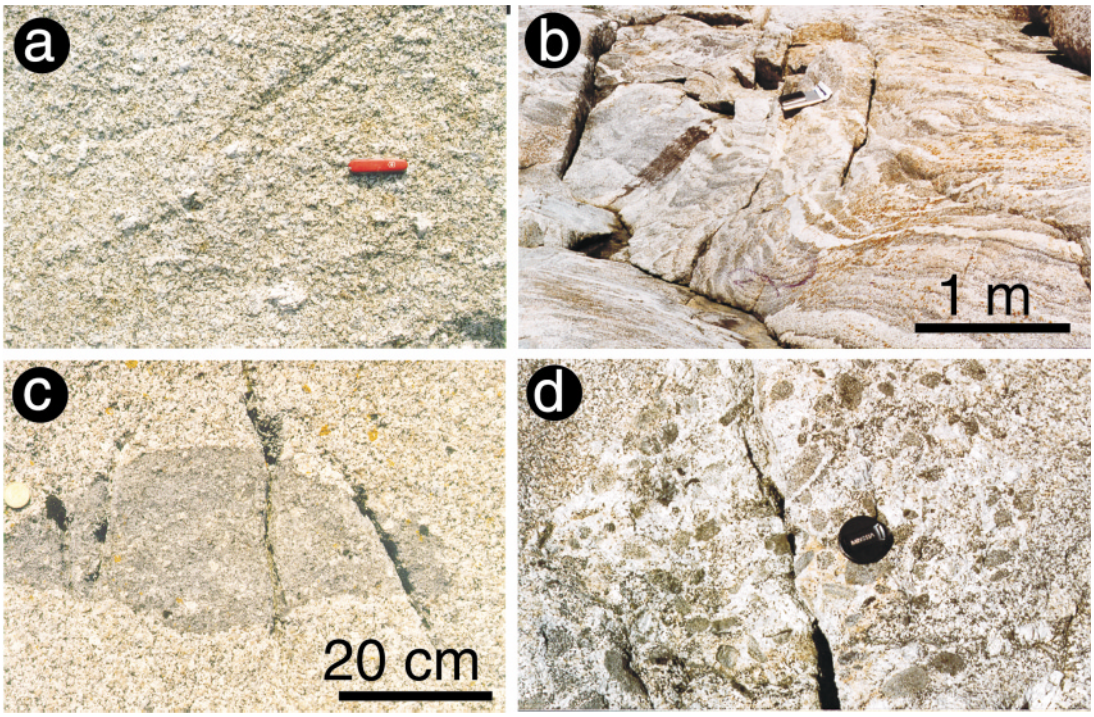


FIG. 2. Outcrop photos of leucomonzogranite, the host rock at Peggys Cove. (a) K-feldspar- megacrystic leucomonzogranite with coarse, knobby, K-feldspar megacrysts. (b) Well-developed magmatic layering. (c) Melanocratic xenolith of probable metasedimentary origin. (d) Abundant, small melanocratic xenoliths enveloped by coarse, K-feldspar-rich pegmatite.

The granite is devoid of an obvious structural fabric, but numerous steeply dipping joints of generally N–S and E–W orientation occur. Joint measurements over the entire study-area indicated no differences, hence all data are presented together in Figure 3. The joints have a conjugate orientation, but do not quite match the general orientations of joints in the SMB, which Horne *et al.* (1992) related to regional stress during emplacement of the batholith. Where the highest frequency of joints occurs, there is an appearance of comminution of the granite and fabric development.

*General features of aplite–pegmatite sheets*

The aplite–pegmatite sheets occur as (1) extensive, thin (1–20 cm) sheets draping the undulating surface of the host monzogranite (Fig. 4a). The sheets are dominated by medium- to very fine-grained and texturally complex aplite, that change laterally to intricately layered aplite–pegmatite of ≤1–2 m thickness (Fig. 4c). Dykes of fine-grained aplite are considered to be part of this group (Fig. 5a). There are also (2) 1–2 m sheets

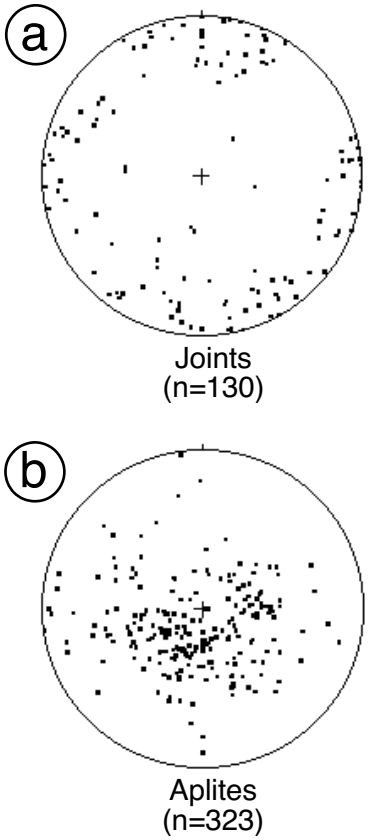


FIG. 3. Stereoplots of structural data from Peggys Cove: (a) joints in the host leucomonzogranite, (b) aplite sheets in the host-rock leucomonzogranite. Note the steeply dipping, orthogonal orientation of the joints, which contrasts with the relatively flat-lying nature of the aplites.

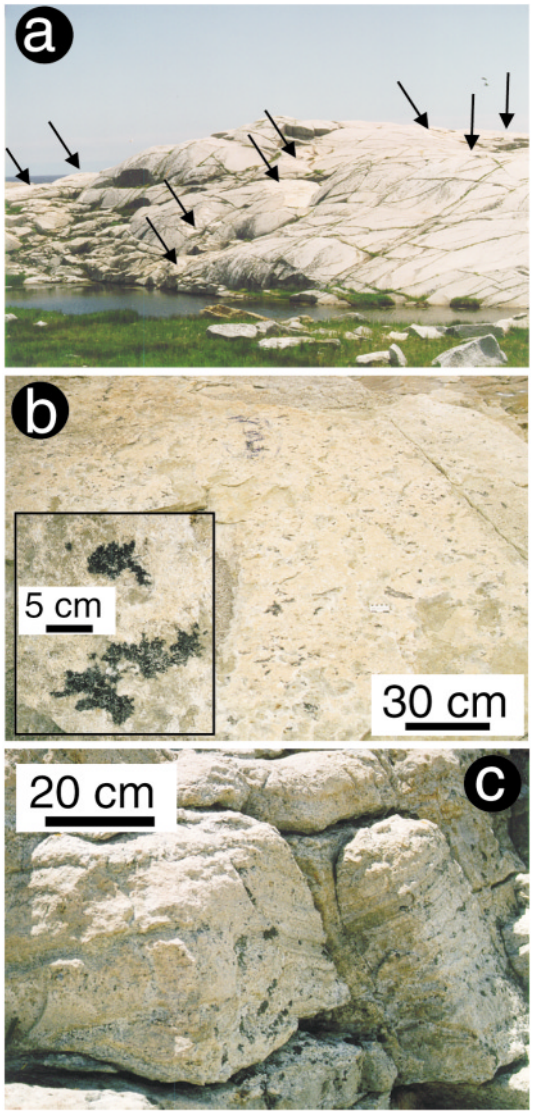


FIG. 4. Outcrop photos showing typical features of the aplite–pegmatite sheets at Peggys Cove. (a) Undulating, glacially scoured surface of granite draped by aplite sheet (indicated by arrows). View is looking west from parking-lot area. (b) Close-up of aplite sheet in Figure 4a showing disseminated rosettes of tourmaline in fine-grained, light beige, sacchroidal aplite. Inset shows a close-up of coarse rosettes of tourmaline. (c) Development of layered aplite–pegmatite in the aplite sheet of Figure 4a, where it thickens.

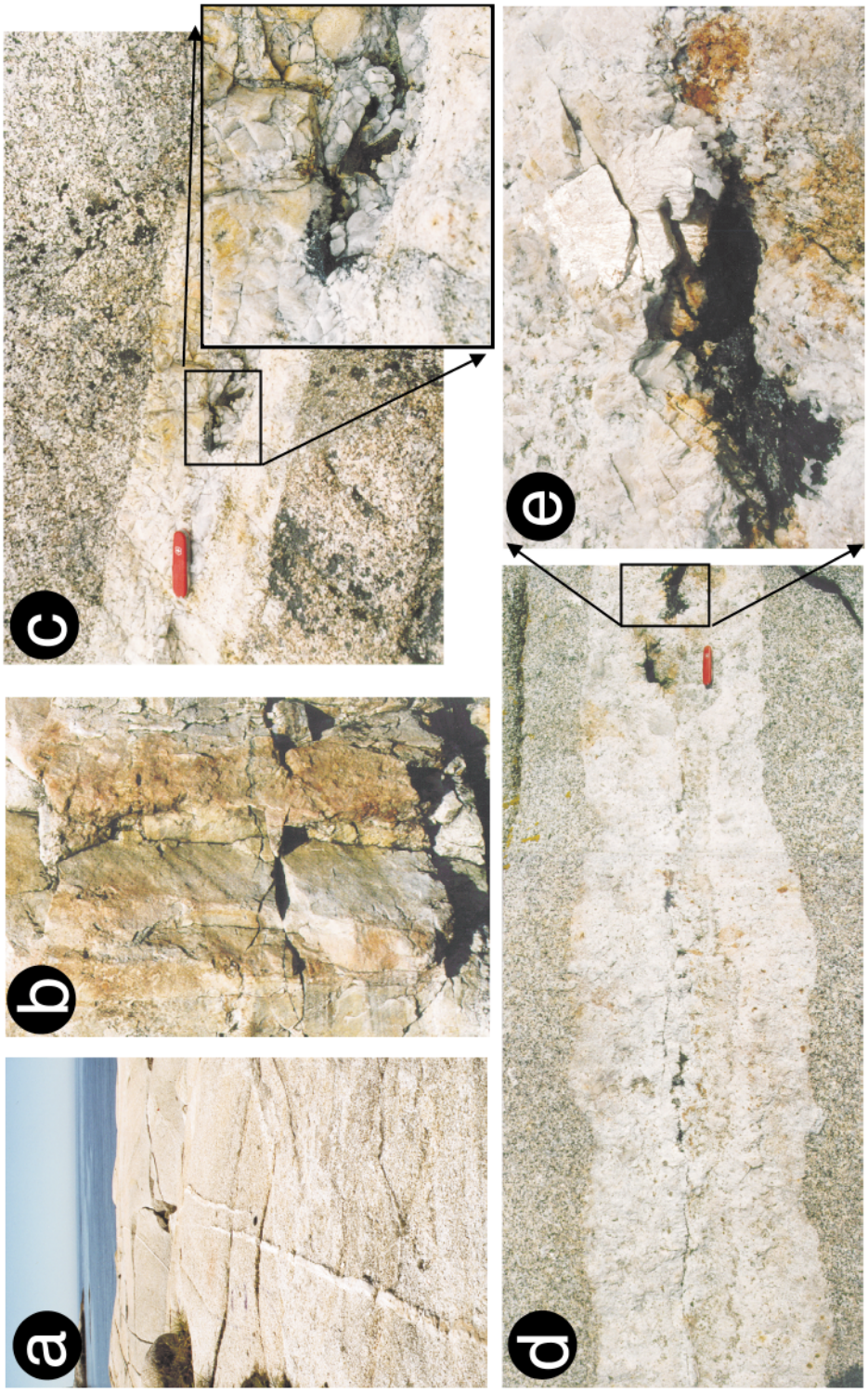
a
b
c
d
e

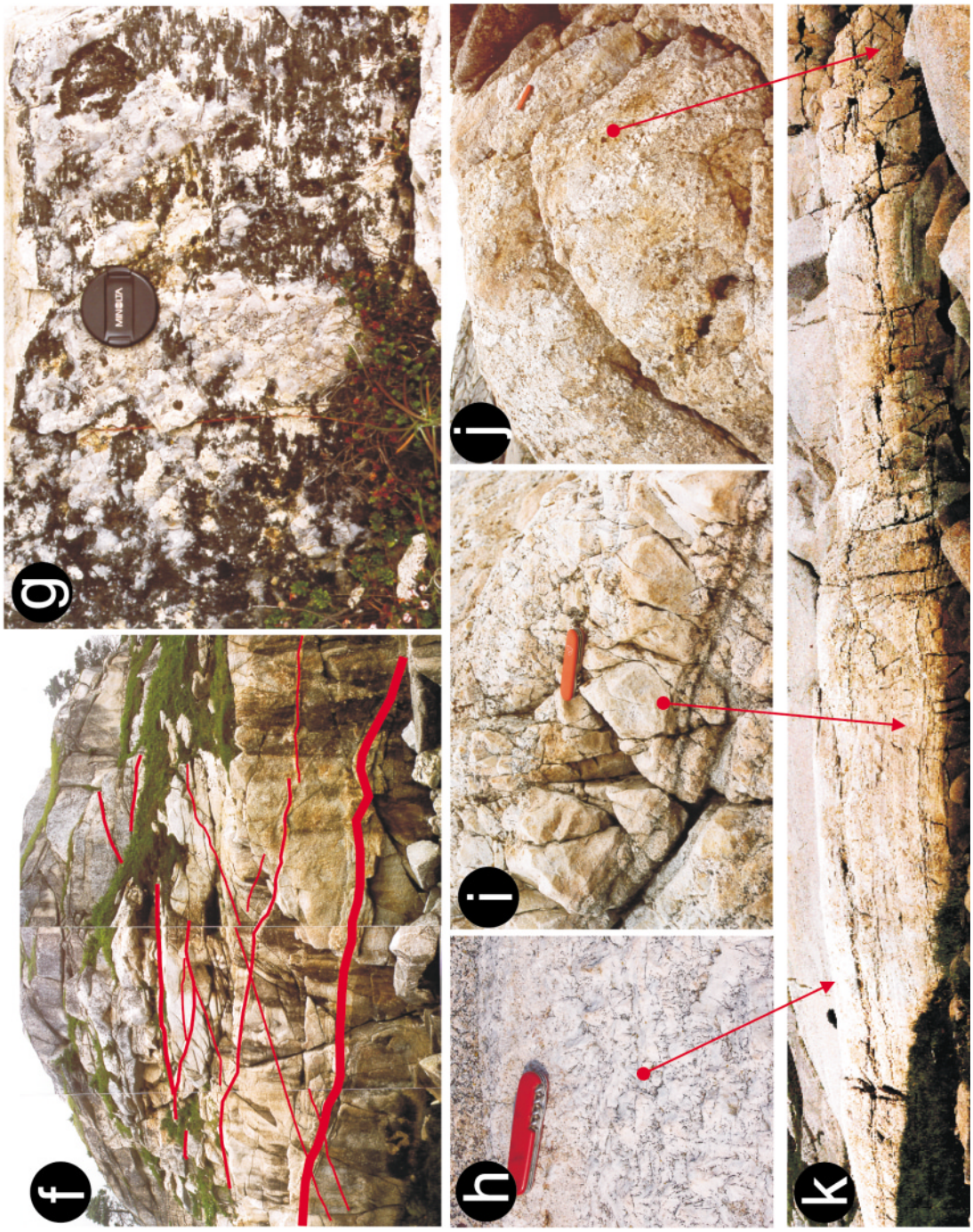

FIG. 5. Outcrop photos showing features of the aplite–pegmatite sheets at Peggys Cove. (a) *En échelon* array of aplitic dykes just east of the post-office lighthouse. Photo is *ca.* 2 m wide at the bottom. (b) Line-rock texture in bottom of zoned aplite–pegmatite sheet. Photo is *ca.* 0.4 m high. (c) Layered aplite–pegmatite sheet with bottom half consisting of fine-grained aplite and upper half comprising coarse, K-feldspar-rich pegmatite. Inset photo shows close-up of the quartz–tourmaline pod. Note

zoned from a lower fine-grained aplite to an upper coarse-grained pegmatite with graphic texture (Figs. 5b, c, d, e). In the latter case, the K-feldspar crystals are ≤10–20 cm and are oriented perpendicular to the aplite–monzogranite contact (Figs. 5c, e, h). Commonly, a graphic texture surrounds the K-feldspar inward from the contact. These sheets have small (*i.e.*, <1 m) late-stage pockets of quartz – K-feldspar – tourmaline – muscovite that are randomly distributed within the sheets. Finally, there are (3) intricately banded aplite – pegmatite – leucogranite sheets of ≤3 m. At one location (Fig. 5k), a *ca.* 3-m-thick section consists of numerous multi-cm thick, undulating bands of aplite – pegmatite – leucogranite that define a banding (Figs. 5i, j) that is traced for several tens of meters.

Textural variability characterizes most aplite–pegmatite sheets, most notably with the development of coarse segregations (≤20–50 cm) or pockets of variable mixtures of quartz, K-feldspar, tourmaline and, rarely, muscovite toward the center of the sheets (Figs. 5c, e). These pockets are overlain by coarse pegmatite and underlain by banded aplite; in the latter, a mm- to cm-scale banding (Fig. 5b) similar to the line-rock texture, so prevalent in zoned pegmatites, occurs (London 1992a). This tripartite division of the pegmatite–aplite sheets is very similar to zoned pegmatites described, for example, from San Diego County, California (Foord 1977, Stern *et al*. 1986).

Signs of an alteration halo, a phenomenon common in evolved pegmatites elsewhere (*e.g.*, Tanco pegmatite, Manitoba; Selway *et al*. 2000), have not been observed at Peggys Cove. As noted by London (1992a), it is very common to find evidence of infiltration of the volatile component of pegmatites in the surrounding wallrock, as might be manifest by the development of secondary B-bearing minerals.

*Nature of tourmaline in aplite–pegmatite sheets*

Tourmaline occurs in the following textures within the aplite–pegmatite sheets (1) Coarse rosettes of euhedral tourmaline are found disseminated within aplite sheets (Fig. 4b) grading laterally into pegmatite–aplite sheets (Fig. 4c). (2) Rosettes occur along contacts between coarse-grained leucogranite and fine-grained aplite within zoned sheets, the tourmaline layers being laterally continuous for several tens of m. (3) A core of tourmaline may be found in aplite sheets that have a thin (*i.e.*, 1–2 cm) quartz-rich center. (4) Segregations or pods of tourmaline are found within zoned pegmatites, either intergrown with quartz (Fig. 5c) or as coarse monomineralic areas (Fig. 5e); these pods, with maximum dimensions of 10–30 cm, contain the largest concentration of tourmaline. (5) Tourmaline lines fractures that cut several zones within an pegmatite–aplite sheet. This tourmaline represents a late-hydrothermal or metasomatic type similar in occurrence to some documented by Tindle *et al.* (2002). Finally, (6) rare tourmaline fibers occur at the upper contact of sheets (Fig. 5g).

*Pocket features*

Occurring within the pegmatitic parts of the sheets are ovoid areas with coarse aggregates of variable percentages of quartz, feldspar, muscovite and tourmaline with a central cavity of 1–5 cm. Such pockets are commonly occupied by gem-quality crystals of various minerals in pegmatites (Foord 1977, Stern *et al*. 1986), but no such features occur in the study area.

*Structural features of aplite–pegmatite sheets*

The aplite–pegmatite sheets have a uniform orientation, and the following observations are relevant. (1) Multiple sheets are commonly arranged in an *en échelon* manner (Fig. 5a). Cross-cutting relationships occur among sheets, commonly with a conjugate relationship with inter-limb angles of ≤40–50° (Fig. 5f). (2) Terminations are tapered or wedge-shaped, as in shear veins (Fig. 5a). (3) Contacts with the surrounding granitic rock are "welded" *versus* sheared. (4) Coarse crystals, generally K-feldspar but also quartz, in the marginal zones in many cases have a comb texture. Thus, in most cases movement either during or after emplacement and crystallization did not occur (see exception below). Finally, (5) the sheets are generally flat-dipping, with the majority dipping gently southward (Fig. 3b). These orientations contrast with the orientations of the joints in the

pen knife for scale. (d) Layered aplite–pegmatite sheet with bottom half consisting of fine-grained aplite and upper half coarse, K-feldspar-rich pegmatite. Outcrop is located just north of the wharf area and is *ca.* 2 m wide. (e) Close-up of previous photo showing tourmaline pocket and cleavage face of coarse K-feldspar crystal, one of several that line the upper part of the tourmaline-rich pocket *ca.* 30 cm in width. (f) Composite photo of granitic outcrop containing numerous flat-lying sheets (more prominent ones are highlighted in red) of aplite–pegmatite showing mutual cross-cutting relationships. Note that the sheets are arranged like flat-lying shear veins in some cases and have tapered terminations. (g) Tourmaline fibers growing on the upper surface of a pegmatite–aplite sheet. Orientations and step-like features of the tourmaline fibers indicate northward movement. (h, i, j, k) Large, layered aplite–pegmatite sheet *ca.* 3 m in height displaying internal organization with alternating layers of aplite, leucogranite and coarse K-feldspar-rich pegmatite in aplite sheet (photo taken facing east). The upper contact is marked by a zone dominated by coarse, oriented K-feldspar crystals (h), whereas the central zone is characterized by layered aplite – leucogranite – pegmatite (i), and the southern end is characterized by coarse, layered, K-feldspar-rich leucogranite to pegmatite. The sheet is located along the coast, south of the cafeteria at Peggys Cove.

host monzogranite (Fig. 3a) and depart markedly from the orientations of dykes and veins in the SMB (Horne *et al*. 1992), which are prominently NW-trending and steeply dipping. However, Horne *et al*. (1992) did show a minimal amount of data (<2% of area) clustered in the center of their stereoplot for the dykes; thus a small number of flat-lying dykes are generally present in the SMB, albeit fewer than are apparent at Peggys Cove. In a single locality, tourmaline fibers lining the upper contact of a pegmatite sheet with steps into the underlying fine-grained aplite indicate a north-directed sense of movement (Fig. 5g).

## Petrography of Pegmatites and Aplites

Examination of both pegmatite and aplite samples indicate similar features for the major silicate phases, these being quartz, albitic feldspar, K-feldspar, muscovite and cordierite. The aplite–pegmatite sheets are characterized by: (1) a well-defined graphic texture, generally developed with K-feldspar, but also plagioclase, (2) a rare myrmekite texture in plagioclase that is always in close proximity to the graphic texture, (3) comb-textured quartz and K-feldspar, (4) late subhedral to anhedral, zoned tourmaline, (5) minor chloritized cordierite of subhedral to euhedral shape, (6) variably perthitic K-feldspar with film and flame texture; bead perthite is rare. In addition, the degree of mottled texture in K-feldspar, generally indicative of strain associated with the orthoclase–microcline inversion, and amount of microcline grid twinning, usually restricted to areas around albite exsolution, ranges from rare to abundant. Within pegmatite samples, there is a consistent paragenesis of early sodic plagioclase plus or minus quartz, followed by quartz and K-feldspar, in a graphic intergrowth. Muscovite and tourmaline, where present, are late paragenetically. Re-equilibration of minerals is manifest by development of a perthitic texture in K-feldspar, strained K-feldspar with grid twinning, replacement of plagioclase by K-feldspar, fine-grained white mica decorating plagioclase, and development of irregular grain-boundaries.

The aplites and coarse leucogranite parts of the sheets are dominated by idiomorphic textures with variable conversion to xenomorphic textures where subsolidus re-equilibration has been most extreme (*e.g.,* Taylor & Pollard 1988). Miarolitic cavities contain the same assemblage as the host rock. The K-feldspar contains film, flame and beaded perthite textures and mottled textures occur along with grid twinning, especially in smaller intergranular grains. Muscovite is highly variable in abundance, from nearly absent to generally 3–5%, but where aplite–pegmatite contacts are observed, up to 10–15% occurs and the grains tend to be coarser. Rare biotite occurs in the aplites, but it is commonly altered to chlorite.

## Analytical Techniques

The $^{40}Ar/^{39}Ar$ analyses of three high-quality separates of muscovite irradiated at McMaster University nuclear reactor (Hamilton, Ontario) were done at the Geochronology Laboratory of Queen's University (Kingston, Ontario) following the procedures outlined in Clark *et al.* (1998). Errors for the individual steps, age spectra and isotope-correlation diagrams represent the analytical precision at a $2\sigma$ level, assuming that the errors in the ages of the flux monitors are negligible, which is suitable for comparing within-spectrum variation and for determining which steps constitute a plateau (McDougall & Harrison 1988). A conservative estimate for the error in the J value is 0.5%.

Powdered whole-rock samples (–200 mesh) were analyzed for major and trace elements on fused and pressed pellets, respectively, using an automated Philips 2400 X-ray-fluorescence (XRF) spectrometer at St. Mary's University, Nova Scotia. In addition, high-quality mineral separates and some of the powdered whole-rock samples were analyzed for trace (Li, Mo, Cs, Hf, Ta, Bi, Th, U) and rare-earth (*REE*) elements by solution chemistry by ICP–MS (Memorial University, Newfoundland) using the method of Jenner *et al.* (1990). Analyses of minerals were done using polished thin sections and grain mounts with a JEOL 733 Superprobe at Dalhousie University (Halifax, Nova Scotia) using the following operating conditions: 1–3 μm but defocussed to 10 μm for feldspars, beam current 10 nA, and accelerating voltage 15 kV. Stable isotope analyses of whole rocks and silicate minerals were done at Queen's University using standard methods, as described in Kyser *et al.* (1998). Fluid inclusion thermometry was done using a USGS-type gas-flow heating–cooling stage housed at the Nova Scotia Department Natural Resources, Halifax (Kontak 1998). Precipitate mounds generated from artificial thermal decrepitation of fluid inclusions (Haynes *et al.* 1988) were also analyzed using the JEOL 733 Superprobe with conditions similar to those described above.

The structural states of the alkali feldspar were determined using a Philips Analytical X-ray diffractometer (XRD) with PC–APD diffraction software at Dalhousie University, Halifax, with the following operating conditions: Cu$K\alpha$ radiation, goniometer speed of 1°2θ/minute, and chart recorder speed of 1 cm/min.

## Age Dating

Three samples of muscovite analyzed for $^{40}Ar/^{39}Ar$ dating (Table 1) represent the following occurrences: (1) aplite with crenulate layering where muscovite occurs within miarolitic cavities (PCG–99–11), (2) a pocket zone with coarse-grained quartz – K–feldspar – muscovite in a layered aplite–pegmatite sheet (PCG–

99–16; Fig. 5k), and (3) a quartz – tourmaline – K–feldspar – muscovite segregation in an aplite sheet (PCG–99–18). Results of the analyses (Fig. 6) indicate similar age spectra for the three samples of muscovite, with age plateaus of 367.4, 373.8 and 371.0 Ma. For all samples, the spectra indicate a simple thermal history with no evidence of subsequent reheating. The results of the isotopic measurements (Table 1) can be obtained from the Depository of Unpublished Data, CISTI, National Research Council, Ottawa, Ontario K1A 0S2, Canada.

## Diffraction Studies of Alkali Feldspar

Diffractograms were obtained for seven separates of K-rich alkali feldspar from pegmatites in order to assess the degree of Si/Al order, itself an indication of the thermal evolution of the samples (*e.g.,* Brown & Parsons 1989). The results indicate the dominance of either a monoclinic or triclinic phase, but samples also contain a mixture of the two phases. The degree of obliquity (Δ), determined using the equation of Goldsmith & Laves (1954), are 0.68, 0.71 and 0.78 for the three triclinic samples. The monoclinic samples have distinct (131) reflections, but in some of them, broad peaks and low-intensity shoulders occur, indicative of subordinate triclinic material with variable Δ values (Černý & Chapman 1986, Neves & Godinho 1999).

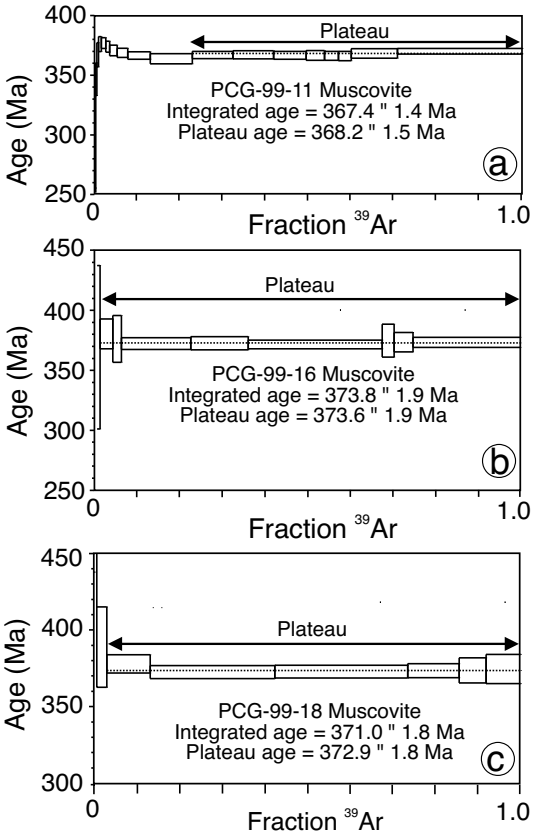


FIG. 6. $^{40}Ar/^{39}Ar$ age spectra for muscovite separates from pegmatites at Peggys Cove. (a) Aplite sample with crenulate layering. (b) Pocket zone containing quartz – muscovite – K-feldspar in aplite–pegmatite. (c) Aplite sheet with coarser pods of quartz – tourmaline – K-feldspar – muscovite.

## Whole-Rock Compositions

Twelve samples of aplite and pegmatite material were analyzed for major and trace elements (Table 2), including: (1) aplites from the margin (PCG–12, 16K, 17A) and interior (PCG–16B) of sheets, (2) isolated domains of aplite (PCG–3A), (3) coarse leucogranite–aplite (PCG–16D, 16I), (4) muscovite–tourmaline pods (PCG–14A, 14B), and (5) coarse K-feldspar (PCG–15C, 16F, 16H). The following points are noted with respect to the major-element abundances: (1) all aplites and leucogranite samples are silica-rich (74–78 wt.% $SiO_2$), have uniform aluminum contents (13 wt.% $Al_2O_3$), have $K_2O/Na_2O$ >1.5 except for one sample at *ca.* 1, are peraluminous (A/CNK values = 1.09 to 1.2; 2% normative Crd), and are depleted in $TiO_2$, CaO, MnO and MgO; (2) the two samples of muscovite–tourmaline pods are very similar in their composition, and (3) samples of coarse segregations of K-feldspar from zoned pegmatites have bulk compositions of $Or_{59}Ab_{41}$, $Or_{56}Ab_{44}$ and $Or_{72}Ab_{28}$.

Normative compositions of the samples plot in distinct fields in the Q–Ab–Or plot (Fig. 7a). The aplite samples fall near the pseudoternary minimum for $H_2O$-saturated haplogranite (Tuttle & Bowen 1958) and near the average of fine-grained leucomonzogranite for the SMB ($n$ = 100, Ham *et al.* 1989), but they also define a trend plotting toward K-feldspar-rich samples. The coarse-grained leucogranites also plot near the fine-grained aplites. The data are compared to the minima for $H_2O$-saturated granites at 0.5, 1, 3, and 5 kbar in Figure 7a. It is clear that the samples fall near the low-pressure minima. Also shown for comparison are the minima for 4.5 wt.% $B_2O_5$ added at 1 kbar for $H_2O$-saturated and dry granite systems.

The samples are generally depleted in the trace elements considered, except for the muscovite–tourmaline pods, which are enriched in most elements relative to the other samples (Table 2), most notably the transition metals (V, Cr, Co, Ni), high-field strength (Zr, Nb, Ti) and lithophile and alkaline earth elements (Rb, Sr, Ba, Ga). The three K-feldspar-rich samples have the highest Rb contents, but these are well below the 2000 ppm Rb level for K-feldspar from evolved pegmatites of the SMB (Kontak & Martin 1997) and even higher abundances in highly fractionated pegmatites (Černý *et al.* 1985). The compositions of the aplite–leucogranite

samples are generally similar, with uniformly low values of most trace elements, and highly variable Ba, Sr and Rb.

In a plot of wt.% $K_2O$ *versus* Rb (Fig. 7b), the data show a positive correlation, with the K-feldspar-rich samples most enriched in Rb. In order to assess the degree of fractionation of the samples, comparative data for the SMB are shown for: (1) whole-rock samples, and (2) K-feldspar separates from pegmatite segregations in various settings of the SMB. Whereas there is a trend that is similar to that of the SMB, the Peggys Cove samples are chemically not as evolved as the batholith. In addition, the coarse-grained, K-feldspar-rich zones in the pegmatites are not as evolved as similar segregations in pegmatites of the SMB (Fig. 7b).

Six samples of aplite analyzed for their *REE* contents indicate similar results (Fig. 8) with: (1) chondrite-normalized abundances of 2 to 10, except for Eu; (2) generally flat, gull-wing type patterns typical of evolved felsic rocks that have crystallized monazite (*e.g.,* Miller

TABLE 2. WHOLE-ROCK GEOCHEMISTRY OF GRANITIC SAMPLES, PEGGY'S COVE, NOVA SCOTIA

| Sample | PCG-99 3A | PCG-99 12 | PCG-99 14A | PCG-99 14E | PCG-99 15C | PCG-99 16B | PCG-99 16D | PCG-99 16F | PCG-99 16H | PCG-99 16I | PCG-99 16K | PCG-99 17A |
|---|---|---|---|---|---|---|---|---|---|---|---|---|
| Rock | aplite | aplite | Ms–Tur pod | Ms–Tur pod | Kfs | aplite* | coarse lcgr-aplite | Ksp | Kfs | coarse lcgr-aplite | aplite** | aplite |
| $SiO_2$ wt.% | 78.19 | 74.69 | 65.04 | 67.13 | 75.20 | 75.48 | 76.01 | 75.22 | 74.45 | 75.71 | 75.08 | 76.62 |
| $TiO_2$ | 0.05 | 0.06 | 0.96 | 0.93 | 0.04 | 0.05 | 0.05 | 0.04 | 0.05 | 0.05 | 0.05 | 0.04 |
| $Al_2O_3$ | 13.10 | 13.98 | 21.13 | 17.92 | 13.68 | 13.68 | 13.36 | 13.70 | 13.32 | 13.68 | 13.00 | 13.62 |
| $Fe_2O_3$ | 0.55 | 0.32 | 8.68 | 7.55 | 0.39 | 0.36 | 0.65 | 0.28 | 0.47 | 0.69 | 0.58 | 0.37 |
| MnO | 0.02 | 0.01 | 0.24 | 0.39 | 0.01 | 0.00 | 0.02 | 0.00 | 0.01 | 0.02 | 0.02 | 0.00 |
| MgO | 0.03 | 0.04 | 1.70 | 2.11 | 0.02 | 0.03 | 0.10 | 0.01 | 0.03 | 0.09 | 0.08 | 0.05 |
| CaO | 0.48 | 0.38 | 0.15 | 0.14 | 0.30 | 0.28 | 0.31 | 0.14 | 0.15 | 0.62 | 0.52 | 0.39 |
| $Na_2O$ | 3.59 | 3.12 | 0.34 | 0.27 | 3.03 | 3.31 | 2.86 | 2.58 | 2.14 | 4.01 | 3.26 | 2.98 |
| $K_2O$ | 4.55 | 6.08 | 4.75 | 3.52 | 6.44 | 5.03 | 5.63 | 7.57 | 8.20 | 4.09 | 5.14 | 6.30 |
| $P_2O_5$ | 0.13 | 0.19 | 0.16 | 0.14 | 0.14 | 0.14 | 0.11 | 0.16 | 0.15 | 0.12 | 0.14 | 0.21 |
| LOI | 0.65 | 0.93 | 7.74 | 9.01 | 0.40 | 1.35 | 0.68 | 0.39 | 0.37 | 0.62 | 0.71 | 0.70 |
| Total | 101.34 | 99.80 | 100.89 | 99.11 | 99.65 | 99.71 | 99.78 | 100.09 | 99.33 | 99.70 | 98.58 | 101.29 |
| V ppm | ND | ND | 132 | 117 | ND | ND | ND | 3 | ND | ND | ND | ND |
| Cr | 8 | 9 | 97 | 78 | 7 | 12 | 15 | 1 | 5 | 11 | 13 | 6 |
| Co | ND | ND | 26 | 23 | ND | ND | ND | ND | ND | ND | ND | ND |
| Zr | 22 | 22 | 189 | 212 | 4 | 26 | 22 | 2 | 3 | 16 | 16 | 17 |
| Ba | ND | 230 | 672 | 4361 | ND | 173 | 0 | 124 | 192 | ND | 161 | 258 |
| La | 2 | ND | 63 | 55 | 5 | ND | ND | 3 | ND | 2 | ND | 5 |
| Ce | ND | 17 | 84 | 63 | 24 | 37 | ND | 26 | 36 | 22 | 33 | 30 |
| Nd | 13 | 8 | 41 | 29 | 2 | 8 | 8 | ND | 9 | 5 | 8 | 5 |
| Ni | ND | ND | 44 | 29 | 1 | 1 | ND | ND | 3 | ND | ND | ND |
| Cu | ND | ND | 15 | 11 | ND | ND | ND | ND | ND | ND | ND | ND |
| Zn | 17 | 15 | 10 | 8 | 18 | 24 | 18 | 10 | 12 | 24 | 15 | 15 |
| Ga | 17 | 17 | 27 | 23 | 15 | 20 | 16 | 16 | 14 | 16 | 16 | 17 |
| Rb | 251 | 266 | 148 | 121 | 303 | 221 | 207 | 381 | 253 | 180 | 183 | 216 |
| Sr | 27 | 34 | 680 | 629 | 15 | 23 | 27 | 9 | 26 | 15 | 42 | 39 |
| Y | ND | ND | 35 | 34 | ND | ND | ND | ND | ND | ND | ND | ND |
| Nb | 5 | 5 | 18 | 17 | 1 | 7 | 5 | 1 | 3 | 5 | 4 | 3 |
| Sn | 8 | 8 | 4 | 4 | 7 | 8 | 8 | 7 | 7 | 8 | 8 | 8 |
| Pb | 41 | 54 | 10 | 11 | 42 | 114 | 49 | 47 | 55 | 42 | 42 | 57 |
| Th | 6 | 6 | 15 | 14 | 6 | 7 | 4 | 2 | 4 | 6 | 7 | 6 |
| U | 1 | 1 | 4 | 3 | 1 | 2 | 1 | ND | 1 | 1 | 2 | 1 |
| La ppm | 2.45 | 2.24 | | | | | 2.83 | | | 3.20 | 1.64 | 2.04 |
| Ce | 4.76 | 5.95 | | | | | 6.75 | | | 6.91 | 3.78 | 5.28 |
| Pr | 0.70 | 0.80 | | | | | 0.86 | | | 0.78 | 0.50 | 0.69 |
| Nd | 2.81 | 3.14 | | | | | 3.31 | | | 2.64 | 1.95 | 2.65 |
| Sm | 0.94 | 1.16 | | | | | 1.22 | | | 0.82 | 0.80 | 1.00 |
| Eu | 0.10 | 0.04 | | | | | 0.10 | | | 0.04 | 0.15 | 0.14 |
| Gd | 0.98 | 0.96 | | | | | 1.20 | | | 0.64 | 0.85 | 0.85 |
| Tb | 0.21 | 0.18 | | | | | 0.26 | | | 0.14 | 0.19 | 0.18 |
| Dy | 1.46 | 1.05 | | | | | 1.82 | | | 0.91 | 1.29 | 1.02 |
| Ho | 0.30 | 0.17 | | | | | 0.39 | | | 0.18 | 0.25 | 0.19 |
| Er | 1.03 | 0.52 | | | | | 1.37 | | | 0.62 | 0.84 | 0.60 |
| Tm | 0.17 | 0.09 | | | | | 0.22 | | | 0.11 | 0.14 | 0.10 |
| Yb | 1.24 | 0.68 | | | | | 1.60 | | | 0.82 | 1.05 | 0.75 |
| Lu | 0.18 | 0.09 | | | | | 0.23 | | | 0.12 | 0.15 | 0.11 |

* Fine-grained aplite; ** marginal part of aplite. Symbols: lcgr: leucogranite, Ms: muscovite, Tur: tourmaline.

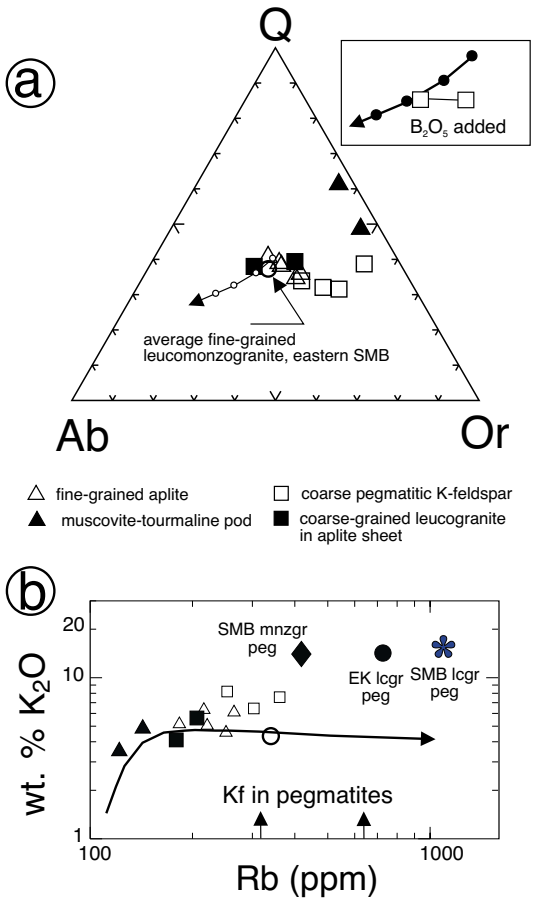


FIG. 7. Whole-rock compositions of aplite–pegmatite samples. (a) Plot of normative quartz (Q) – albite (Ab) – orthoclase (Or). Data are compared to the average composition of fine-grained leucomonzogranite (circle) in the South Mountain Batholith (Ham *et al.* 1989, $n = 100$). The arrow indicates the projection of the pseudoternary minima for 0.5, 1, 3 and 5 kbar in $H_2O$-saturated granite (Tuttle & Bowen 1958). Inset box shows the effect of adding 4. 5 wt.% $B_2O_5$ to $H_2O$-saturated (near cotectic) and undersaturated granite at P = 1 kbar (Manning & Pichavant 1988). (b) Binary element plot of wt.% $K_2O$ *versus* Rb (ppm), in which Peggys Cove data are compared to K-feldspar samples from pegmatites of various settings in the South Mountain Batholith, namely segregations in monzogranites (SMB mnzgr), evolved pegmatites in the New Ross area (SMB lcgr peg) and segregations in the East Kemptville leucogranite (EK lcgr peg). The arrows on the X axis indicate the Rb contents (ppm) for two K-feldspar separates from pegmatites at Peggys Cove (data in Table 4). The curved line traces the evolution of the South Mountain Batholith based on whole-rock samples (dataset of Ham *et al.* 1989). Average composition of fine-grained leucomonzogranite in the South Mountain Batholith (Ham *et al.* 1989, $n = 100$) is shown by circle.

& Mittlefehldt 1982), and (3) pronounced negative Eu anomalies due to feldspar fractionation. In Figure 8b, three aplite–leucogranite samples from the large layered aplite–pegmatite sheet (Fig. 5k) are plotted separately. There is no systematic relationship between sample position within the sheet (*i.e.,* margin *versus* core) and their *REE* content. The *REE* patterns for the aplite samples are similar to some *REE* patterns for evolved phases (leucomonzogranites and aplites) of the SMB (Kontak *et al.* 1988, Clarke *et al.* 1993, Dostal & Chatterjee 1995), but in general contrast with the more fractionated patterns typical of granites from both early and late phases of the SMB, as represented by granodiorite–monzogranite and leucogranites, respectively (Fig. 8b).

## MINERAL COMPOSITIONS

### *Major and minor elements*

Representative compositions of the major silicate phases are summarized in Tables 3 and 4.

*Alkali feldspar* analyzed includes K- and Na-rich feldspars and the varied perthites; a typical pegmatitic K-feldspar examined with back-scattered electron (BSE) imaging (Fig. 9a) illustrates the nature of the film and flame perthite textures. Raster analysis of the K-feldspar indicates bulk compositions of $Or_{72}Ab_{28}$ to $Or_{84}Ab_{16}$, although some go to $Or_{65}Ab_{35}$ and $Or_{95}Ab_5$ (Fig. 9b). In contrast, point analysis of K-feldspar indicates that most compositions fall in the range $Or_{86}Ab_{14}$ to $Or_{100}$ (Fig. 9b). Thus only in a few cases did complete re-equilibration at subsolidus conditions occur (*i.e.*, $Or_{96–100}$; Fig. 9b). Compositions of albite occurring as exsolution lamellae and isolated grains in K-feldspar range from $Ab_{86}$ to $Ab_{100}$ (Fig. 9c). The phosphorus contents of alkali feldspar are generally below 0.5 wt.%, and most are below the detection limit of 0.2 wt.%; a few samples contain between 0.5 to 1.0 wt.% $P_2O_5$ (Fig. 9d). These results contrast markedly with values of 1 to 2 wt. % $P_2O_5$ for pegmatitic alkali feldspar in the SMB (Kontak *et al.* 1996). The barium content of feldspars range from below the detection limit of *ca.* 0.20 wt.% BaO to a maximum of *ca.* 0.6 wt.%. BaO. A single case of K-feldspar ($Or_{98}Ab_2$) occurring as a vein cutting tourmaline in sample PCG–023 (Table 2) contains up to 1.2 wt.% BaO.

*Plagioclase* in the leucogranites and aplites varies in composition from $An_{12}$ to $An_0$ (Fig. 10), as is typical of this mineral phase in evolved granites, including the SMB (MacDonald *et al.* 1992). There is a progression in plagioclase toward more sodic compositions that correlates with textures indicative of subsolidus equilibration, with end-member albite ($An_{0–2}$) typical of pitted areas (Fig. 11e).

*Muscovite* in pegmatites, leucocratic granite and aplite, and within cavities of leucogranites in sheeted aplite–pegmatite, has a uniform composition. BSE im-

aging and point analyses indicate a homogeneous composition with: 0.6 ± 0.4 wt.% MgO, 1.4 ± 0.6 wt.% $FeO_T$, 0.6 ± 0.2 wt.% $Na_2O$, and 0.2 to 0.5 wt.% $TiO_2$. Muscovite has <5% paragonite component and limited substitution toward celadonite. There is a positive correlation between FeO and MgO, but the data define a large range in the MgO:FeO ratio (1:1 to 1:6; Fig. 11d). This variation reflects differences among samples, as the Mg:Fe ratio for muscovite within a sample is uniform. Neither F nor Cl were detected during analysis (*i.e.,* ≤0.2 wt.%). Small grains of secondary muscovite in feldspar are notably depleted in FeO, MgO and $TiO_2$ compared to the coarser, primary muscovite grains (Fig. 12). The exception to this generalization pertains to secondary muscovite within altered cordierite; it contains 8 wt.% FeO and 2 wt.% MgO.

Grains of an *apatite-group mineral* fall into two groups based on composition and occurrence: (1) Mn-rich grains that are disseminated within the matrix of aplite and leucogranite, and (2) Mn-depleted grains disseminated within feldspar grains (Figs. 11a, b). The former tend to be coarser, whereas the latter are associated with turbid areas within pitted feldspar (Figs. 11d, e). The strong negative correlation between wt.% CaO and MnO in the apatite (Fig. 11a) reflects Ca ⇌ Mn exchange, and there also is an increase in wt.% $SiO_2$ in grains deficient in phosphorus (Fig. 11c). All apatite grains analyzed are depleted in both F and Cl, thus similar to the F- and Cl-deficient nature of muscovite, and are considered to be hydroxylapatite.

*Tourmaline* (Table 4) from all varieties of occurrence were analyzed, but we found no distinct chemical differences. Tourmaline is strongly zoned in terms of wt.% $SiO_2$ (30–45), $Al_2O_3$ (26–40), FeO (6–15), MgO (0–5) and $Na_2O$ (1–3), with a strong positive correlation among $SiO_2$ and $Al_2O_3$ and $Na_2O$, and negative correlation between MgO and FeO. The samples are deficient in Li (see below), and calculated amounts based on mineral stoichiometry are *ca.* ≤0.5 wt.% $Li_2O$ (Table 4). In binary plots (Fig. 13), the data correspond to schorl, dravite and foitite, with the majority of compositions corresponding to schorl. Based on imaging, the grains seem to have a broad, chemically homogeneous core and a narrow, strongly zoned border, which is characterized by up to 23 wt.% $FeO_T$. This Fe enrichment is similar to that in tourmaline from late-stage aplites and pegmatites in the Hub Kapong batholith, Thailand (Manning 1982). The Mg-rich nature of the majority of the tourmaline analyzed contrasts markedly with the generally Mg-depleted nature of tourmaline in aplites and granites (*sensu stricto*), as documented by several investigators (*e.g.,* Manning 1982, Sinclair & Richardson 1992, Stern *et al*. 1986, Jolliff *et al.* 1986, London & Manning 1995). In addition, the tourmaline is depleted in Mn, which contrasts with the common enrichment of this element in pegmatitic tourmaline (Stern *et al*. 1986). Although not shown herein, the compositional data are comparable to a dataset for tourmaline from a variety of granitic settings in the Meguma Terrane (Clarke *et al*. 1989).

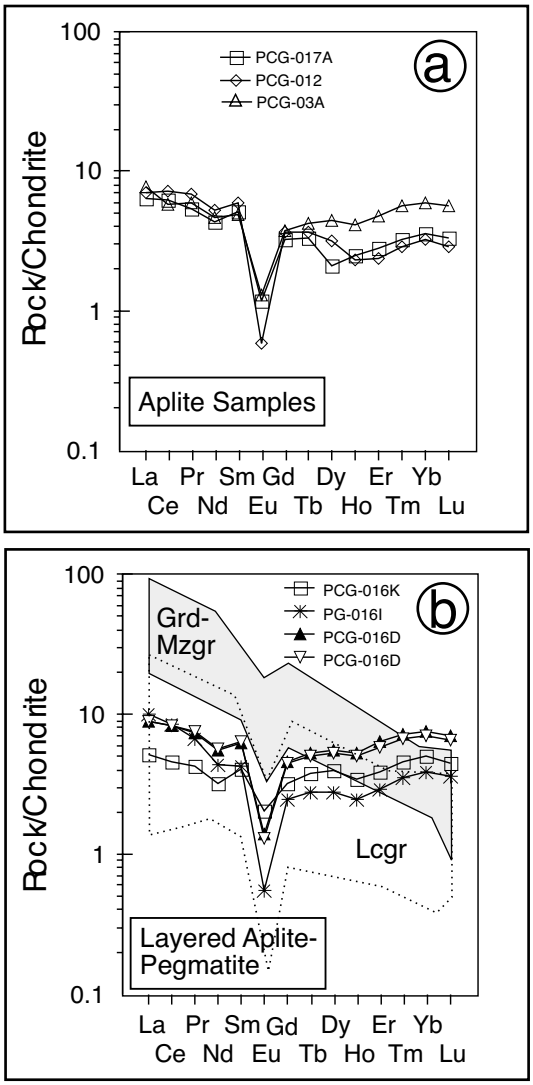


FIG. 8. Chondrite-normalized plots of rare-earth element concentrations (chondrite values of Masuda *et al*. 1973) for whole-rock samples of aplite from layered aplite–pegmatite rock at Peggys Cove. (a) Three samples of aplite at Peggys Cove. (b) Samples of aplite from the layered aplite–pegmatite shown in Figure 5k. Note that the three samples have similar abundances and patterns regardless of position, *i.e.*, bottom contact (PCG–016k) *versus* center area (PCG–016D, 016I). Sample PCG–016D was analyzed in duplicate; excellent reproducibility of the data is indicated. Data are compared to the range for granodiorite–monzogranite (Grd–Mzgr; Muecke & Clarke 1981) and leucogranites (Lcgr; Clarke *et al*. 1993) of the South Mountain Batholith.

TABLE 3. REPRESENTATIVE COMPOSITIONS OF MINERALS, PEGMATITE–APLITE SHEETS, PEGGYS COVE, NOVA SCOTIA

| Sample | Mineral | $SiO_2$ | $TiO_2$ | $Al_2O_3$ | FeO | MnO | MgO | CaO | $Na_2O$ | $K_2O$ | $P_2O_5$ | BaO | Total |
|---|---|---|---|---|---|---|---|---|---|---|---|---|---|
| PCG-01B | Kfs | 64.84 | - | 19.23 | N.D. | - | - | N.D. | 1.08 | 15.23 | 0.52 | N.D. | 100.90 |
| PCG-01B | Kfs | 64.05 | | 18.58 | N.D. | | | N.D. | 1.90 | 14.03 | 0.36 | N.D. | 98.92 |
| PCG-04 | Kfs | 64.94 | - | 18.79 | N.D. | - | - | N.D. | 0.33 | 15.74 | N.D. | N.D. | 99.80 |
| PCG-9A | Kfs | 64.20 | - | 19.02 | N.D. | - | - | N.D. | 1.14 | 15.18 | 0.46 | N.D. | 100.01 |
| PCG-9A | Ab | 67.51 | - | 19.89 | N.D. | - | - | 0.29 | 10.44 | N.D. | 0.39 | N.D. | 98.52 |
| PCG-010 | Kfs | 64.11 | | 18.79 | N.D. | | | N.D. | 0.88 | 15.13 | N.D. | 0.68 | 99.59 |
| PCG-010 | Ab | 66.54 | | 21.02 | N.D. | | | 1.28 | 9.92 | 0.14 | N.D. | N.D. | 98.90 |
| PCG-015A | Ab | 66.32 | - | 21.23 | N.D. | - | - | 1.89 | 10.02 | 0.18 | 0.00 | N.D. | 99.64 |
| PCG-015A | Kfs | 64.57 | - | 18.94 | N.D. | - | - | 0.00 | 0.62 | 15.23 | 0.47 | N.D. | 99.83 |
| PCG-015A | Ab | 66.28 | - | 21.63 | N.D. | - | - | 1.97 | 10.33 | 0.19 | 0.36 | N.D. | 100.76 |
| PCG-016B | Ab | 69.76 | - | 20.10 | N.D. | - | - | 0.20 | 9.14 | 0.04 | N.D. | N.D. | 99.24 |
| PCG-016B | Kfs | 65.57 | - | 17.94 | N.D. | - | - | N.D. | 0.49 | 15.52 | N.D. | 0.17 | 99.68 |
| PCG-019 | Ab | 67.76 | - | 19.59 | N.D. | - | - | N.D. | 8.45 | 3.49 | 0.38 | N.D. | 99.86 |
| PCG-019 | Kfs | 65.10 | - | 18.83 | N.D. | - | - | N.D. | 0.97 | 15.09 | N.D. | N.D. | 100.00 |
| PCG-023 | Ab | 68.59 | - | 19.55 | N.D. | - | - | 0.19 | 11.96 | N.D. | N.D. | N.D. | 100.29 |
| PCG-023 | Kfs | 62.09 | - | 19.50 | 0.73 | - | - | N.D. | 0.39 | 14.98 | N.D. | 0.81 | 98.50 |
| PCG-023 | Kfs | 64.90 | - | 18.31 | 0.33 | - | - | N.D. | 0.22 | 15.85 | N.D. | 0.53 | 100.14 |
| PCG-07B | Ms | 47.17 | N.D. | 36.73 | 1.15 | N.D. | 0.62 | N.D. | 0.46 | 9.77 | - | - | 95.90 |
| PCG-09C | Ms | 47.26 | N.D. | 34.40 | 2.35 | N.D. | N.D. | N.D. | 0.70 | 9.62 | - | - | 94.35 |
| PCG-010 | Ms | 46.59 | N.D. | 34.59 | 1.70 | N.D. | 1.05 | N.D. | 0.47 | 9.96 | - | - | 94.36 |
| PCG-010 | Ms | 46.39 | N.D. | 36.08 | 2.24 | N.D. | 0.82 | N.D. | 0.47 | 10.80 | - | - | 96.79 |
| PCG-011 | Ms | 45.81 | N.D. | 35.47 | 2.01 | N.D. | 0.42 | N.D. | 0.66 | 9.35 | - | - | 93.72 |
| PCG-14B | Ms | 46.30 | N.D. | 36.11 | 2.10 | N.D. | 0.35 | N.D. | 0.56 | 9.44 | - | - | 94.84 |
| PCG-012 | Ms | 47.32 | 0.29 | 36.02 | 1.14 | N.D. | 0.52 | N.D. | 0.36 | 9.33 | - | - | 94.98 |
| PCG-16C | Ms | 46.16 | N.D. | 35.70 | 1.98 | N.D. | 0.39 | N.D. | 0.69 | 8.49 | - | - | 93.41 |
| PCG-016E | Ms | 47.10 | 0.41 | 36.43 | 1.45 | N.D. | 0.29 | N.D. | 0.55 | 8.90 | - | - | 95.14 |
| PCG-023 | Ms | 46.44 | 0.48 | 35.74 | 1.66 | N.D. | 0.43 | N.D. | 0.40 | 9.28 | - | - | 94.46 |
| PCG-023 | Hap | N.D. | - | N.D. | N.D. | 1.75 | N.D. | 55.29 | N.D. | N.D. | 44.13 | - | 101.17 |
| PCG-012 | Hap | 0.00 | - | 0.02 | 0.62 | 5.98 | 0.04 | 49.81 | N.D. | N.D. | 43.05 | - | 98.87 |
| PCG-012 | Hap | 1.99 | - | 0.68 | 0.14 | 0.07 | 0.04 | 55.97 | N.D. | 0.82 | 41.77 | - | 98.66 |
| PCG-012 | Hap | 2.53 | - | 0.82 | N.D. | N.D. | 0.03 | 55.02 | 0.25 | 1.00 | 41.41 | - | 97.71 |
| PCG-012 | Hap | 0.43 | - | N.D. | 0.63 | 6.08 | N.D. | 49.10 | N.D. | N.D. | 42.46 | - | 97.64 |
| PCG-016B | Hap | N.D. | - | N.D. | N.D. | 3.41 | N.D. | 53.06 | N.D. | N.D. | 44.28 | - | 100.75 |
| PCG-016B | Hap | 3.00 | - | 0.87 | N.D. | N.D. | 0.04 | 54.59 | 0.36 | N.D. | 42.16 | - | 97.15 |
| PCG-019 | Hap | 0.25 | - | N.D. | N.D. | N.D. | N.D. | 56.80 | N.D. | N.D. | 44.07 | - | 100.87 |

| Sample | Mineral | Si | Ti | Al | Fe | Mn | Mg | Ca | Na | K | P | Ba |
|---|---|---|---|---|---|---|---|---|---|---|---|---|
| PCG-01B | Kfs | 2.952 | 0.000 | 1.032 | 0.000 | 0.000 | 0.000 | 0.000 | 0.096 | 0.888 | 0.024 | 0.000 |
| PCG-01B | Kfs | 2.968 | 0.000 | 1.016 | 0.000 | 0.000 | 0.000 | 0.000 | 0.168 | 0.832 | 0.016 | 0.000 |
| PCG-04 | Kfs | 2.992 | 0.000 | 1.024 | 0.000 | 0.000 | 0.000 | 0.000 | 0.032 | 0.928 | 0.000 | 0.000 |
| PCG-09A | Kfs | 2.952 | 0.000 | 1.032 | 0.000 | 0.000 | 0.000 | 0.000 | 0.104 | 0.888 | 0.016 | 0.000 |
| PCG-09A | Ab | 2.976 | 0.000 | 1.032 | 0.000 | 0.000 | 0.000 | 0.016 | 0.896 | 0.000 | 0.016 | 0.000 |
| PCG-010 | Kfs | 2.976 | 0.000 | 1.032 | 0.000 | 0.000 | 0.000 | 0.000 | 0.080 | 0.896 | 0.000 | 0.016 |
| PCG-010 | Ab | 2.928 | 0.000 | 1.088 | 0.000 | 0.000 | 0.000 | 0.064 | 0.848 | 0.008 | 0.000 | 0.000 |
| PCG-015A | Ab | 2.912 | 0.000 | 1.096 | 0.000 | 0.000 | 0.000 | 0.088 | 0.856 | 8.000 | 0.000 | 0.000 |
| PCG-015A | Kfs | 2.968 | 0.000 | 1.024 | 0.000 | 0.000 | 0.000 | 0.000 | 0.056 | 0.896 | 0.016 | 0.000 |
| PCG-015A | Ab | 2.888 | 0.000 | 1.112 | 0.000 | 0.000 | 0.000 | 0.096 | 0.872 | 0.008 | 0.016 | 0.000 |
| PCG-016B | Ab | 3.032 | 0.000 | 1.032 | 0.000 | 0.000 | 0.000 | 0.008 | 0.768 | 0.000 | 0.000 | 0.000 |
| PCG-016B | Kfs | 3.032 | 0.000 | 0.976 | 0.000 | 0.000 | 0.000 | 0.000 | 0.040 | 0.912 | 0.000 | 0.000 |
| PCG-019 | Ab | 2.992 | 0.000 | 1.016 | 0.000 | 0.000 | 0.000 | 0.000 | 0.720 | 0.200 | 0.016 | 0.000 |
| PCG-019 | Kfs | 2.992 | 0.000 | 1.024 | 0.000 | 0.000 | 0.000 | 0.000 | 0.056 | 0.888 | 0.000 | 0.000 |
| PCG-023 | Ab | 2.992 | 0.000 | 1.008 | 0.000 | 0.000 | 0.000 | 0.008 | 1.008 | 0.000 | 0.000 | 0.000 |
| PCG-023 | Kfs | 2.920 | 0.000 | 1.080 | 0.032 | 0.000 | 0.000 | 0.000 | 0.032 | 0.896 | 0.000 | 0.016 |
| PCG-023 | Kfs | 3.000 | 0.000 | 1.000 | 0.016 | 0.000 | 0.000 | 0.000 | 0.024 | 0.936 | 0.000 | 0.008 |
| PCG-07B | Ms | 3.091 | 0.000 | 2.838 | 0.066 | 0.000 | 0.066 | 0.000 | 0.055 | 0.814 | 34.001 | 0.000 |
| PCG-09C | Ms | 3.168 | 0.000 | 2.717 | 0.132 | 0.000 | 0.000 | 0.000 | 0.088 | 0.825 | 34.648 | 0.000 |
| PCG-010 | Ms | 3.124 | 0.000 | 2.728 | 0.099 | 0.000 | 0.110 | 0.000 | 0.066 | 0.847 | 34.364 | 0.000 |
| PCG-010 | Ms | 3.058 | 0.000 | 2.805 | 0.121 | 0.000 | 0.077 | 0.000 | 0.055 | 0.902 | 33.638 | 0.000 |
| PCG-011 | Ms | 3.091 | 0.000 | 2.816 | 0.110 | 0.000 | 0.044 | 0.000 | 0.088 | 0.803 | 34.001 | 0.000 |
| PCG-14B | Ms | 3.080 | 0.000 | 2.838 | 0.121 | 0.000 | 0.033 | 0.000 | 0.077 | 0.803 | 33.880 | 0.000 |
| PCG-12 | Ms | 3.124 | 0.011 | 2.805 | 0.066 | 0.000 | 0.055 | 0.000 | 0.044 | 0.781 | 34.364 | 0.121 |
| PCG-16C | Ms | 3.102 | 0.000 | 2.827 | 0.110 | 0.000 | 0.044 | 0.000 | 0.088 | 0.726 | 34.122 | 0.000 |
| PCG-016E | Ms | 3.102 | 0.022 | 2.827 | 0.077 | 0.000 | 0.033 | 0.000 | 0.066 | 0.748 | 34.122 | 0.242 |
| PCG-023 | Ms | 3.102 | 0.022 | 2.805 | 0.099 | 0.000 | 0.044 | 0.000 | 0.055 | 0.792 | 34.122 | 0.242 |
| PCG-023 | Hap | 0.000 | 0.000 | 0.000 | 0.000 | 0.260 | 0.000 | 9.884 | 0.000 | 0.000 | 6.292 | 0.000 |
| PCG-012 | Hap | 0.000 | 0.000 | 0.000 | 0.078 | 0.884 | 0.000 | 9.256 | 0.000 | 0.000 | 6.318 | 0.000 |
| PCG-012 | Hap | 0.338 | 0.000 | 0.130 | 0.000 | 0.000 | 0.000 | 10.114 | 0.000 | 0.182 | 5.954 | 0.000 |
| PCG-012 | Hap | 0.416 | 0.000 | 0.156 | 0.000 | 0.000 | 0.000 | 9.958 | 0.078 | 0.208 | 5.928 | 0.000 |
| PCG-012 | Hap | 0.078 | 0.000 | 0.000 | 0.104 | 0.910 | 0.000 | 9.178 | 0.000 | 0.000 | 6.266 | 0.000 |
| PCG-016B | Hap | 0.000 | 0.000 | 0.000 | 0.000 | 0.494 | 0.000 | 9.620 | 0.000 | 0.000 | 6.344 | 0.000 |
| PCG-016B | Hap | 0.494 | 0.000 | 0.182 | 0.000 | 0.000 | 0.000 | 9.776 | 0.130 | 0.000 | 5.954 | 0.000 |
| PCG-019 | Hap | 0.052 | 0.000 | 0.000 | 0.000 | 0.000 | 0.000 | 10.218 | 0.000 | 0.000 | 6.266 | 0.000 |

Symbols: Kfs: K-feldspar, Ab: albite, Ms: muscovite, Hap: hydroxylapatite, N.D.: not detected. The structural formulas are recalculated on the basis of eight atoms of oxygen for K-feldspar and albite, eleven for muscovite, and twenty-six for hydroxylapatite.

Trace amounts of subhedral to anhedral *zircon* occur associated with hydroxylapatite in pitted feldspar (Fig. 11d). These grains are too small to analyze reliably, hence no Hf or *REE* data are available.

An unidentified mineral phase containing Si, Ca, Ba, Sr and $SO_4$ occurs as anhedral secondary grains within fractured tourmaline. The presence of this phase is noted because it bears on our interpretation of the whole-rock composition of the muscovite–tourmaline pods, discussed below.

*Trace and rare-earth elements*

K-feldspar and tourmaline mineral separates were analyzed for trace and *REE* abundances (Table 5) and chondrite-normalized plots are shown in Figure 14. The two pegmatitic K-feldspar have trace element (*i.e.,* Ba, Sr, Rb, Pb, Cs) contents, Rb:Sr ratios, and levels of *REE* that are intermediate between values typical for K-feldspar hosted by monzogranite and unevolved pegmatites of the SMB, rather than evolved pegmatites (Kontak & Martin 1997). The contrasting Eu anomalies for the two samples are unusual, and we have no explanation at present. The *REE* contents are also enriched compared to K-feldspar from chemically evolved, zoned pegmatites of the Black Hills, South Dakota (Walker *et al.* 1986), which have chondritic values less than 1.

Tourmaline separates (Table 5) from pegmatite (PCG–010, 020) and aplite (PCG–023) have variable abundances of trace elements, *e.g.,* Li (16 to 19 ppm),

TABLE 4. COMPOSITIONS OF TOURMALINE FROM APLITE–PEGMATITE SHEETS, PEGGYS COVE, NOVA SCOTIA

| Sample | | PCG-2000 4 | PCG-2000 4 | PCG-2000 4 | PCG-2000 1 | PCG-2000 1 | PCG-99 02B | PCG-99 02B | PCG-99 7 | PCG-99 7 | PCG-99 23 | PCG-99 23 | PCG-99 21A | PCG-99 21A |
|---|---|---|---|---|---|---|---|---|---|---|---|---|---|---|
| $SiO_2$ | wt.% | 35.53 | 35.51 | 35.50 | 35.27 | 35.30 | 36.70 | 36.48 | 35.62 | 35.93 | 35.29 | 35.37 | 35.14 | 34.29 |
| $TiO_2$ | | N.D. | 0.51 | 0.38 | 0.88 | N.D. | 0.18 | 0.21 | 0.50 | 0.04 | 0.83 | 0.90 | 0.27 | 0.53 |
| $Al_2O_3$ | | 32.98 | 33.67 | 31.28 | 33.11 | 32.76 | 34.22 | 33.67 | 34.44 | 32.51 | 33.33 | 33.22 | 34.69 | 33.58 |
| FeO | | 13.23 | 9.22 | 11.57 | 9.71 | 13.56 | 7.16 | 7.73 | 8.22 | 9.76 | 9.50 | 9.45 | 13.74 | 14.67 |
| MgO | | 1.03 | 3.74 | 3.68 | 3.75 | 0.72 | 4.17 | 3.83 | 4.22 | 4.90 | 3.90 | 3.71 | 0.11 | 0.20 |
| CaO | | N.D. | 0.32 | 0.37 | 0.29 | N.D. | 0.03 | 0.03 | 0.16 | 0.23 | 0.22 | 0.19 | 0.03 | 0.01 |
| MnO | | N.D. | N.D. | 0.24 | N.D. | 0.26 | 0.04 | 0.17 | 0.04 | 0.06 | 0.20 | 0.09 | 0.34 | 0.25 |
| $Na_2O$ | | 1.21 | 1.69 | 2.05 | 1.89 | 1.31 | 2.35 | 1.98 | 1.73 | 1.98 | 1.89 | 1.81 | 1.74 | 1.86 |
| $H_2O^*$ | | 3.52 | 3.60 | 3.55 | 3.59 | 3.50 | 3.67 | 3.63 | 3.64 | 3.60 | 3.60 | 3.60 | 3.58 | 3.52 |
| $B_2O_3^*$ | | 10.18 | 10.41 | 10.27 | 10.38 | 10.13 | 10.64 | 10.51 | 10.54 | 10.45 | 10.45 | 10.42 | 10.39 | 10.22 |
| $Li_2O^*$ | | 0.32 | 0.24 | 0.17 | 0.24 | 0.30 | 0.60 | 0.57 | 0.29 | 0.09 | 0.26 | 0.31 | 0.37 | 0.28 |
| Total | | 98.00 | 98.90 | 99.05 | 99.11 | 97.85 | 99.80 | 98.81 | 99.44 | 99.56 | 99.49 | 99.08 | 100.41 | 99.58 |
| Structural formula based on 31 anions (O,OH,F) | | | | | | | | | | | | | | |
| *T* | Si *apfu* | 6.063 | 5.930 | 6.008 | 5.903 | 6.055 | 5.996 | 6.030 | 5.875 | 5.977 | 5.870 | 5.898 | 5.880 | 5.834 |
| | Al | 0.000 | 0.070 | 0.000 | 0.097 | 0.000 | 0.004 | 0.000 | 0.125 | 0.023 | 0.130 | 0.102 | 0.120 | 0.166 |
| | B | 3.000 | 3.000 | 3.000 | 3.000 | 3.000 | 3.000 | 3.000 | 3.000 | 3.000 | 3.000 | 3.000 | 3.000 | 3.000 |
| *Z* | Al | 6.000 | 6.000 | 6.000 | 6.000 | 6.000 | 6.000 | 6.000 | 6.000 | 6.000 | 6.000 | 6.000 | 6.000 | 6.000 |
| | Mg | 0.000 | 0.000 | 0.000 | 0.000 | 0.000 | 0.000 | 0.000 | 0.000 | 0.000 | 0.000 | 0.000 | 0.000 | 0.000 |
| *Y* | Al | 0.633 | 0.558 | 0.239 | 0.435 | 0.623 | 0.586 | 0.560 | 0.571 | 0.352 | 0.405 | 0.427 | 0.721 | 0.567 |
| | Ti | 0.000 | 0.064 | 0.048 | 0.111 | 0.000 | 0.022 | 0.026 | 0.062 | 0.005 | 0.104 | 0.113 | 0.034 | 0.068 |
| | Mg | 0.262 | 0.931 | 0.928 | 0.936 | 0.184 | 1.016 | 0.944 | 1.038 | 1.215 | 0.967 | 0.922 | 0.027 | 0.051 |
| | Mn | 0.000 | 0.000 | 0.034 | 0.000 | 0.038 | 0.006 | 0.024 | 0.006 | 0.008 | 0.028 | 0.013 | 0.048 | 0.036 |
| | $Fe^{2+}$ | 1.888 | 1.288 | 1.637 | 1.359 | 1.945 | 0.978 | 1.069 | 1.134 | 1.358 | 1.322 | 1.318 | 1.923 | 2.087 |
| | $Li^*$ | 0.217 | 0.160 | 0.113 | 0.159 | 0.210 | 0.392 | 0.378 | 0.190 | 0.062 | 0.175 | 0.207 | 0.246 | 0.191 |
| | Sum *Y* | 3.000 | 3.001 | 2.999 | 3.000 | 3.000 | 3.000 | 3.001 | 3.001 | 3.000 | 3.001 | 3.000 | 2.999 | 3.000 |
| *Z* | Ca | 0.000 | 0.057 | 0.067 | 0.052 | 0.000 | 0.005 | 0.005 | 0.028 | 0.041 | 0.039 | 0.034 | 0.005 | 0.002 |
| | Na | 0.400 | 0.547 | 0.673 | 0.613 | 0.436 | 0.744 | 0.635 | 0.553 | 0.639 | 0.610 | 0.585 | 0.565 | 0.614 |
| | K | 0.000 | 0.000 | 0.000 | 0.000 | 0.000 | 0.010 | 0.000 | 0.011 | 0.002 | 0.004 | 0.002 | 0.002 | 0.037 |
| | □ | 0.600 | 0.396 | 0.260 | 0.335 | 0.564 | 0.240 | 0.360 | 0.408 | 0.318 | 0.347 | 0.379 | 0.428 | 0.348 |
| OH | | 4.000 | 4.000 | 4.000 | 4.000 | 4.000 | 4.000 | 4.000 | 4.000 | 4.000 | 4.000 | 4.000 | 4.000 | 4.000 |
| Name | | Foitite | Schorl | Schorl | Schorl | Foitite | Dravite | Schorl | Schorl | Schorl | Schorl | Schorl | Schorl | Schorl |

Sample locations: PCG-2004: pod of tourmaline in pegmatite; PCG-2000-1: tourmaline-lined fracture in pegmatite; PCG-99-2B: pegmatite; PCG-99-7: coarse segregation in pegmatite core; PCG-99-23: tourmaline in aplite; PCG-99-21A: pocket zone in pegmatite. Mineral formulae calculated using program in Tindle *et al.* (2002); * refers to amounts inferred from stoichiometry. □: vacancy, *apfu*: atoms per formula unit.

Rb and Sr (4 to 11 ppm), Zr (95 to 20 ppm), Ba (933 to 395 ppm) and Pb (4 to 6 ppm). The low Nb:Ta ratio (0.5–0.7) is similar to those in evolved rocks in the SMB (Dostal & Chatterjee 2000), signifying some internal evolution of the pegmatites, but the Li contents are very low compared to tourmaline from evolved pegmatite-forming melts (*e.g.,* Jolliff *et al.* 1986, Tindle *et al.* 2002). The chondrite-normalized *REE* patterns are generally flat, with a negative Eu anomaly, and are similar to the patterns for the whole-rock samples, thus consistent with observations that tourmaline does not preferentially incorporate any *REE* (Jolliff *et al*. 1987). The low Σ*REE* is similar to that found for tourmaline from the interior of the Bob Ingersoll pegmatite (Jolliff *et al.* 1987) and quartz–tourmaline veins associated with granite at the Dachang tin deposit, China (Jiang *et al.* 1999), but depleted compared to tourmaline from granodiorite and related veins in the Salikvan porphyry Cu–Mo deposit (Yavuz *et al.* 1999).

## Fluid Inclusions

A variety of pegmatite samples containing variable modal proportions of quartz – feldspar – muscovite – tourmaline were prepared for fluid-inclusion study. From this initial suite, a few selected samples were used for detailed thermometric and decrepitate analyses. Our observations and thermometric measurements focus on areas of inclusions with uniform proportions of phases (*i.e.,* L:V ratios) and shapes, which equate to fluid inclusion assemblages (FIA) of Goldstein & Reynolds (1994).

### *Petrographic observations*

The quality and abundance of inclusions vary considerably, ranging from absent to inundating areas. Although inclusions are present in both quartz and tourmaline, the latter proved difficult to use and are,

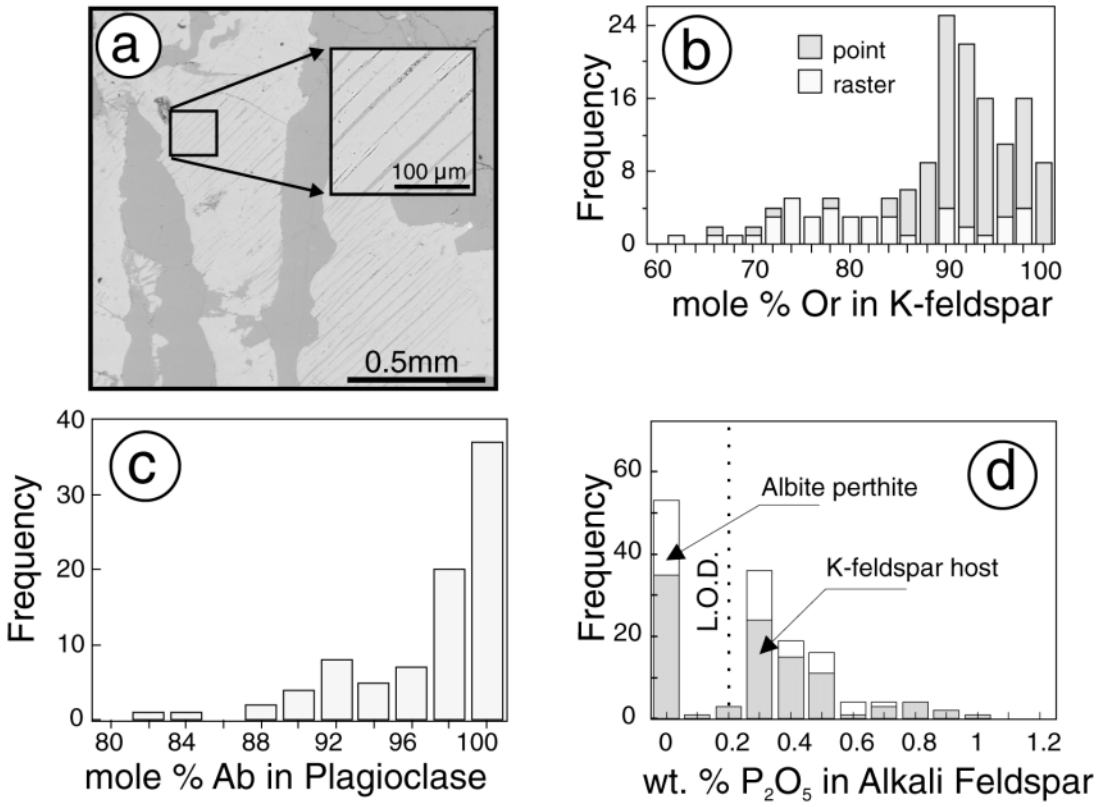


FIG. 9. Compositional data for perthitic K-feldspar in pegmatites. (a) Back-scattered electron image of perthitic alkali feldspar (light grey) intergrown with quartz (dark grey) in graphic-textured pegmatite sample. Inset figure shows film perthite. Raster-type data for the inset area are interpreted to give the primary bulk-composition of the alkali feldspar. (b) Histogram plot of point and raster analyses of perthitic alkali feldspar. (c) Histogram plot of albite lamellae in perthitic K-feldspar. (d) Histogram plot of wt.% $P_2O_5$ for K-feldspar host (point-type analysis) and albite lamellae in perthitic K-feldspar. LOD is the limit of detection.

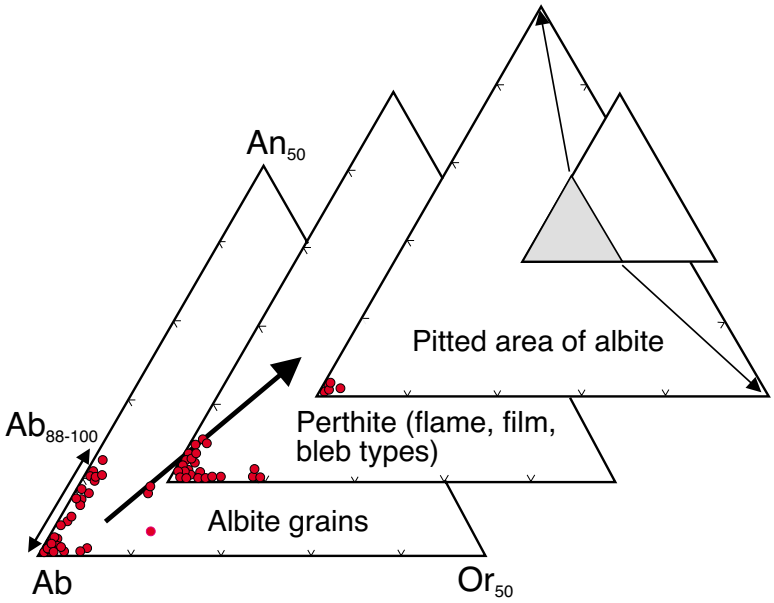


FIG. 10. Plots of compositions of plagioclase and albite lamellae in perthitic K-feldspar from aplite and pegmatite. Arrow indicates the trend of inferred re-equilibration, as reflected by the composition of the plagioclase.

TABLE 5. TRACE-ELEMENT DATA FOR MINERAL SEPARATES, PEGGYS COVE PEGMATITES, NOVA SCOTIA

| Sample | PCG-99 | | | PCG-99 | |
|---|---|---|---|---|---|
| Mineral | 23 Tur | 20 Tur | 10 Tur | 20 Kfs | 023A Kfs |
| Li ppm | 19.4 | 18.9 | 16.9 | 4.6 | 2.1 |
| Rb | 11.2 | 5.6 | 0.3 | 623.7 | 315.4 |
| Sr | 4.8 | 9.0 | 1.2 | 15.6 | 60.0 |
| Y | 2.3 | 1.9 | 0.7 | 0.5 | 0.7 |
| Zr | 20.5 | 18.9 | 4.8 | 1.2 | 5.7 |
| Nb | 1.2 | 1.2 | 1.7 | 0.2 | 0.1 |
| Mo | 0.3 | 0.2 | 0.3 | 0.1 | N.D. |
| Cs | N.D. | 0.1 | N.D. | 5.4 | 2.4 |
| Ba | 33.7 | 395.1 | 0.5 | 52.3 | 252.0 |
| Hf | 1.9 | 1.7 | 0.4 | 0.1 | 0.7 |
| Ta | 1.6 | 1.5 | 3.4 | 0.2 | N.D. |
| Tl | 0.1 | 0.0 | N.D. | 2.7 | 1.3 |
| Pb | 5.1 | 6.7 | 4.4 | 42.2 | 68.0 |
| Bi | N.D. | N.D. | 1.5 | 0.1 | N.D. |
| Th | 0.4 | 0.3 | 0.3 | N.D. | 0.2 |
| U | 2.3 | 2.2 | 2.4 | 0.2 | 0.3 |
| La | 0.51 | 0.46 | 0.32 | 4.03 | 3.51 |
| Ce | 1.13 | 1.04 | 1.02 | 2.97 | 2.12 |
| Pr | 0.16 | 0.14 | 0.15 | 2.34 | 1.63 |
| Nd | 0.61 | 0.58 | 0.55 | 1.52 | 1.06 |
| Sm | 0.23 | 0.24 | 0.19 | 0.88 | 0.79 |
| Eu | 0.03 | 0.04 | N.D. | 0.01 | 4.52 |
| Gd | 0.27 | 0.27 | 0.15 | 0.49 | 0.60 |
| Tb | 0.05 | 0.06 | 0.03 | 0.29 | 0.41 |
| Dy | 0.41 | 0.42 | 0.18 | 0.23 | 0.41 |
| Ho | 0.08 | 0.09 | 0.03 | 0.14 | 0.33 |
| Er | 0.27 | 0.27 | 0.11 | 0.13 | 0.33 |
| Tm | 0.04 | 0.05 | 0.03 | 0.27 | 0.37 |
| Yb | 0.38 | 0.39 | 0.18 | 0.09 | 0.37 |
| Lu | 0.06 | 0.06 | 0.02 | N.D. | 0.22 |

Symbols: Tur: tourmaline, Kfs: K-feldspar, N.D.: not detected.

therefore, not discussed further. No inclusions could readily be related to growth features in quartz using plane transmitted light, hence they are considered to be pseudosecondary and secondary (Roedder 1984, Goldstein & Reynolds 1994). Inclusions are mostly concentrated along healed fracture planes aligned orthogonally to each other or at the intersections of such planes (Fig. 15a). These inclusions have variable L:V ratios and shapes, suggestive of necking, but FIAs with consistent L:V ratios do occur (Figs. 15a, b). Between the healed fracture planes are areas of isolated, larger fluid inclusions (*i.e.,* ≤60–80 μm) of irregular shape, with a halo of smaller (≤5–10 μm), equant or regularly shaped inclusions. These large inclusions may or may not have a subparallel alignment (*e.g.,* Fig. 15c *versus* 15d). In addition, similar inclusions along healed fracture planes are clearly of secondary origin (Figs. 15g, h). Planes decorated with these irregularly shaped inclusions cut planes containing equant inclusions. These irregular inclusions are have a stellate or three-prong radial shape in their most irregular form and resemble decrepitated inclusions observed in experimental studies (Sterner & Bodnar 1989, Vityk & Bodnar 1995) and in metamorphic rocks (Sisson & Hollister 1990, Boullier *et al.* 1991, 1997). Such inclusion textures are interpreted to form as a result of rapid changes in pressure, in this case, of fluid overpressuring (*i.e.,* $P_{internal} < P_{confining}$). The inclusion shapes are also similar to those produced in isobaric cooling experiments [see Fig. 6 of Vityk & Bodnar

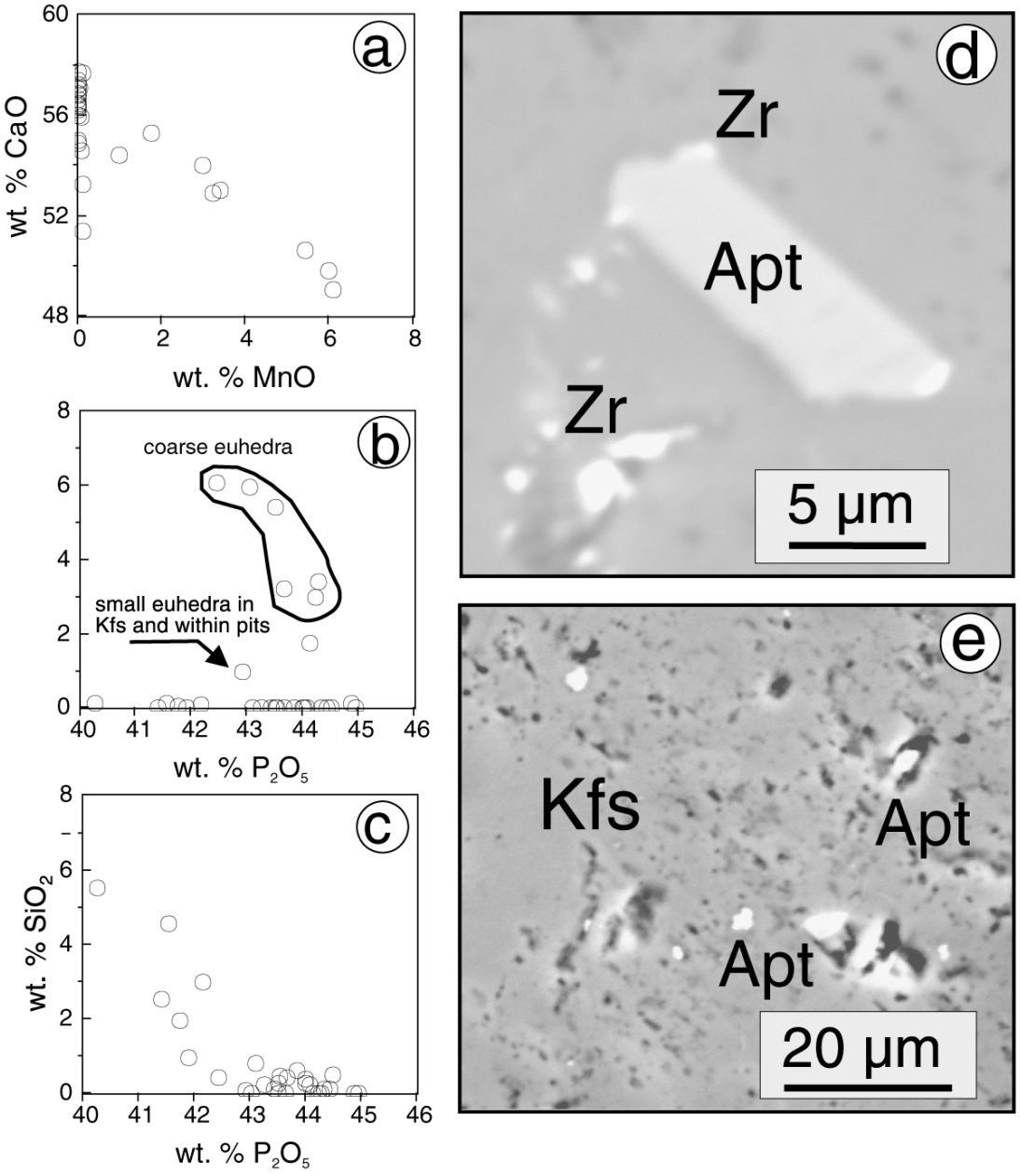


FIG. 11. Binary element plots for hydroxylapatite in aplite and pegmatite, along with back-scattered and secondary electron images. Note the two groups of compositions based on the amount of Mn, as discussed in the text. (a) Wt.% CaO *versus* wt.% MnO; (b) wt.% MnO *versus* wt.% $P_2O_5$. Circled data pertain to coarse, isolated, euhedral grains of hydroxylapatite. (c) Wt.% $SiO_2$ *versus* wt.% $P_2O_5$. (d, e) Back-scattered electron images showing the nature of hydroxylapatite hosted by K-feldspar. Note the presence of zircon (Zr) adjacent the hydroxylapatite (Apt) and the pitted nature of the K-feldspar (Kfs) with inclusions of hydroxylapatite.

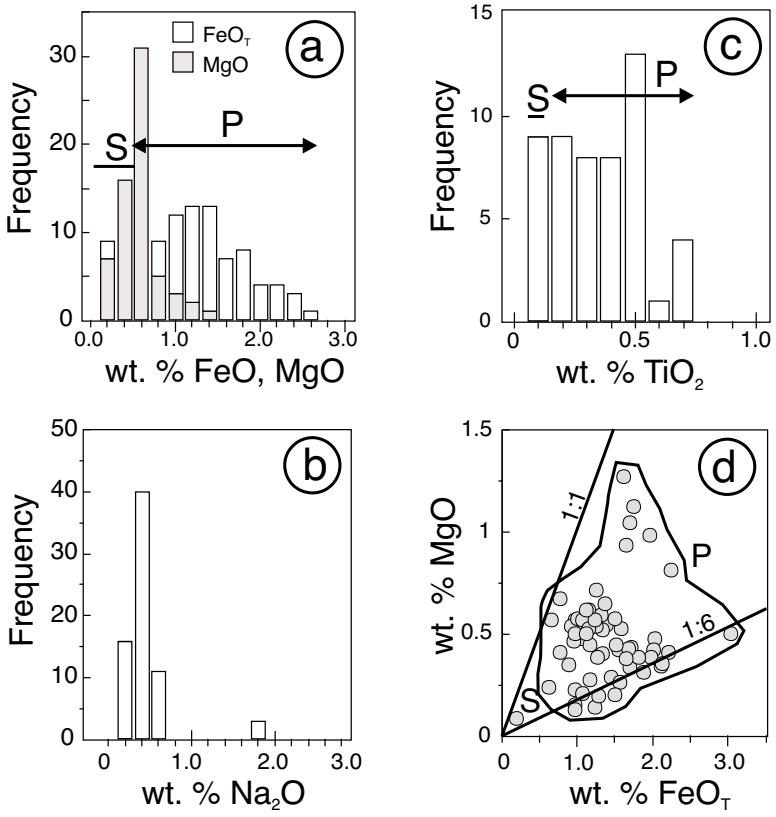


FIG. 12. Composition (wt. %) of muscovite in aplite and pegmatite summarized in histogram and binary element plots: (a) FeO and MgO, (b) $Na_2O$, (c) $TiO_2$, and (d) MgO *versus* FeO. The compositional ranges of primary (P) and secondary (S) grains are noted.

(1995)] and similar to those seen in vein and pegmatitic quartz of the eastern SMB (Carruzzo *et al*. 2001).

Inclusions or areas of FIA are classified into the following types at room temperature (*ca*. 25°C): (1) two-phase liquid–vapor (L–V) type of regular, equant or negative shape to more irregular shape (Figs. 15b, c) of ≤5–20 μm, but attaining 40–60 μm. The L:V ratio of these inclusions is consistent within a population, but varies among populations, thus indicating fluid entrapment over a range of PT conditions. Type-1 inclusions dominate samples and occur as isolated groups, or along healed fracture planes. In the latter case, extensive necking may characterize such areas. Thermometric analyses indicate that type-1 inclusions can be subdivided into aqueous (type-1a) and carbonic (type-1b) types; they are not uniformly distributed among samples. (2) Three-phase L–V–Halite inclusions of ≤10–20 μm. These are rare and occur along healed fracture planes as equant to elongate inclusions and coexist with type-1 inclusions, indicating therefore only a slight difference in their bulk composition. (3) V-rich inclusions of equant or negative shape are ≤20 μm, and occur along healed fractures. These inclusions, which are exceptionally rare, are not observed to coexist with either type-1 or -2 inclusions, and there is no evidence to suggest that they owe their origin to post-entrapment changes. This type of V-rich inclusion is not to be confused with V-rich inclusions having a large range in L:V ratio and whose origin relates to necking. (4) Multi-solid–L–V inclusions of irregular shape and ≤30–50 μm occur with L:V type inclusions. The solids are of variable shape and birefringence and may be micas and feldspar trapped accidentally during crystallization and alteration within the pegmatite (?). (5) Monophase L-rich inclusions of equant shape decorate planes and record post-entrapment necking. Finally, (6) the decrepitated inclusions described above consist of a central, V-rich inclusion of irregular shape that is surrounded by smaller, two-phase L–V inclusions (Figs. 15e, f).

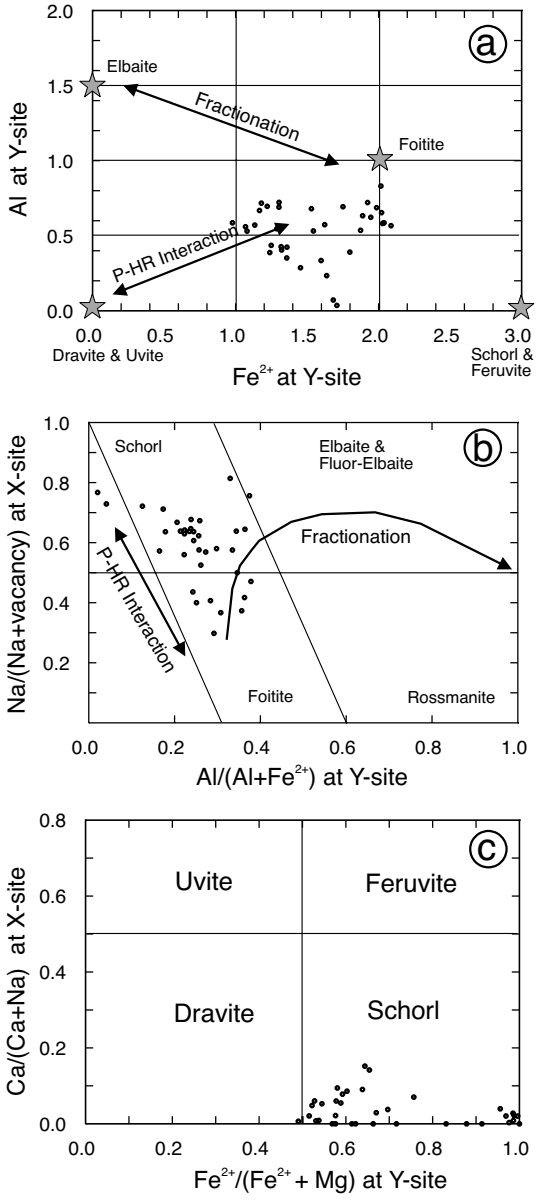


FIG. 13. Composition of tourmaline in aplite and pegmatite in binary plots [atoms per formula unit based on structural formula with 31 anions (O, OH, F)]. The plots are after Tindle *et al*. (2002), and the classification scheme follows that of Hawthorne & Henry (1999) and Selway & Novák (1997). The lines designated P–HR (pegmatite – host rock) Interaction and Fractionation are from Tindle *et al.* (2002) and are based on interpretation of a database for evolved tourmaline-bearing pegmatites.

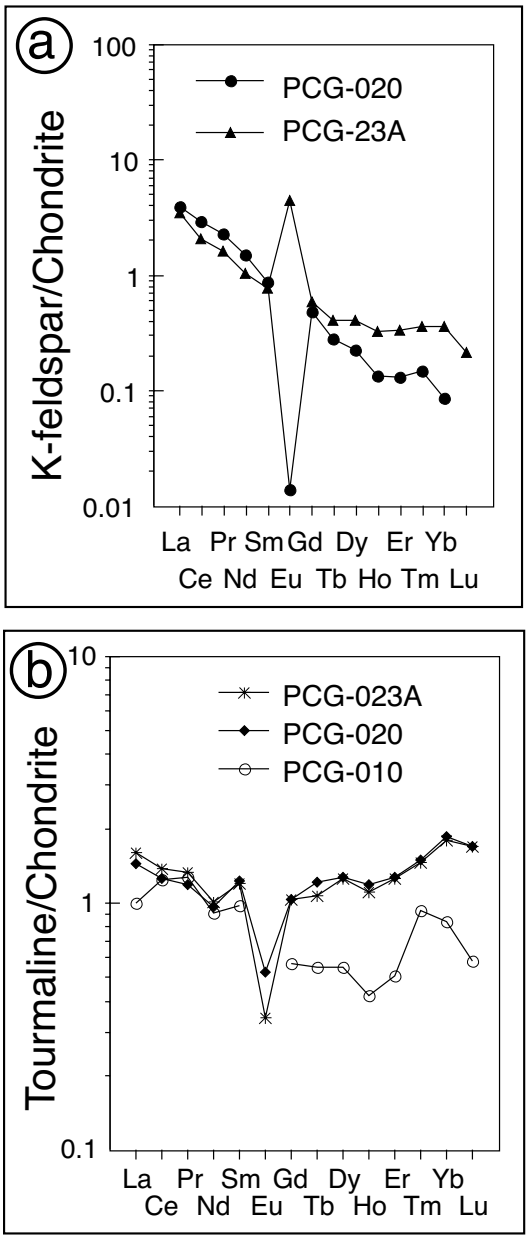


FIG. 14. Chondrite-normalized (chondrite values of Masuda *et al*. 1973) rare-earth element plots for K-feldspar (a) and tourmaline (b) mineral separates from aplite and pegmatites: PCG–010: tourmaline – muscovite – K-feldspar pocket in layered aplite–pegmatite sheet, PCG–020: quartz – K-feldspar – muscovite pocket and tourmaline pocket in layered aplite with line-rock texture, PCG–023A: coarse quartz – K-feldspar pocket in coarse pegmatite in tourmaline-bearing aplite sheet.

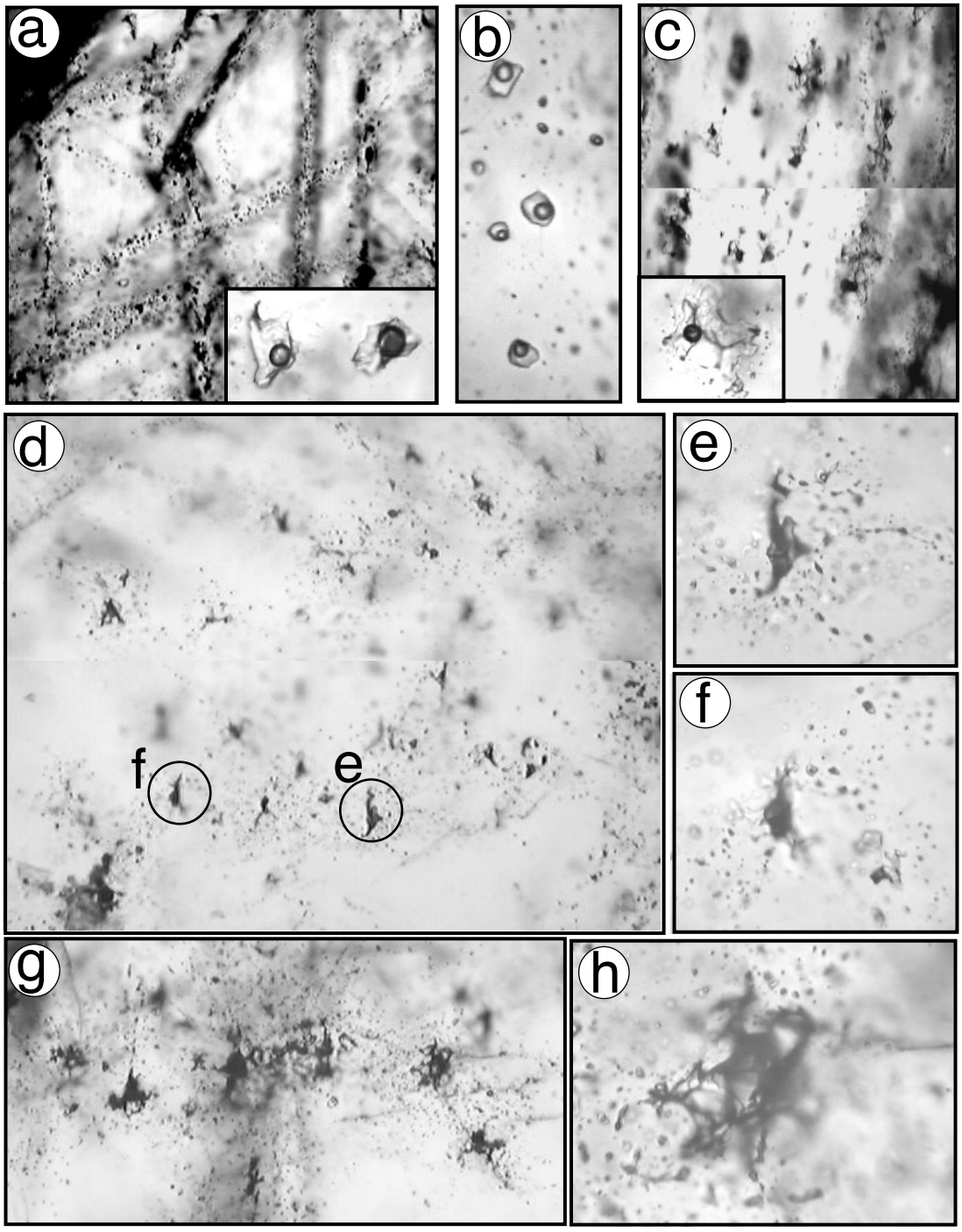


FIG. 15. Photomicrographs of quartz-hosted fluid inclusions in pegmatite. (a) Abundant fluid inclusions along steeply dipping healed fracture-planes. Note the orthogonal orientation of the fracture planes. Width of photo *ca.* 1 mm. Inset shows typical large (50 μm) aqueous L–V inclusions that occur between the fracture planes. (b) Planar array of negatively shaped aqueous–carbonic fluid inclusions (20–30 μm) of uniform L:V ratio in quartz. (c) Array of irregular fluid inclusions with partially

*Thermometric measurements*

Thermometric measurements (Fig. 16) indicate that two broad groups of fluids, these being aqueous and carbonic types. The aqueous inclusions represent variable mixtures of $H_2O$–NaCl–$CaCl_2$ based on their temperature of first melting (Fig. 16a; Crawford 1981) and hydrohalite–ice melting relationships are subdivided into three groups (I, II, III; Fig. 17). Ice melting in the aqueous inclusions occurred at –35 to 0°C, with the majority in the –10 to –25°C range. The carbonic inclusions display triple-freezing behavior during cooling runs (Roedder 1984), and the $CO_2$ component melts at –56.6 ± 0.3°C, indicating essentially pure $CO_2$, and $CO_2$–clathrate melting occurred between +8° and +9.5°C. Homogenization of the $CO_2$ phase to V occurred between +21° and +23°C, but the variation within a FIA is ±0.2°C.

Inclusions homogenized to the liquid phase over a temperature range of 140° to 400°C (Fig. 16b), but the range within a FIA is ≤5°C. There are significant differences among samples with, for example, PCG–21A having a much lower (160–200°C) and smaller range in $T_h$ values than in other samples, whereas in PCG–2000–3 the carbonic inclusions have higher $T_h$ values than aqueous inclusions. For the aqueous inclusions, the $T_h$ data for the different groups in Figure 17 (I, II, III) cover the same broad range. Although not shown in Figure 16, note that some carbonic inclusions homogenized to the V phase in the 374–380°C range. The few halite-bearing fluid inclusions homogenized by halite dissolution at 130° to 133°C ($n = 5$), with final homogenization of the inclusions (to liquid) at 183°C. In the decrepitated inclusions, the small equant inclusions around the central irregular inclusion have $T_h$ values of 350–360°C.

*Fluid composition* (*salinities*)

For aqueous inclusions of groups II and III, the ternary system $H_2O$–$CaCl_2$–NaCl (Vanko *et al*. 1988) or equivalent table (Goldstein & Reynolds 1994) was used to estimate salinity, whereas for group-I inclusions, the temperature of ice melting was used; for halite-bearing inclusions, the temperature of halite dissolution was used (Bodnar & Vityk 1994). For carbonic inclusions, salinities were determined using the temperature of clathrate melting (Collins 1979). Fluid salinities (Fig. 16c) are generally 20–25 wt.% eq. NaCl, and in fluids II and III the ratio $CaCl_2/(CaCl_2 + NaCl)$ exceeds 0.5. The highest salinity measured (29 wt.% eq. NaCl, sample PCG–22) pertains to a halite-bearing inclusion, whereas the lowest (1–6 wt.% equiv. NaCl) pertains to a small number of aqueous inclusions. The salinity of carbonic inclusions is ≤5 wt.% eq. NaCl.

*Salinity versus homogenization temperature*

Two trends are distinguished in a $T_h$ *versus* salinity plot (Fig. 18), with both involving decreasing temperature, but with different salinities. Trend 1 consists of highly saline fluids, including both Ca- and Na-rich types (*i.e.,* groups I, II, III), which record a decrease in $T_h$ values with little apparent change in their salinity. The second trend is not as well defined, but there clearly is a group of inclusions that record progressively lower salinities with a corresponding decrease in $T_h$ values. For trend 2, there are no data for sample PCG–21A, which may be an artifact of data collection. The carbonic inclusions would occupy a separate area in Figure 18, with salinities ≤5 wt.% eq. NaCl and $T_h$ values of 300–380°C.

*Compositions of decrepitate mounds*

A semiquantitative determination of fluid composition was assessed using decrepitate mounds (*cf.* Haynes *et al*. 1988). The only cations detected were K, Na and Ca, although the suite of elements sought included Al, Fe, Mg, Mn, Ba, Sr, P and S. The data are summarized in Ca–Na–K plots (Fig. 19). All inclusions contain Cl, but a few Ca-rich mounds also contain S.

The decrepitate data indicate that three fluid compositions are present: (i) a K–Na fluid with K/(K + Na) in the range 0.2 to 0.92, with minor Ca (maximum 15–20%), (ii) a Na–Ca fluid with Na/(Na + Ca) in the range 1 to 0.4, with minor K (≤10%), and (iii) a Ca-rich fluid with minor Na or K (≤10%). The three fluids correspond in general to groups I, II, III defined from the hydrohalite–ice melting (Fig. 17). Additional points regarding these data are: (1) the limited exchange of the K–Na fluid with the Ca-rich fluid, (2) the difference in solute composition recorded for the two samples analyzed, with each sample only recording two of the three types of fluid, (3) the marked chemical distinction between the Na- and Ca-rich mounds, and (4) deficiency

decrepitated textures defining a preferential alignment of their long dimensions. Width of photo: 300 μm. Inset figure shows an enlargement of a representative fluid inclusion (40 μm) from this assemblage. (d, e, f) Assemblage of irregular, decrepitated inclusions randomly distributed within quartz. These inclusions are candidates for a primary origin. Note the stellate shapes and halo of smaller aqueous L–V inclusions about the central, V-rich inclusion. The circled inclusions enlarged in Figures 15e and 15f are *ca.* 60–80 μm in longest dimension. Width of photo in (d) is 0.8 mm. (g, h). Irregularly shaped, naturally decrepitated fluid inclusions along a healed fracture-plane. Width of photo: 0.8 mm. Note the halo of smaller aqueous L–V inclusions about the large central inclusion. One of the large decrepitated inclusions enlarged in Figure 15h is 60 μm wide.

of the Ca-rich mounds in Cl compared to the Na-rich mounds.

The results of the decrepitate mounds are very similar to results derived for quartz-hosted inclusions from mineralized quartz veins and pegmatites from the New Ross pluton within the central SMB [Fig. 1b of Carruzzo *et al*. (2001)]. Thus the data are not unique to this part of the SMB. However, the data contrast markedly with decrepitate data for inclusions in mineralized pegmatites, greisens and quartz veins at the East Kemptville tin deposit (Kontak *et al*. 2001), which are characterized by elevated Fe, Mn, Sr and Ba, in addition to Na, K and Ca.

## Stable Isotopes

Stable isotope data for whole-rock samples and mineral separates are summarized in Table 6. Whole-rock

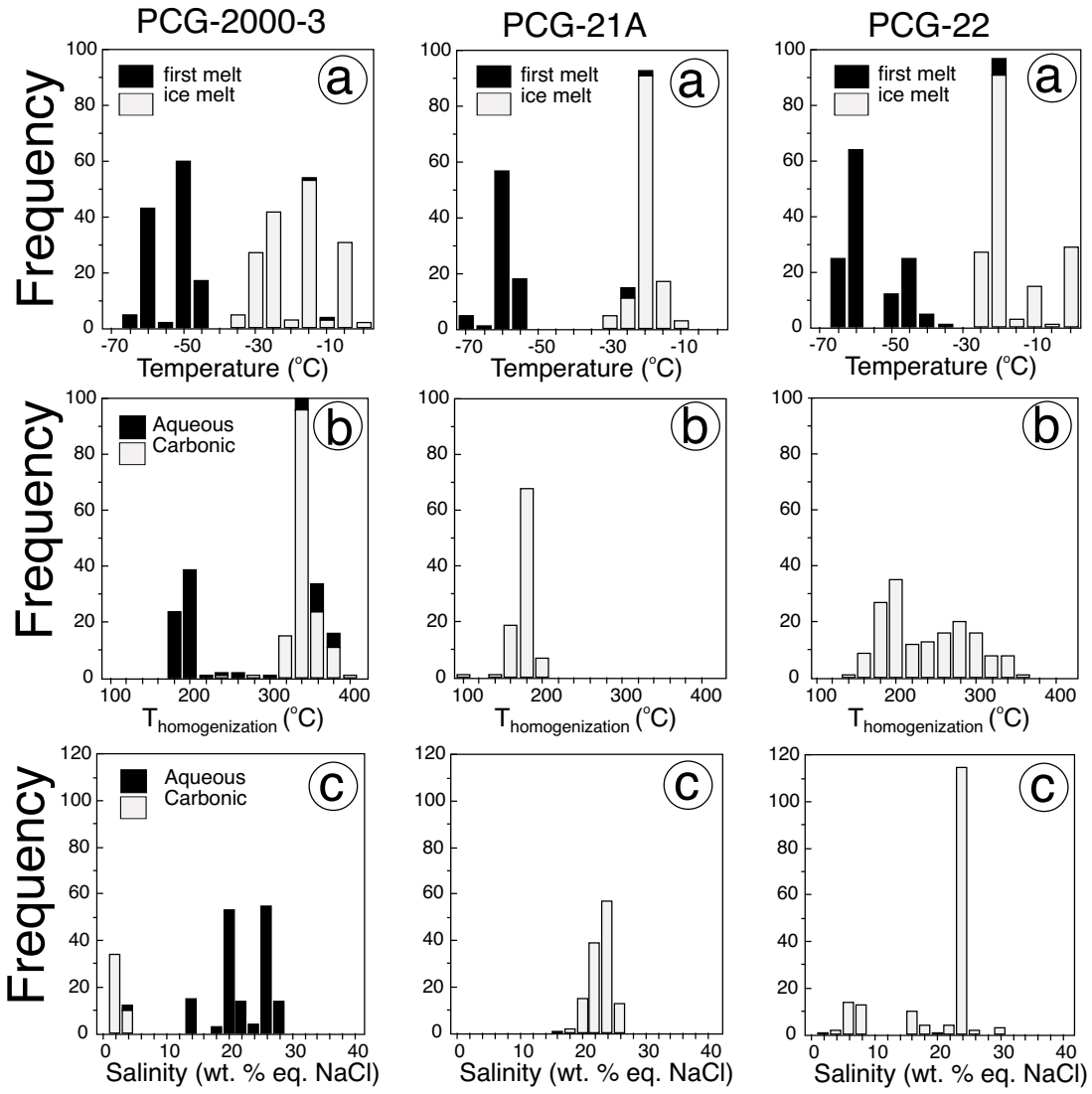


FIG. 16. Thermometric and salinity data for fluid inclusions hosted by quartz of pegmatite arranged by sample. (a) Plots of first melting or inferred eutectic temperatures and ice-melting temperatures. (b) Plots of homogenization temperatures. Note that for sample PCG–2000–3, data for aqueous and carbonic inclusions are plotted separately. (c) Plots of salinity as wt.% equivalent NaCl.

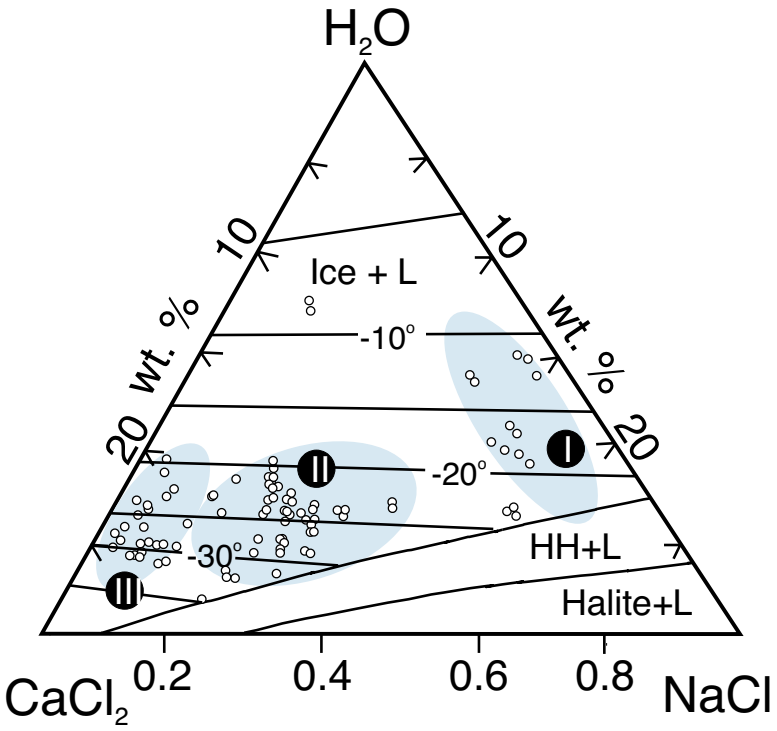


FIG. 17. Partial phase diagram for the ternary system $H_2O$–NaCl–$CaCl_2$ (after Vanko *et al.* 1988) showing the bulk compositions for $L_{H2O}$–V aqueous fluid inclusions hosted by quartz in pegmatite. The data plotted are for aqueous L–V inclusions in which both hydrohalite (HH) and ice melting were determined. Note that the data are subdivided into three groupings (I, II, III) corresponding to different bulk-compositions (in wt.%), as discussed in the text. Note that for group I, there are many more data present than shown, but they plot along the $H_2O$–NaCl join, where hydrohalite melts at the eutectic (*i.e.*, –21.8°C).

$\delta^{18}O$ data for aplite and aplitic parts of layered pegmatite range from +11.7 to +14.7‰ with a mean of +12.7‰ ($n$ = 7), but a single sample is well outside the mean of the others at +14.7‰. Compared to a $\delta^{18}O$ compilation of data for the SMB (Fig. 20), the Peggys Cove samples are enriched in $^{18}O$ and, excluding the most $^{18}O$-enriched sample, overlap best the range for metasedimentary rocks of the Meguma Group.

The $\delta^{18}O$ and $\delta D$ mineral data for the pegmatites include analyses of quartz, K-feldspar, muscovite and tourmaline, and complement data for pegmatites in the SMB presented by Kontak *et al*. (1991). The measured $\delta^{18}O$ values for these pegmatite minerals are: (1) +10.5 to +12.5‰ for quartz ($n$ = 7), (2) +10.3 to +11.9‰ for K-feldspar ($n$ = 5), (3) +8.4 to +8.9‰ for muscovite ($n$ = 3), and (4) +9.4 to +9.7‰ for tourmaline ($n$ = 3). These $\delta^{18}O$ values compare the following measurements on pegmatites from the eastern part of the SMB (from Kontak *et al*. 1991): quartz = +8.9 to +17.6‰ ($n$ = 20), K-feldspar = +8.9 to +12.3‰ ($n$ = 15), muscovite = +8.2 to +9.3‰ ($n$ = 3) and tourmaline = +10.4‰.

The fractionation of $^{18}O$ among coexisting minerals (*i.e.,* $\Delta_{quartz–mineral}$) is temperature-dependent; thus temperatures for coexisting minerals are calculated using the appropriate fractionation-factors (Table 7). For the ten mineral pairs analyzed, calculated temperatures range from 650° to 350°C ($n$ = 5 pairs), and several record isotopic disequilibrium (*e.g.,* ($\Delta_{quartz–mineral} \leq 0$), which result in unrealistic temperatures. Thus the data record equilibrium at magmatic conditions at *ca.* 650°C to later subsolidus re-equilibration to 350°C, and also indicate some disequilibrium among minerals.

The $\delta D$ values determined for muscovite and tourmaline (Table 6) fall in narrow ranges of –69 to –77‰ ($n$ = 4) and –51 to –66‰ ($n$ = 3), respectively. There are no $\delta D$ values for the eastern part of the SMB at present, but Kontak *et al*. (2001) reported $\delta D$ values of –30 and –51‰ for muscovite in pegmatite from the East

Kemptville deposit in the westernmost part of the SMB (Fig. 1).

## Discussion

### *$^{40}Ar/^{39}Ar$ dating*

The results of $^{40}Ar/^{39}Ar$ dating of muscovite indicate identical ages of *ca.* 371 Ma, which are similar to previous Ar/Ar (mica) and U/Pb (zircon, monazite) ages for both the SMB and satellite intrusions in the Meguma Terrane (Clarke *et al.* 1997). Thus, the aplite–pegmatite sheets are both co-spatial and co-temporal with the SMB. Combining the age data with the blocking temperatures for the geochronometers implies rapid post-crystallization cooling of the area to below *ca.* 350°C (McDougall & Harrison 1988). Thus, the age dates indicate that the origin of the aplite–pegmatite sheets is temporally linked to the evolution of the SMB. In addition, we emphasize that the low-temperature gas fraction of the age plateaus lack any discordance. There is, therefore, no evidence to suggest that a subsequent thermal disturbance of ≥300–350°C has affected the area.

### *Al–Si order in K-feldspar*

The Al–Si order in K-feldspar reflects the interplay of various factors, including cooling rate, fluid interaction and strain [see Martin (1974) and Brown & Parsons (1989) for reviews]. At Peggys Cove, there is a large range in the degree of Al–Si order over short distances (*i.e.,* m-scale), suggesting variable conditions. Given that lack of evidence for alteration and proximity of samples studied, variations in degree of fluid interaction and in cooling rate are considered unlikely reasons for the heterogeneous degree of order (*e.g.,* Martin 1974, Cherry & Trembath 1978, Neves & Godinho 1999). However, petrographic observations reveal a heterogeneous distribution of strain, which may account for the highly random occurrence of the K-feldspar polymorphs. This interpretation is consistent with: (1) the presence of tourmaline fibers within the pegmatites (Fig. 5g), (2) the presence of highly ordered triclinic K-

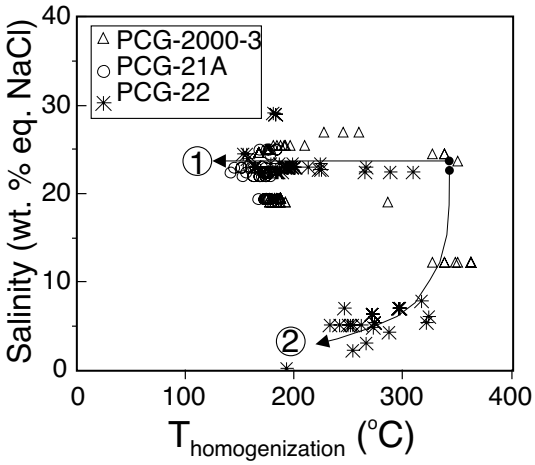


FIG. 18. Plot of salinity *versus* homogenization temperature (°C) for aqueous inclusions in quartz of the pegmatites. The significance of trends 1 and 2 is discussed in the text.

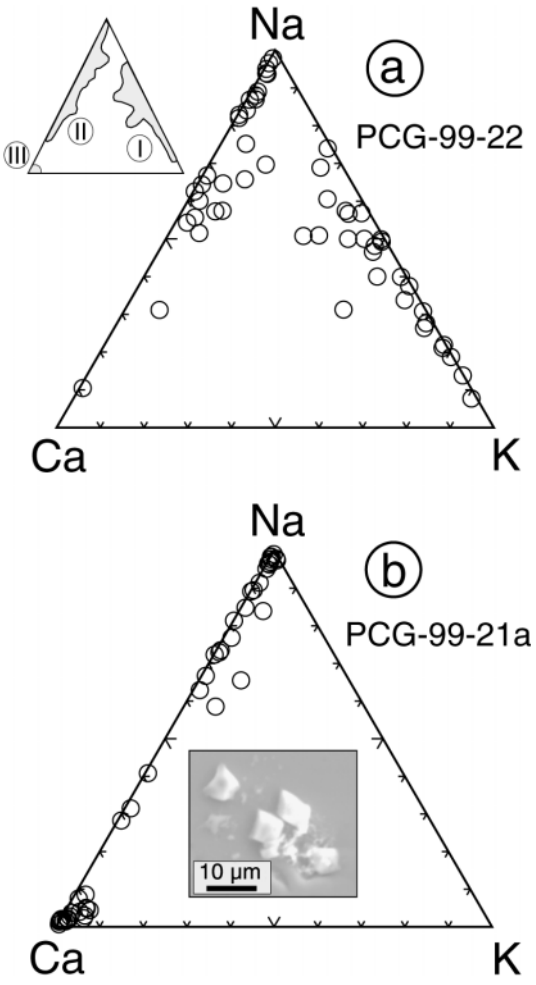


FIG. 19. (a, b) Plots (in wt.%) of Ca–Na–K for decrepitate mounds in quartz in pegmatites. The significance of the three groups (I, II, III) distinguished in the plot is discussed in the text. The inset figure in lower plot is a combined secondary electron and back-scattered electron image of a NaCl-rich decrepitate mound typical of fluid II.

feldspar in the deformed granite at East Kemptville within the SMB (Kontak *et al.* 1996), (3) the presence of decrepitated fluid inclusions that probably record changing fluid pressure (see below), and (4) the suggestions of several investigators that the SMB is a late syntectonic intrusion (*e.g.,* Horne *et al.* 1992, Benn *et al.* 1997, 1999).

*Petrographic features of the aplite–pegmatite sheets*

The aplite–pegmatite sheets have a simple mineralogy, dominated by quartz and feldspar with minor muscovite and trace cordierite, with pockets of quartz, tourmaline and muscovite. These observations, combined with the presence in thin section of idiomorphic textures and film perthite, are consistent with a magmatic origin for the rocks. The minor amount of muscovite, rarity of miarolitic cavities, and late-stage development of pocket zones containing tourmaline, all suggest that the melts were $H_2O$-undersaturated for most of their crystallization history, a feature typical of pegmatites (London 1992a) and other layered aplite–pegmatites (*e.g.,* Webber *et al*. 1999), and that they evolved toward a common end-product, this being a Si- and B-rich metaluminous melt.

The presence of coarse, oriented K-feldspar at wallrock contacts and a consistent tripartite internal division (Figs. 5c, d), which is similar to classic suites of zoned pegmatites (*e.g.,* San Diego County), indicate a single dilational event with minimal shearing during crystallization. The presence of delicate, fine-scale linerock in the bottom half of zoned sheets also attests to the quiescence of the environment, with subtle changes in chemical and physical conditions and mass transfer relating to the origin of the texture (Stern *et al.* 1986, Webber *et al.* 1997, 1999).

The presence of euhedral cordierite in pegmatites is well documented within the SMB (Maillet & Clark 1985, MacDonald *et al.* 1992), thus its occurrence at Peggys Cove is expected and consistent with the peraluminous nature of the melts (*i.e.,* 1.09 < A/CNK < 1.2). As suggested by Clarke (1995), the occurrence of cordierite in granitic pegmatite probably reflects the reaction:

$$L \rightarrow \text{Na–K aqueous fluid} + \text{Crd} \qquad (1).$$

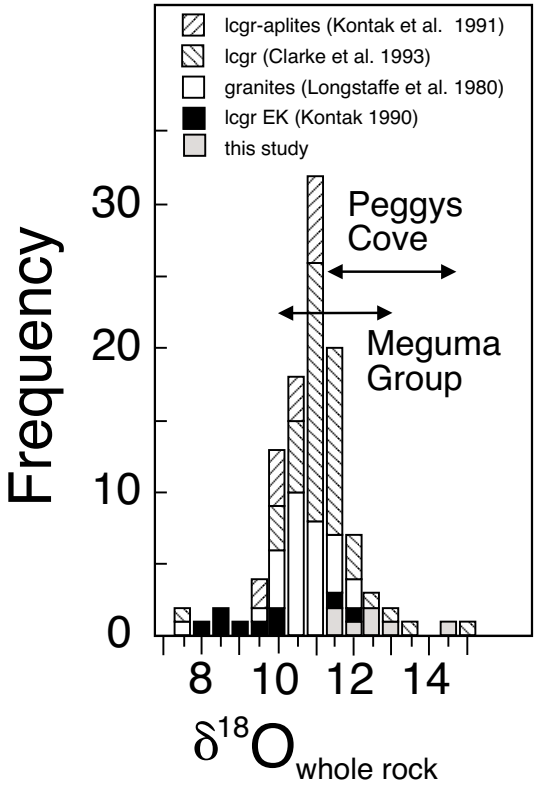


FIG. 20. Summary of whole-rock $\delta^{18}O$ data for the South Mountain Batholith. Lcgr refers to leucogranite samples. The range of values for the Meguma Group metasedimentary rocks is from Longstaffe *et al.* (1980). Note that the majority of the data for the SMB fall in the range +10 to +12‰ and that samples from Peggys Cove plot to heavier values. Data plotted are: (1) leucogranites and aplites associated with pegmatites in the east-central SMB ($10.7 \pm 0.6$‰, $n = 15$; Kontak *et al.* 1991); (2) leucogranites of the eastern part of the SMB ($11.3 \pm 1.0$‰, $n = 47$; Clarke *et al*. 1993); (3) granites (*sensu lato*) of the SMB ($11 \pm 1.0$, $n = 30$; Longstaffe *et al.* 1980), and (4) the East Kemptville leucogranite ($8.9 \pm 0.7$‰ , $n = 8$; Kontak 1990).

TABLE 6. STABLE ISOTOPE DATA FOR PEGGYS COVE PEGMATITES, NOVA SCOTIA

| Sample | Mineral/Rock | $\delta^{18}O$(‰) | $\delta D$(‰) |
|---|---|---|---|
| PCG–99–04 | tourmaline | 9.4 | –72.0 |
| PCG–99–05 | muscovite | 8.9 | –52,–49 |
| PCG–99–06 | quartz | 10.5 | – |
| PCG–99–06 | tourmaline | 9.6 | –76.0 |
| PCG–99–010 | quartz | 12.3 | – |
| PCG–99–010 | K-feldspar | 11.1 | – |
| PCG–99–010 | tourmaline | 9.7 | –77.0 |
| PCG–99–011 | quartz | 12.4 | – |
| PCG–99–011 | feldspar | 11.5 | – |
| PCG–99–011 | muscovite | 8.6 | –64.0 |
| PCG–99–020 | quartz | 12.5 | – |
| PCG–99–020 | K-feldspar | 10.3 | – |
| PCG–99–016J | quartz | 11.1 | – |
| PCG–99–016J | muscovite | 8.4 | –66.0 |
| PCG–99–022 | quartz | 10.5 | – |
| PCG–99–022 | K-feldspar | 11.9 | – |
| PCG–99–023A | quartz | 10.9 | – |
| PCG–99–023A | K-feldspar | 10.9 | – |
| PCG–99–023B | tourmaline | 9.0 | –68.0 |
| PCG–99–03A | whole rock | 11.9 | – |
| PCG–99–012 | whole rock | 12.8 | – |
| PCG–99–016B | whole rock | 13.0 | – |
| PCG–99–016D | whole rock | 11.7 | – |
| PCG–99–016I | whole rock | 12.3 | – |
| PCG–99–016K | whole rock | 12.7 | – |
| PCG–99–017A | whole rock | 14.7 | – |

Diffusive loss of alkalis increases the peraluminosity index (A/CNK), thereby favoring cordierite formation. The rarity of cordierite in line rock and local pegmatite pockets, although consistent with this model, suggests that either egress of an alkali fluid was uncommon or that the bulk composition (*i.e.,* deficiency in Fe and Mg) was not conducive to cordierite formation.

The heterogeneous development of strained quartz and mottled K-feldspar with local grid twinning reflects heterogeneous strain partitioning within the rocks. These features are considered to have occurred during post-crystallization cooling of the area rather than during some later event, as evidence for a subsequent thermal event is not supported by the Ar–Ar dating. The distinct orientation of the healed fracture planes decorated with fluid inclusions (Fig. 15a) also records the presence of an ambient stress-regime during pegmatite formation.

### *Whole-rock composition*

Uniform whole-rock composition for the aplites and the compositions near the minimum in the system Qtz–Ab–Or indicate a magmatic origin. There was clearly insufficient B in the melt to affect the location of the cotectic. However, the enrichment of tourmaline in pockets and locally within banded aplite–leucogranite suggests that B locally may have influenced the late-stage evolution of the melt. However, in general a limited amount of fractional crystallization is inferred from: (1) a restricted range in composition of the aplites and abundance of most granophile and lithophile elements (*e.g.,* Rb, Li, Sn, Nb, and Ta), and values of petrologically meaningful elemental ratios (*e.g.,* K/Rb, Fig. 7b), (2) depletion in Ca, Mg and Ti, which is reflected in rarity of biotite and lack of calcic plagioclase, and (3) uniformity of the whole-rock *REE* data, both in terms of abundances and patterns, and only moderate negative Eu anomaly, which contrasts with much more depleted signatures seen in more chemically evolved rocks of the SMB (Dostal & Chatterjee 1995, Kontak *et al.* 2001).

The only apparent elemental enrichment occurs within muscovite–tourmaline pods, where there are relatively elevated concentrations of V, Cr, Co, Zr, Ba and Sr . There are several possible explanations for this enrichment: (1) enrichment of V, Cr and Ba in white mica is not unusual, and thus a crystal-chemical control is plausible. In this case, there is an inference that the melt also was enriched in these elements. (2) The presence of secondary phases within the tourmaline, such as Ba-enriched K-feldspar and an unidentified Ca–Sr–Ba–$SO_4$ phase, reflects the influence of these mineral phases on whole-rock composition. (3) The presence of secondary hydroxylapatite and zircon occluding pits in K-feldspar (Figs. 11d, e) suggests some hydrothermal mobilization of elements. Certainly Zr enrichment in the muscovite–tourmaline pods may relate to such mobility, and the general enrichment of Sr in apatite would also explain the elevated Sr contents. The muscovite–tourmaline pods represent areas of continued subsolidus equilibration and fluid-mediated mobility of elements. This late mobilization may relate to a late buildup of $H_2O$ in the latest melts due to the capacity of B to depresses the solidus and enhance $H_2O$ solubility (*e.g.,* Manning & Pichavant 1988).

In terms of the *REE* data, the Peggys Cove aplites are less depleted in the *HREE* and are much less fractionated [*i.e.,* lower $(La/Lu)_N$ values] compared to data for the SMB as a whole (Fig. 8b). Thus, it appears that a simple fractional crystallization model cannot account for the *REE* patterns of the aplites as derivatives of granites of the SMB.

TABLE 7. FRACTIONATION FACTORS AND CALCULATED TEMPERATURES FOR MINERAL PAIRS, PEGGYS COVE PEGMATITE, NOVA SCOTIA

| Sample | Mineral pair | Δ | T (°C) | Reference |
|---|---|---|---|---|
| PCG–99–06 | Qtz–Tur | 0.9 | >700°C | Zheng (1993b) |
| PCG–99–010 | Qtz–Tur | 2.6 | 500°C | Zheng (1993b) |
| | Qtz–Kfs | 1.2 | 650°C | Zheng (1993a) |
| PCG–99–011 | Qtz–Kfs | 0.9 | >700°C | Zheng (1993a) |
| | Qtz–Ms | 3.8 | 450°C | Bottinga & Javoy (1975) |
| PCG–99–020 | Qtz–Kfs | 2.2 | 350°C | Zheng (1993b) |
| PCG99–016J | Qtz–Ms | 2.7 | 550°C | Zheng (1993b) |
| PCG–99–022 | Qtz–Kfs | –1.4 | ND | Zheng (1993b) |
| PCG–99–023A | Qtz–Kfs | 0.0 | ND | Zheng (1993b) |
| PCG–99–023A,B | Qtz–Tur | 1.9 | 600°C | Zheng (1993b) |

Abbreviations after Kretz (1983); Δ: mineral fractionation, ND: not determined.

### *Mineral compositions*

The mineral compositions, interpreted also in the context of textures, indicates that the phases analyzed reflect growth or equilibration under conditions that varied from magmatic through to hydrothermal.

The composition of muscovite compares to that for the SMB (Ham & Kontak 1988) and the larger dataset of muscovite compositions for granitic rocks compiled by Miller *et al.* (1981) and Zane & Rizzo (1999). The composition of our muscovite compares to that from granitic rocks in general and, more specifically, suites of pegmatites and aplites as compiled by Zane & Rizzo (1999). In this study, the limited chemical variation is consistent with the apparent primary texture of the muscovite. It is not surprising, therefore, that in the $\Sigma$Al–Si–$M^{2+}$ diagram of Monier & Robert (1986; Fig. 21), the data plot in a tight cluster and indicate equilibration at *ca.* 600°C. The secondary muscovite has a distinct composition, as noted above.

The textures and composition of K-feldspar reflect a progression from high-temperature magmatic conditions to lower-temperature equilibration. The preservation of film perthite in isolated domains (Fig. 9a) and bulk compositions of such areas (Fig. 9b) attest to a magmatic origin. In contrast, the development of flame and bead perthites cross-cutting film perthite reflects fluid incursion (Brown & Parsons 1989). Based on EMPA point analyses, the K-feldspar reacted with the fluid down to *ca.* 300°C. The role of a fluid phase is also reflected by the pitted textures (Fig. 11e; Worden *et al.* 1990, Teertstra *et al.* 1999) and associated formation of secondary hydroxylapatite and zircon.

The phosphorus content of feldspars in peraluminous granites is a good monitor of degree of fractionation (*e.g.,* London *et al*. 1990, London 1992b), and the SMB is no exception. Kontak *et al.* (1996) have shown that there is a systematic increase of P in both K- and Na-rich feldspars toward more evolved compositions, consistent with the general increase of $P_2O_5$ in whole-rock samples (Ham *et al*. 1989). Thus, the values of ≤0.5 wt.% $P_2O_5$ in feldspar of the pegmatitic samples (Fig. 9d) contrast markedly with values of up to 1–2 wt. % $P_2O_5$ in feldspar from pegmatitic samples in the SMB (Kontak *et al*. 1996). Thus, the melt from which feldspar formed was not evolved relative to pegmatite-forming melts elsewhere in the SMB.

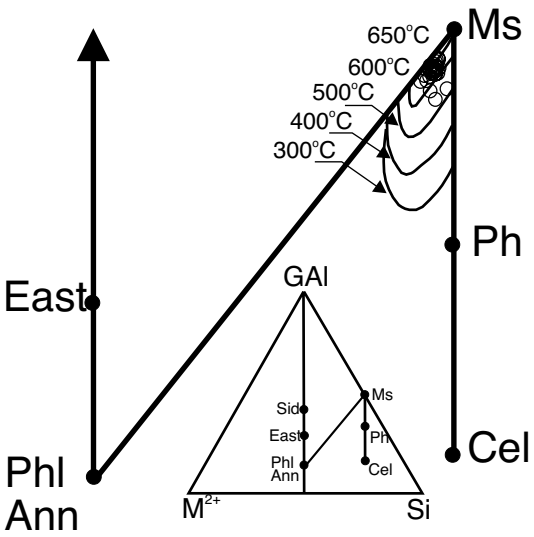


FIG. 21. Plot of muscovite compositions in the $M^{2+} - \Sigma Al - Si$ diagram of Monier & Robert (1986), with isotherms for temperatures of 650° to 350°C. Note that the muscovite data plot in a restricted field near the 650–600°C isotherms. Abbreviations are East: eastonite, Phl: phlogopite, Ann: annite, Cel: celadonite, Ph: phengite, Ms: muscovite.

In a manner similar to P, the trace-element contents (*e.g.,* Ba, Sr, Rb) and appropriate ratios (K/Rb, Rb/Sr) in K-feldspar are also good monitors of chemical fractionation (*e.g.*, Černý *et al.* 1985). Compared to the SMB (Kontak & Martin 1997), the K-feldspar in pegmatites has Rb (300–600 ppm), Pb (40–70 ppm), Rb/Sr (5–40) and K/Rb (150–300) values that are comparable to K-feldspar from granodiorite and monzogranite rather than pegmatites. However, the Ba contents deviate from this apparent trend and are markedly depleted (50–250 ppm) compared to values typical of K-feldspar from pegmatites from the eastern SMB. Given that the $K_D$ for Ba (Icenhower & London 1996) favors enrichment in K-feldspar of this bulk composition rather than the melt, these data imply that the primary melt and, by inference, the source, were deficient in Ba.

Tourmaline, dominantly schorl, is strongly zoned, and there is a consistent late-stage enrichment of Fe toward the margin of all grains, which reflects a late-stage internal evolution of the pegmatites. However, of more significance are the following points: (1) the tourmaline compositions are coincident with the metasedimentary field rather than granitic suites in the Al–Fe–Mg diagram of Henry & Guidotti (1985; not shown), and (2) the data show trends suggestive of contamination rather than fractionation (Fig. 13) on the basis of the chemical variation of tourmaline compositions for several evolved tourmaline-bearing pegmatites (Tindle *et al*. 2002). This suggestion of pegmatite – host-rock interaction, in this case melanocratic xenoliths of presumed metasedimentary origin (*i.e.,* Meguma Group), is consistent with the Mg-rich nature of the tourmaline compared to tourmaline in granitic pegmatites in general, as alluded to earlier.

The composition and morphology of the hydroxylapatite indicates an early magmatic stage given that it: (1) occurs within the matrix, (2) is characterized by a coarse, subhedral to euhedral habit, and (3) is adjacent feldspar grains that retain primary textural features. In contrast, the Mn-deficient hydroxylapatite, although of euhedral to subhedral shape, invariably occurs within pitted feldspar (Fig. 12e); in some cases, the Mn-deficient grains also occur as inclusions in some of these small cavities. Thus, the Mn-deficient hydroxylapatite is considered to reflect growth in a fluid-mediated environment during the subsolidus stage of pegmatite evolution, which probably involved release of P from feldspar. We do note that Mn deficiency of apatite-group minerals alone is not indicative of a secondary origin, as both Kontak (1991) and O'Reilly (1992) noted Mn enrichment (to 7 wt.% MnO) in secondary "apatite" within Meguma Zone granites.

Trace amounts of zircon were observed as micrometric grains adhering to or adjacent to euhedral hydroxylapatite (Fig. 12) and also within the pits. Thus, as already noted above, Zr was evidently mobile during or after the textural modification of the feldspar and formation of secondary hydroxylapatite.

*Stable isotope data*

The $\delta^{18}O$ whole-rock values are more strongly positive compared to the majority of $\delta^{18}O$ whole-rock data for the SMB (Fig. 20), and the absolute values suggest a process of enrichment by either crustal contamination *via* sediments or interaction with a $^{18}O$-enriched fluid. Petrographic observations of the aplites precludes extensive deuteric alteration and, hence, significant modification of their primary $\delta^{18}O$ values. This would indicate that contamination of the melt may have occurred at the magmatic stage or that the source itself was enriched in $^{18}O$. Note that the quartz also records elevated values, with the data clearly divided into two groupings, one with $\delta^{18}O$ values of +10.5 to +11.2‰ ($n$ = 4) and the other with $\delta^{18}O$ values of +12.2 to +12.5‰ ($n$ = 3). This variation is well outside the range attributable to fractionation (Sheppard 1986) and must, therefore, originate at the source. The two most likely candidates are cooling and contamination. The difference in $\delta^{18}O$ values of 2‰ implies a temperature difference of 150–200°C, thereby indicating pegmatite formation down to 500° to 450°C, which is unrealistic for the samples with the elevated $\delta^{18}O$ values given that higher temperatures are inferred based on oxygen isotope geothermometry and fluid inclusion thermometry (P corrected). Thus, contamination is considered a viable explanation and one that has been suggested before for similar variation in $\delta^{18}O$ values of quartz in pegmatitic rocks (Longstaffe 1982).

The mineral $\delta^{18}O$ values indicate both equilibrium and disequilibrium conditions (Table 7). The maximum oxygen isotopic temperatures calculated (600–650°C), in agreement with the muscovite-derived temperatures above, are consistent with the expected temperature of pegmatite formation (London 1992a). Lower temperatures (to 350°C) reflect continued exchange during subsolidus cooling, a common feature of pegmatites (Longstaffe 1982) and coincident with the lower limit of P-corrected temperatures based on fluid-inclusion homogenization (see below) and feldspar re-equilibration (see above).

The $\delta^{18}O$ values for the fluid in equilibrium with the minerals of the pegmatites were calculated (Table 8) using limiting values of 650° and 500°C, with $\delta^{18}O_{H2O}$ values ranging from +8.5 to +11.6‰ (650°C) to +7.5 to +10.8‰ (500°C). These values are within the range for normal magmatic $H_2O$, albeit at the extreme end of $^{18}O$ enrichment (Sheppard 1986), which is consistent with the peraluminous nature and crustal source for the SMB (MacDonald *et al*. 1992, Clarke *et al*. 1997). If another fluid reservoir was involved in pegmatite evolution, it was relatively insignificant. The slightly higher $\delta^{18}O_{H2O}$ values for K-feldspar–$H_2O$ fractionation reflects the tendency of this mineral to continue to exchange during subsolidus cooling (*e.g.,* Javoy 1977).

The $\delta D_{H2O}$ values calculated using tourmaline and muscovite $\delta D$ data for 650° and 500°C differ significantly (Table 8). At 650°C, the $\delta D_{H2O}$ values for tourmaline are –64 to –73‰ compared to –44 to –57‰ for muscovite, but both are within the range for normal magmatic $H_2O$ (Sheppard 1986). However, since muscovite and tourmaline are not observed to coexist, direct comparison of their isotopic composition is not possible.

*Fluid inclusions: P–T conditions of entrapment, fluid composition and source reservoirs*

Before examining the nature and origin of the fluids, the inclusions are examined in terms of their P–T evolution in light of: (1) petrographic features suggesting their primary to secondary origin, (2) thermometric data indicating different populations, the most dominant being a *ca.* 25 wt.% eq. NaCl type, with a lesser aqueous–carbonic type and a minor low-salinity type, (3) decrepitate textures indicating fluctuating pressure during and after inclusion entrapment, and (4) pegmatite formation at *ca.* 370 Ma at a pressure of 3–3.5 kbar (Raeside & Mahoney 1996).

Taking into consideration the above, the fluid-inclusion data are interpreted as follows (Fig. 22): (1) the maximum P-corrected $T_h$ values of *ca.* 650°C equate to values consistent with magmatic conditions, but do not extend above the $H_2O$-saturated solidus for haplogranite (Tuttle & Bowen 1958), thus indicating that some depression of the solidus is required if the fluids are to be considered primary; (2) on the basis of the $T_h$ data, most of the inclusions reflect entrapment below the solidus; (3) cooling was initially isobaric down to below 350°C, consistent with decrepitate textures for the inclusions that resemble those formed during implosion, as would be expected in an environment undergoing isobaric cooling (Vityk & Bodnar 1995); (4) the carbonic inclusions must have been trapped during cooling of the pegmatites and cannot represent entrapment of primary, magmatic fluids, and (5) the minimum $T_h$ data for the aqueous inclusions correspond to P-corrected temperatures of *ca.* 350°C, which is considered significant because: (i) this would approximate the ambient temperature at a depth of the granite emplacement equivalent to 3–3.5 kbar for a reasonable geothermal gradient (*i.e.,* 25–30°C/km); (ii) this is the Ar-blocking temperature for muscovite, and (iii) if uplift commenced from this point, fluids would be trapped along the iso-$T_h$ line of 150°C during uplift, which coincides with the minimum $T_h$ values recorded. For the above reasons stated, the P–T path shown in Figure 22 has been constructed and is discussed in more detail below.

With regard to the carbonic inclusions, some inclusions homogenize to the V and L phase at the same temperature, indicating entrapment of such inclusions during fluid unmixing. Thus, it is not surprizing that the isochoric projections for the carbonic inclusions correspond to the inferred trapping temperature at *ca.* 3–3.5 kbar (Fig. 22). However, the rarity of carbonic inclu-

sions homogenizing by V-phase expansion indicates that fluid unmixing was rare and intermittent.

The dominant fluid in the aplite–pegmatite system was moderately saline and of mixed Na–K–Ca composition with a bulk equivalent composition of 22–24 wt.% equiv. NaCl; a minor amount of a lower-salinity fluid also occurs. This fluid composition compares to that of magmatic fluids associated with pegmatites and greisen mineralization elsewhere in the SMB (Halter *et al.* 1998, Kontak *et al.* 2001, Carruzzo *et al.* 2001) and is also similar to magmatic fluids found in some highly evolved felsic systems, including pegmatites (*e.g.,* Linnen & Williams-Jones 1994, Samson & Sinclair 1992). The composition of the decrepitate mounds and modeling of the thermometric data in the system NaCl–$CaCl_2$–$H_2O$ indicate that the saline fluid can be subdivided into subgroups (*i.e.,* K–Na, Na–Ca, Ca); their nature and origin are addressed below.

The K–Na fluid is represented by data on the Na–K limb of the Na–K–Ca plot for decrepitate data (Fig. 19) and Na-rich fluids of the NaCl–$CaCl_2$–$H_2O$ plot (fluid I; Fig. 17). The variation in K:Na of this fluid may relate to one or both of the following: (1) changes in the physical and chemical conditions within the magma (*e.g.,* Cline & Bodnar 1994, Campbell *et al.* 1995), or (2) fluid:rock interaction as the system cools (Orville 1963, Lagache & Weisbrod 1977, Lagache 1984). The apparent secondary nature of many inclusions suggests the second possibility, with the fluid becoming more sodic during cooling.

TABLE 8. CALCULATED VALUES FOR $\Delta^{18}O_{H2O}$ AND $\Delta D_{H2O}$ AT 650° AND 500°C FOR FLUIDS INVOLVED IN PEGMATITE FORMATION, PEGGYS COVE, NOVA SCOTIA

| | $\delta^{18}O_{H2O}$ | | | | $\delta D_{H2O}$ | |
|---|---|---|---|---|---|---|
| Sample | Tur | Ms | Qtz | Kfs | Tur | Ms |
| PCG-99-04 | 8.9/9.3 | - | - | - | -68.2/-54.6 | - |
| PCG-99-05 | - | 10.1/9.6 | - | - | - | -44.2/-33.2 |
| PCG-99-06 | 9.1/9.5 | - | 8.7/7.5 | - | -72.2/-58.6 | - |
| PCG-99-010 | 9.2/9.6 | - | 10.5/9.3 | 10.8/10 | -73.2/-59.6 | - |
| PCG-99-011 | - | 9.8/9.3 | 10.6/9.4 | 11.2/10.4 | - | -57.2/-46.2 |
| PCG-99-020 | - | - | 10.7/9.5 | 10.0/9.2 | - | - |
| PCG-99-016J | - | 9.6/9.1 | 9.3/8.1 | - | - | -59.2/-48.2 |
| PCG-99-022 | - | - | 8.7/7.5 | 11.6/10.8 | - | - |
| PCG-99-023A | - | - | 9.1/7.9 | 10.6/9.8 | - | - |
| PCG-99-023B | 8.5/8.9 | - | - | - | -64.2/-50.6 | - |

Abbreviations after Kretz (1983). Fractionation equations used are as follows: For $\delta^{18}O_{H2O}$: Tourmaline – $H_2O$: Zheng (1993b); Muscovite – $H_2O$: Zheng (1993b); Quartz – $H_2O$: Zheng (1993a); K-feldspar – $H_2O$ (Zheng 1993a). For $\delta D_{H2O}$: Tourmaline – $H_2O$: Kotzer *et al.* (1993)/Muscovite – $H_2O$: Suzuoki & Epstein (1976). In each case, two values are presented, the first for 650°C, the second for 500°C.

The Na–Ca fluid (fluid II) is represented by data on the Na–Ca limb of the Na–K–Ca plot for the decrepitate data and the Na–Ca fluids in the NaCl–$CaCl_2$–$H_2O$ plot. The Na-rich nature of the fluid in sample PCG–99–21a and the absence of K–Na fluid indicate that the higher-temperature fluid in sample PCG–99–22 either did not penetrate this sample or was not trapped. The higher $T_h$ data for this sample (PCG–99–22; Fig. 16a) is consistent with this interpretation. In this model, the majority of fluid II (Fig. 17) must have been trapped during cooling of the system (*i.e.,* post-crystallization), as suggested in Figure 22 for fluids with $T_h$ of 200°C.

The Ca-rich fluid (fluid III) is unusual for magmatic systems. In fact, we are unaware of such a fluid within felsic magmatic systems, although this fluid is well documented within mafic systems (*e.g.,* Vanko *et al.* 1992, Kelly & Robinson 1992). Thus, a non-magmatic reservoir for this fluid is considered, and the proximal Meguma Group is a likely source. The following points are consistent with this interpretation: (1) the fact that S, albeit in minor amounts, is only detected in the Ca-rich fluid, and that sulfides are known to occur within the Meguma Group rocks; (2) the presence of carbonate within the Meguma Group; (3) infiltration of a Ca-rich component from the contact-metamorphic aureole of intrusions is well documented [*e.g.,* Bowman (1998) for review], and (4) there is a possible contribution from chemical corrosion of the metasedimentary xenoliths within the host leucomonzogranite at Peggys Cove (Fig. 2c). Relevant to this discussion also is modeling of fluid:rock interaction by Smith (1995), who could not reproduce the Ca-rich nature of a similar fluid found in Sn–W mineralized greisens of Cornwall by equilibration of a fluid with granitic assemblages that included sodic plagioclase ($An_{20}$). Could it be that such Ca-rich fluids also reflect infiltration of a fluid from an external, metasedimentary reservoir at Cornwall? The timing of infiltration of the Ca-rich fluid is inferred to be late on the basis of: (1) their low $T_h$ values (*i.e.,* 200°C), which pressure-correct to *ca.* 350–400°C, and (2) the fact that this fluid only mixes with the Na-rich fluid, which itself is inferred to have formed late.

The low-salinity fluid also reflects incursion of an extraneous fluid unrelated to pegmatite formation. Given the gap in the salinity between this fluid and the higher-salinity fluid (Fig. 16), a mixing origin involving the two fluids is considered unlikely. However, the high values of $T_h$ (220–300°C) suggest that incursion of this fluid probably occurred during cooling and uplift of the SMB.

### *Inferred P–T conditions of aplite–pegmatite formation*

The conditions of emplacement of the aplite–pegmatite sheets can be estimated using the following: (1) calculated temperatures of melt based on Zr and P solubilities; (2) isochoric projections of pegmatitic fluids using $T_h$ and compositional data, as discussed above;

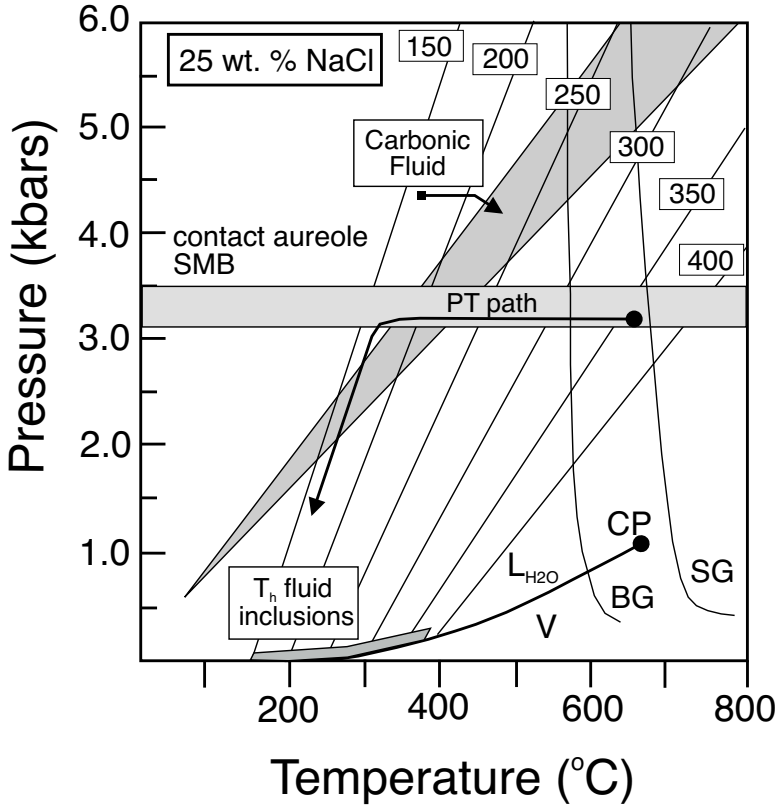


FIG. 22. Pressure–temperature diagram summarizing the relevant information relating to the P–T history of aplite–pegmatite sheets at Peggys Cove. Source of information as follows: (1) the Iso–$T_h$ (*i.e.*, isochoric) lines and L–V curve for a 25 wt.% equiv. NaCl fluid from Bodnar & Vityk (1994), (2) the solidi for $H_2O$-saturated haplogranite (SG) and volatile (B,Li,F,$H_2O$)-rich Beauvoir granite (BG) from Tuttle & Bowen (1958) and Pichavant *et al.* (1987), respectively, (3) homogenization data from Figure 19c, (4) the contact aureole of the SMB from Raeside & Mahoney (1996), (5) isochoric projection for aqueous–carbonic fluid calculated using FLINCOR program (Brown 1989), and (6) the isochoric P–T path for the Peggys Cove area.

(3) experimentally determined solidi for various granitic systems; (4) constraints imposed by the presence of the low-temperature quartz polymorph, occurrence of primary peraluminous phases (muscovite, cordierite; also andalusite elsewhere in the SMB; Clarke *et al.* 1976) and presence of two feldspars, and (5) the calculated P–T conditions of the contact aureole of the SMB (Raeside & Mahoney 1996). From these foregoing constraints, the inferred PT path for the melts responsible for the aplite–pegmatite in the Peggys Cove area is shown in Figure 22.

Melt temperatures of ≤650–700°C based on Zr and P solubilities (Watson & Harrison 1983, Montel 1993) are similar to values calculated using Zr geothermometry for the Calamity Peak granite–pegmatite complex by Duke *et al.* (1992). A lower temperature of melt solidification, but not necessarily lower P, would be consistent with the known solidi of volatile-rich systems (*e.g.,* Beauvoir granite; Fig. 22), although it is not apparent that the pegmatite–aplite system at Peggys Cove was enriched in the necessary volatiles [*i.e.,* several wt.% B, F; see London (1992a) for review]. The maximum P-corrected $T_h$ values for the fluid inclusions generally coincide with the intersection of the Beauvoir granite solidus and contact aureole of the SMB (Fig. 22). Is this evidence for solidification of the aplite–pegmatite sheets at lower temperatures? If not, then the data indicate that primary fluids were not trapped and the observed fluid inclusions represent secondary inclusions trapped during isobaric cooling.

The absence of fluid inclusions with $T_h$ values *ca.* ≥380°C precludes both a lower P for melt crystallization or rapid post-crystallization uplift history following a counter-clockwise P–T path, unless the trapping of inclusions occurred much later and relates to an unknown hydrothermal event. Rather, an isobaric cooling curve is preferred, which permits trapping of fluids during cooling and is consistent with subsequent uplift of the SMB. The trajectory in Figure 22 is also constrained by assuming a geothermal gradient of *ca.* 25–30°C, which indicates a T of *ca.* 300°C at *ca.* 3 kbar, which incidentally coincides with the 200°C iso-$T_h$ line. Given the abundance of fluid-inclusion $T_h$ data at *ca.* 160° to 190°C, we contend that the extension of this isochore to 3–3.5 kbar represents thermal equilibrium of the granite with the country rock and the point at which the P–T curve for the pegmatites leaves the isobaric trend. This temperature also coincides with the lowest oxygen isotopic temperature calculated (Table 7).

The textures of the fluid inclusions are highly variable, with shapes reflecting both non-equilibrium (*e.g.,* Figs. 15c, d, g) and equilibrium (Fig. 15b) conditions after entrapment. In the former case, the inclusions resemble decrepitates produced in experimental studies due to implosion ($P_i < P_c$: Vityk & Bodnar 1995). That the inclusions did not subsequently attain regular shapes indicates that equilibration at their new environment was arrested. Similarly decrepitated inclusions reported in mesothermal quartz veins are interpreted to reflect overpressures of 2–3 kbar (Robert *et al.* 1995).

### *Emplacement of the aplite–pegmatite sheets and internal evolution*

The occurrence and nature of the aplite–pegmatite sheets are not unusual in terms of layered pegmatites, but their petrogenesis is unusual in that they are not products of a chemically evolved reservoir. In addition, the orientations of the sheets are unusual compared to examples elsewhere in the SMB (Horne *et al.* 1992): they are generally flat rather that subvertical.

With respect to the overall structural setting and evolution of the sheets, the following points are first noted: (1) the flat-lying sheets record filling of subhorizontal dilatant zones within the host granite that were first filled with felsic melt. Coarse, oriented K-feldspar with a comb texture indicates that post-crystallization movement was minimal. The internal evolution and separation of the sheets into fine-grained aplitic bottoms and coarse-grained K-feldspar-rich tops also indicate that the zones of infill represent single dilational events rather than multiple openings. (2) The aplite–pegmatite sheets are very heterogeneous with respect to their internal evolution and lateral continuity; (3) sheets have a morphology similar to shear-type veins; (4) orientations of aplites are at times similar to conjugate-shear veins, and *en échelon* arrays are common (Figs. 5a, f), and (5) tourmaline fibers at the upper contact of a zoned sheet indicate north-directed compression, consistent with the kinematics of the regional Acadian deformation.

Formation of the flat sheets within monzogranite also indicates that these rocks deformed by a combined brittle–ductile mechanism. Such failure within granite does not require complete crystallization, but once a rigid framework is established at 70–75% crystallization, the partially solidified magma can deform (Vigneresse *et al.* 1996). In order for this to occur, however, high internal fluid pressures would be required in order to overcome the vertical normal stress ($\sigma_V$; Brisbin 1986) generated by the overlying 12–15 km of cover (MacDonald *et al.* 1992, Raeside & Mahoney 1996). The presence of a horizontal stress ($\sigma_H$) related to regional compression would enhance formation of the flat sheets given the 3–3.5 kbar depth of emplacement. Formation of the dilatant zones, requiring vertical extension, overlapped conditions under which shear-type veins formed (*e.g.,* Fig. 5f). These features are analogous to the subvertical and flat veins observed crosscutting each other in the Sigma gold mine, Quebec (Sibson *et al.* 1988), although in this case, the orientation of the shear veins is different than at Peggys Cove. In the case at Sigma, periodic buildup of fluid pressure was proposed as a means of forming the contrasting arrays of veins. Such a mechanism might apply at Peggys Cove, that is periodic release of a fluid from within the magma chamber generated *via* exsolution of volatiles, perhaps in conjunction with relaxation of regional stresses. A similar model of fluid overpressuring was proposed by Kirkham & Sinclair (1988) and Lowenstern & Sinclair (1996) for aplite–pegmatite systems.

### *Model for formation of the tourmaline-bearing pegmatite–aplite sheets at Peggys Cove*

In terms of petrogenesis of the aplite–pegmatite sheets, the important observations are: (1) occurrence within a biotite leucomonzogranite and apparent absence of a spatially related, chemically evolved granite, as are other aplites and pegmatites within the SMB and the Halifax Pluton (MacDonald & Horne 1988, MacDonald *et al.* 1992); (2) neither whole-rock (high K/Rb) nor mineral (high Rb and low P in feldspar, low Cl and F in muscovite) compositions of the pegmatites indicate crystallization from a chemically evolved melt; (3) absence of an alteration zone around the pegmatite–aplite sheets due to diffusive loss of volatiles (London 1992a); (4) elevated $\delta^{18}O$ values for aplites indicative of a crustal reservoir, and (5) tourmaline compositions that are unusual for evolved granitic pegmatites and that suggest some contribution from another reservoir. These observations would be consistent with a local process that generated small fractions of melt enriched in volatiles ($H_2O$, B). In this respect, the presence of the melanocratic xenoliths enveloped by pegmatite (Fig. 2d) is considered critical, as they may represent a micro-

scale example of the process that formed the larger sheets; such a model follows.

Given the proximity of the Meguma Group both laterally (*i.e.,* a few hundred m off shore) and vertically (proximal to the roof of intrusion; MacDonald *et al.* 1992), the incorporation of Meguma xenoliths was common, as evidenced from their abundance in the host rock. Partial digestion of these xenoliths would liberate volatiles, which may have locally enriched areas of the melt in $H_2O$ and B. Sudden decompression of the magma, perhaps in response to regional tectonic processes, would promote separation of small batches of volatile-rich melt. Formation of the aplite–pegmatite sheets and associated internal fabrics are features that are commonly associated with fluctuating $P(H_2O)$ (Kirkham & Sinclair 1988, Lowenstern & Sinclair 1996), as might be expected to occur within an active tectonic regime. Thus, the tourmaline-bearing aplite–pegmatite sheets may reflect a form of melt contamination, not unlike that encountered in cases of assimilation and fractional crystallization. Additional support for this origin includes: (1) the fluid-inclusion compositions that indicate a considerable Ca component to the pegmatitic fluid. The origin of this component is likely from a non-magmatic reservoir, given the depletion of calcium in these aplite–pegmatite sheets. (2) Values of $\delta^{18}O$ of +12 to +13‰ for the aplites, which are much higher than the +10 to +11‰ values typical for samples of the SMB (Fig. 20).

In summary, the formation of pegmatite–aplite sheets at Peggys Cove is considered to be contingent on several processes. First, contamination of a monzogranitic melt by partial digestion of Meguma Group metasedimentary xenoliths, which liberated volatiles ($H_2O$, B) that were dissolved in the melt. Subsequent decompression of the area, possibly related to periodic relaxation of regional stresses, caused sudden formation of volatile-rich melt, which created conditions of sudden overpressuring or hydrofracturing of the partially crystallized melt (*i.e.,* 75%), resulting in formation of flat dilatant zones. These dilatant zones were immediately infilled by the volatile-rich melt, which subsequently evolved internally to the layered pegmatite–aplite sheets now observed. The undulating nature of the sheets may reflect subsequent folding of these rocks while still ductile (*cf.* Benn *et al.* 1997, 1999).

## Acknowledgements

This project was funded by the Nova Scotia Department of Natural Resources. The support of management is sincerely acknowledged. Analytical data were acquired with the support of NSERC operating grants to Dostal, Kyser and Archibald. Mr. R. McKay, Dalhousie University, is thanked for assistance with the operation of the electron microprobe. Discussions with M. MacDonald, R. Horne, D.B Clarke, and A. Anderson regarding the origin of these spectacular sheets of aplite is appreciated. Reviews of the manuscript by L. Groat, T. Mulja, R.C. Ewing, A.U. Falster, W.B. Simmons, Jr., and R.F. Martin are sincerely acknowledged. This paper is published with permission of the Director, Nova Scotia Department of Natural Resources.

## References

Benn, K., Horne, R.J., Kontak, D.J., Pignotta, G.S. & Evans, N.G. (1997): Syn-Acadian emplacement model for the South Mountain Batholith, Meguma Terrane, Nova Scotia: magnetic fabric and structural analyses. *Geol. Soc. Am., Bull.* **109**, 1279-1293.

_____, Roest, W.R., Rochette, P., Evans, N.G. & Pignotta, G.S. (1999): Geophysical and structural signatures of syntectonic batholith construction: the South Mountain Batholith, Meguma Terrane, Nova Scotia. *Geophys. J. Int.* **136**, 144-158.

Bodnar, R.J. & Vityk, M.O. (1994): Interpretation of microthermometric data for $H_2O$–NaCl fluid inclusions. *In* Fluid Inclusions in Minerals: Methods and Applications (B. De Vivo & M.L. Frezzotti, eds.). Int. Mineral. Assoc., Short Course Notes, 117-130.

Bottinga, Y. & Javoy, M. (1975): Oxygen isotope partitioning among the minerals in igneous and metamorphic rocks. *Rev. Geophys. Space Phys.* **13**, 401-418.

Boullier, A.-M., Firdaous, K. & Boudier, F. (1997): Fluid circulation related to deformation in the Zabargad gneisses (Red Sea rift). *Tectonophys.* **279**, 281-302.

_____, France-Lanord, C., Dubessy, J., Adamy, J. & Champenois, M. (1991): Linked fluid and tectonic evolution in the High Himalaya mountains (Nepal). *Contrib. Mineral. Petrol.* **107**, 358- 372.

Bowman, J.R. (1998): Stable isotope systematics of skarns. *In* Mineralized Intrusion-Related Skarn Systems (D.R. Lentz, *ed.*). *Mineral. Assoc. Can., Short Course Vol.* **26**, 99-145.

Brisbin, W.C. (1986): Mechanics of pegmatite intrusion. *Am. Mineral.* **71**, 644-651.

Brown, P.E. (1989): FLINCOR: a computer program for the reduction of and investigation of fluid inclusion data. *Am. Mineral.* **74**, 1390-1393.

Brown, W.L. & Parsons, I. (1989): Alkali feldspars: ordering rates, phase transformations and behaviour diagrams for igneous rocks. *Mineral. Mag.* **53**, 25-42.

Campbell, A.R., Banks, D.A., Phillips, R.S. & Yardley, W.D. (1995): Geochemistry of Th–U–REE mineralizing magmatic fluids, Capitan Mountains, New Mexico. *Econ. Geol.* **90**, 1271-1287.

Carruzzo, S., Kontak, D.J. & Clarke, D.B. (2001): Granite-related mineral deposits of the New Ross area, South Mountain Batholith, Nova Scotia, Canada: P, T and X

constraints of fluids using fluid inclusion thermometry and decrepitate analysis. *Trans. R. Soc. Edinburgh, Earth Sci.* **91**, 303-319.

ČERNÝ, P. & CHAPMAN, R. (1986): Adularia from hydrothermal vein deposits: extremes in structural state. *Can. Mineral.* **24**, 717-728.

_____, MEINTZER, R.E. & ANDERSON, A.J. (1985): Extreme fractionation in rare-element granitic pegmatites: selected examples of data and mechanisms. *Can. Mineral.* **23**, 381-421.

CHATTERJEE, A.K. & STRONG, D.F. (1985): Geochemical characteristics of the polymetallic tin domain, southwestern Nova Scotia, Canada. *In* Granite-Related Mineral Deposits, Geology, Petrogenesis and Tectonic Setting (R.P. Taylor & D.F. Strong, eds.). *Can. Inst. Mining Metall., Abstr. Vol.*, 41-52.

CHERRY, M.E. & TREMBATH, L.T. (1978): Structural state and composition of alkali feldspars in granites of the St. George pluton, south-western New Brunswick. *Mineral. Mag.* **42**, 391-399.

CLARK, A.H., ARCHIBALD, D.A., LEE, A.W., FARRAR, E. & HODGSON, C.J. (1998): Laser probe $^{40}Ar/^{39}Ar$ ages of early- and late-stage alteration assemblages, Rosario porphyry copper–molybdenum deposit, Collahuasi district, I Region, Chile. *Econ. Geol.* **93**, 326-337.

CLARKE, D.B. (1995): Cordierite in felsic igneous rocks: a synthesis. *Mineral. Mag.* **59**, 311-325.

_____ & CLARKE, G.K.C. (1998): Layered granodiorites at Chebucto Head, South Mountain batholith, Nova Scotia. *J. Struct. Geol.* **20**, 1305-1324.

_____, MACDONALD, M.A., REYNOLDS, P.H. & LONGSTAFFE, F. (1993): Leucogranites from the eastern part of the South Mountain Batholith, Nova Scotia. *J. Petrol.* **34**, 653-679.

_____, _____ & TATE, M.C. (1997): Late Devonian mafic-felsic magmatism in the Meguma Zone, Nova Scotia. *In* The Nature of Magmatism in the Appalachian Orogen (A.K. Sinha, J.B. Whalen & J.P. Hogan, eds.). *Geol. Soc. Am., Mem.* **191**, 107-127.

_____, MCKENZIE, C.B., MUECKE, G.K. & RICHARDSON, S.W. (1976): Magmatic andalusite from the South Mountain batholith, Nova Scotia. *Contrib. Mineral. Petrol.* **56**, 279-287.

_____, REARDON, N.C., CHATTERJEE, A.K. & GREGOIRE, D.C. (1989): Tourmaline composition as a guide to mineral exploration: a reconnaissance study from Nova Scotia using discriminant function analysis. *Econ. Geol.* **84**, 1921-1935.

CLINE, J.S. & BODNAR, R.J. (1994): Direct evolution of brine from a crystallizing silicic melt at the Questa, New Mexico, molybdenum deposit. *Econ. Geol.* **89**, 1780-1802.

COLLINS, P.L.F. (1979): Gas hydrates in $CO_2$-bearing fluid inclusions and the use of freezing data for estimation of salinity. *Econ. Geol.* **74**, 1435-1444.

CRAWFORD, M.L. (1981): Phase equilibria in aqueous fluid inclusions. *In* Fluid Inclusions: Applications to Petrology (L.S. Hollister & M.L. Crawford). *Mineral. Assoc. Can., Short Course Vol.* **6**, 75-100.

DOSTAL, J. & CHATTERJEE, A.K. (1995): Origin of topaz-bearing and related peraluminous granites of late Devonian Davis Lake pluton, Nova Scotia, Canada. *Chem. Geol.* **123**, 67-88.

_____ & _____ (2000): Contrasting behaviour of Nb/Ta and Zr/Hf ratios in a peraluminous granitic pluton (Nova Scotia, Canada). *Chem. Geol.* **163**, 207-218.

DUKE, E.F., PAPIKE, J.J. & LAUL, J.C. (1992): Geochemistry of a boron-rich peraluminous granite pluton: the Calamity Peak layered granite–pegmatite complex, Black Hills, South Dakota. *Can. Mineral.* **30**, 811-833.

FOORD, E.E. (1977): Famous mineral localities: the Himalaya dike system, Mesa Grande district, San Diego County, California. *Mineral. Rec.* **8**, 461-474.

GOLDSMITH, J.R. & LAVES, F. (1954): The microcline–sanidine stability relations. *Geochim. Cosmochim. Acta* **5**, 1-19.

GOLDSTEIN, R.H. & REYNOLDS, T.J. (1994): Systematics of fluid inclusions in diagenetic minerals. *SEPM (Society for Sedimentary Geology), Short Course* **31**.

HALTER, W.E., WILLIAMS-JONES, A.E. & KONTAK, D.J. (1998): Origin and evolution of the greisenizing fluid at the East Kemptville tin deposit, Nova Scotia, Canada. *Econ. Geol.* **93**, 1026-1051.

HAM, L.J. & KONTAK, D.J. (1988): A textural and chemical study of white mica in the South Mountain Batholith, Nova Scotia: primary versus secondary origin. *Maritime Sediments & Atlantic Geology* **24**,111-1121.

_____, MARSH, S.W., COREY, M.C., HORNE, R.J. & MACDONALD, M.A. (1989): Lithogeochemistry of the eastern portion of the South Mountain Batholith, Nova Scotia. *Nova Scotia Department of Mines & Energy, Open-File Rep.* **89-001**.

HAYNES, F.M., STERNER, S.M..& BODNAR, R.J. (1988): Synthetic fluid inclusions in natural quartz. IV. Chemical analysis of fluid inclusions by SEM/EDA: evaluation of method. *Geochim. Cosmochim. Acta* **52**, 969-977.

HAWTHORNE, F.C. & HENRY, D.J. (1999): Classification of the minerals of the tourmaline group. *Eur. J. Mineral.* **11**, 201-215.

HENRY, D.J. & GUIDOTTI, C.V. (1985): Tourmaline as a petrogenetic indicator mineral: an example from the staurolite-grade metapelites of NW Maine. *Am. Mineral.* **70**, 1-15.

HICKS, R.J., JAMIESON, R.A. & REYNOLDS, P.H. (1999): Detrital and metamorphic $^{40}Ar/^{39}Ar$ ages from muscovite and whole-rock samples, Meguma Supergroup, southern Nova Scotia. *Can. J. Earth Sci.* **36**, 23-32.

HORNE, R.J., CAREY, M.C., HAM, L.J. & MACDONALD, M.A. (1988): Primary and secondary structural features in the eastern portion of the South Mountain Batholith, southwestern Nova Scotia: implications for regional stress orientations during intrusion. *Maritime Sediments & Atlantic Geology* **24**, 71-82.

_____, MACDONALD, M.A., COREY, M.C. & HAM, L.J. (1992): Structure and emplacement of the South Mountain Batholith, southwestern Nova Scotia. *Atlantic Geology* **28**, 29-50.

ICENHOWER, J. & LONDON, D. (1996): Experimental partitioning of Rb, Cs, Sr, and Ba between alkali feldspar and peraluminous melt. *Am. Mineral.* **81**, 719-734.

JAVOY, M. (1977): Stable isotopes and geothermometry. *J. Geol. Soc. London* **133**, 609-636.

JENNER, G.A., LONGERICH, H.P., JACKSON, S.E. & FRYER, B.J. (1990): ICP–MS – a powerful tool for high-precision trace-element analysis in earth sciences: evidence from analysis of selected U.S. Geological Survey reference samples. *Chem. Geol.* **83**, 133-148.

JIANG, SHAOYONG, HAN, F., SHEN, JIANZHONG & PALMER, M.R. (1999): Chemical and Rb–Sr, Sm–Nd isotopic systematics of tourmaline from the Dachang Sn-polymetallic ore deposit, Guangxi Province, P.R. China. *Chem. Geol.* **157**, 49-67.

JOLLIFF, B.L., PAPIKE, J.J. & LAUL, J.C. (1987): Mineral recorders of pegmatite internal evolution: *REE* contents of tourmaline from the Bob Ingersoll pegmatite, South Dakota. *Geochim. Cosmochim. Acta* **51**, 2225-2232.

_____, _____ & SHEARER, C.K. (1986): Tourmaline as a recorder of pegmatite evolution: Bob Ingersoll pegmatite Black Hills, South Dakota. *Am. Mineral.* **71**, 472-500.

KELLY, D.S. & ROBINSON, P.T. (1992): Development of brine-dominated hydrothermal system at temperatures of 400–500°C in the upper level plutonic sequence, Troodos ophiolite, Cyprus. *Geochim. Cosmochim. Acta* **54**, 653-661.

KIRKHAM, R.V. & SINCLAIR, W.D. (1988): Comb quartz layers in felsic intrusions and their relationship to porphyry deposits. *In* Recent Advances in the Geology of Granite-Related Mineral Deposits (R.P. Taylor & D.F. Strong, eds.). *Can. Inst. Mining Metall., Spec. Vol.* **39**, 50-71.

KONTAK, D.J. (1990): The East Kemptville topaz–muscovite leucogranite, Nova Scotia. I. Geological setting and whole-rock geochemistry. *Can. Mineral.* **28**, 787-825.

_____ (1991):The East Kemptville topaz–muscovite leucogranite, Nova Scotia. II. Mineral chemistry. *Can. Mineral.* **29**, 37-60.

_____ (1998): A study of fluid inclusions in sulfide and non-sulfide mineral phases from a carbonate-hosted Zn–Pb deposit, Gays River, Nova Scotia, Canada. *Econ. Geol.* **93**, 793-817.

_____, ANSDELL, K., DOSTAL, J., HALTER, W., MARTIN, R. & WILLIAMS-JONES, A.E. (2001): The nature and origin of pegmatites in a fluorine-rich leucogranite, East Kemptville tin deposit, Nova Scotia, Canada. *Trans. R. Soc. Edinburgh: Earth Sci.* **92**, 173-200.

_____, KERRICH, R. & STRONG, D.F. (1991): The role of fluids in the late-stage evolution of the South Mountain batholith, Nova Scotia: further geochemical and oxygen isotopic studies. *Atlantic Geology* **27**, 29-48.

_____ & MARTIN, R.F. (1997): Alkali feldspar in the peraluminous South Mountain batholith, Nova Scotia: trace-element data. *Can. Mineral.* **35**, 959-977.

_____, _____ & RICHARD, L. (1996): Patterns of phosphorus enrichment in alkali feldspar, South Mountain batholith, Nova Scotia, Canada. *Eur. J. Mineral.* **8**, 805-824.

_____, STRONG, D.F. & KERRICH, R. (1988): Crystal – melt ± fluid phase equilibria versus late-stage fluid–rock interaction in granitoid rocks of the South Mountain batholith, Nova Scotia: whole rock geochemistry and oxygen isotope evidence. *Maritime Sediments & Atlantic Geology* **24**, 97-110.

KOTZER, T.G., KYSER, T.K., KING, R.W. & KERRICH, R. (1993): An empirical oxygen- and hydrogen-isotope geothermometer for quartz–tourmaline and tourmaline–water. *Geochim. Cosmochim. Acta* **52**, 3421-3426.

KRETZ, R. (1983): Symbols for rock-forming minerals. *Am. Mineral.* **68**, 277-279.

KYSER, T.K., LESHER, C.E. & WALKER, D. (1998): The effects of liquid immiscibility and thermal diffusion on oxygen isotopes in silicate liquids. *Contrib. Mineral. Petrol.* **133**, 373-381.

LAGACHE, M. (1984): The exchange equilibrium distribution of alkali and alkaline-earth elements between feldspars and hydrothermal solutions. *In* Feldspar & Feldspathoids: Structures, Properties and Occurrences (W.L. Brown, ed.). D. Reidel, Dordrecht, The Netherlands (317-372).

_____ & WEISBROD, A. (1977): The system two alkali feldspars – KCl – NaCl – $H_2O$ at moderate to high temperatures and low pressures. *Contrib. Mineral. Petrol.* **62**, 77-101.

LINNEN, R.L. & WILLIAMS-JONES, A.E. (1994): The evolution of pegmatite-hosted Sn–W mineralization at Nong Sua, Thailand: evidence from fluid inclusions and stable isotopes. *Geochim. Cosmochim. Acta* **58**, 735-747.

LOGOTHETIS, J. (1985): Economic geology of the New Ross–Vaughan complex. *In* Guide to the Granites and Mineral Deposits of Southwestern Nova Scotia (A.K. Chatterjee &

D.B. Clarke, eds.). *Nova Scotia Department Natural Resources, Pap.* **85-3**, 41-62.

LONDON, D. (1992a): The application of experimental petrology to the genesis and crystallization of granitic pegmatites. *Can. Mineral.* **30**, 499-540.

_____ (1992b): Phosphorus in S-type magmas: the $P_2O_5$ content of feldspars from peraluminous granites, pegmatites, and rhyolites. *Am. Mineral.* **77**, 126-145.

_____, ČERNÝ, P., LOOMIS, J.L. & PAN, J.J. (1990): Phosphorus in alkali feldspars of rare- element granitic pegmatites. *Can. Mineral.* **28**, 771-786.

_____ & MANNING, D.A.C. (1995): Chemical variation and significance of tourmaline from southwest England. *Econ. Geol.* **90**, 495-519.

LONGSTAFFE, F.J. (1982): Stable isotopes in the study of granitic pegmatites and related rocks. *In* Granitic Pegmatites in Science and Industry (P. Černý, ed.). *Mineral. Assoc. Can., Short Course Vol.* **8**, 373-404.

_____, SMITH, T.E. & MUEHLENBACHS, K. (1980): Oxygen isotope evidence for the genesis of Upper Paleozoic granitoids from southwestern Nova Scotia. *Can. J. Earth Sci.* **17**, 132-141.

LOWENSTERN, J.B. & SINCLAIR, W.D. (1996): Exsolved magmatic fluid and its role in the formation of comb-layered quartz at the Cretaceous Logtung W–Mo deposit, Yukon Territory, Canada. *Trans. R. Soc. Edinburgh: Earth Sci.* **87**, 291-303.

MACDONALD, M.A. & CLARKE, D.B. (1991): Use of nonparametric ranking statistics to characterize magmatic and post-magmatic processes in the eastern South Mountain Batholith, Nova Scotia, Canada. *Chem. Geol.* **92**, 1-20.

_____ & HORNE, R.J. (1988): Petrology of the zoned, peraluminous Halifax Pluton, south-central Nova Scotia. *Maritime Sediments & Atlantic Geology* **24**, 33-45.

_____, _____, COREY, M.C. & HAM, L.J. (1992): An overview of recent bedrock mapping and follow-up petrological studies of the South Mountain Batholith, southwestern Nova Scotia, Canada. *Atlantic Geology* **28**, 7-28.

MAILLET, L.A. & CLARKE, D.B. (1985): Cordierite in the peraluminous granites of the Meguma Zone, Nova Scotia, Canada. *Mineral. Mag.* **49**, 695-702.

MANNING, D.A.C. (1982): Chemical and morphological variation in tourmalines from the Hub Kapong batholith of peninsular Thailand. *Mineral. Mag.* **45**, 139-147.

_____ & PICHAVANT, M. (1988): Volatiles and their bearing on the behaviour of metals in granitic systems. *In* Recent Advances in the Geology of Granite-Related Mineral Deposits (R.P. Taylor & D.F. Strong, eds.). *Can. Inst. Mining Metall., Spec. Vol.* **39**, 13-24.

MARTIN, R.F. (1974): Controls of ordering and subsolidus phase relations in the alkali feldspars. *In* The Feldspars (W.S. McKenzie & J. Zussman, eds.), Manchester University Press, Manchester, U.K. (313-336).

MASUDA, A., NAKAMURA, N. & TANAKA, T. (1973): Fine structures of mutually normalized rare-earth patterns of chondrites. *Geochim. Cosmochim. Acta* **37**, 239-248.

MCDOUGALL, I. & HARRISON, T.M. (1988): Geochronology and thermochronology by the $^{40}Ar/^{39}Ar$ method. Oxford University Press, Oxford, U.K.

MILLER, C.F. & MITTLEFEHLDT, D.W. (1982): Depletion of light rare-earth elements in felsic magmas. *Geology* **10**, 129-133.

_____, STODDARD, E.F., BRADFISH, L.J. & DOLLASE, W.A. (1981): Composition of plutonic muscovite: genetic implications. *Can. Mineral.* **19**, 25-34.

MONIER, G. & ROBERT, J.-L. (1986): Muscovite solid solutions in the system $K_2O$–MgO–FeO–$Al_2O_3$–$SiO_2$–$H_2O$: an experimental study at 2 kbar $P_{H2O}$ and comparison with natural Li-free white micas. *Mineral. Mag.* **50**, 257-266.

MONTEL, J.M. (1993): A model for monazite/melt equilibrium and application to the generation of granitic magmas. *Chem. Geol.* **110**, 127-146.

MUECKE, G.K. & CLARKE, D.B. (1981): Geochemical evolution of the South Mountain Batholith, Nova Scotia: rare-earth element evidence. *Can. Mineral.* **19**, 133-145.

NEVES, L.J.P.F. & GODINHO, M.M. (1999): Structural state of K-feldspar in some Hercynian granites from Iberia: a review of data and controlling factors. *Can. Mineral.* **37**, 691-700.

O'REILLY, G.A. (1992): Petrograhic and geochemical evidence for a hypogene origin of granite-hosted, vein-type mineralization at the New Ross Mn deposits, Lunenburg County, Nova Scotia, Canada. *Econ. Geol.* **87**, 1275-1300.

_____, FARLEY, E.J. & CHAREST, M.H. (1982): Metasomatic-hydrothermal mineral deposits of the New Ross – Mahone Bay area, Nova Scotia. *Nova Scotia Dep. Mines & Energy, Pap.* **82-2**.

ORVILLE, P.M. (1963): Alkali ion exchange between vapor and feldspar phases. *Am. J. Sci.* **261**, 201-237.

PICHAVANT, M., BOHER, M., STENGER, J.-F., AISSA, M. & CHAROY, B. (1987): Relations de phase des granites de Beauvoir à 1 et 3 kbar en conditions de saturation en $H_2O$. *Géologie de la France* **2-3**, 77-85.

RAESIDE, R.P. & MAHONEY, K.M. (1996): The contact metamorphic aureole of the South Mountain Batholith, southern Nova Scotia. *Geol. Assoc. Can. – Mineral. Assoc. Can., Program Abstr.* **21**, A77.

ROBERT, F., BOULLIER, A.M. & FIRDAOUS, K. (1995): Gold-bearing quartz veins in metamorphosed terranes and their

bearing on the role of fluids in faulting. *J. Geophys. Res.* **100**, 12861-12879.

ROEDDER, E. (1984): Fluid Inclusions. *Rev. Mineral.* **12**.

SAMSON, I.M. & SINCLAIR, W.D. (1992): Magmatic hydrothermal fluids and the origin of quartz–tourmaline orbicules in the Seagull Batholith, Yukon Territory. *Can. Mineral.* **30**, 937-954.

SELWAY, J.B. & NOVÁK, M. (1997): Experimental conditions, normalization procedures and used nomenclature for tourmaline. *In* Tourmaline 1997 (Nové Mesto na Morave) Field Trip Guidebook (M. Novák & J.B. Selway, eds.), 19-21.

_____, _____, ČERNÝ, P. & HAWTHORNE, F.C. (2000): The Tanco pegmatite at Bernic Lake Manitoba. XIII. Exocontact tourmaline. *Can. Mineral.* **38**, 869-876.

SHEPPARD, S.M.F. (1986): Characterization and isotopic variations in natural waters. *In* Stable Isotopes in High Temperature Geological Processes (J.W. Valley, H.P. Taylor, Jr. & H.R. O'Neil, eds.). *Rev. Mineral.* **16**, 165-183.

SIBSON, R.H., ROBERT, F. & POULSEN, K.H. (1988): High angle reverse faults, fluid-pressure cycling, and mesothermal gold–quartz deposits. *Geology* **16**, 551-555.

SINCLAIR, W.D. & RICHARDSON, J.M. (1992): Quartz–tourmaline orbicules in the Seagull Batholith, Yukon Territory. *Can. Mineral.* **30**, 923-935.

SISSON, V.B. & HOLLISTER, L.S. (1990): A fluid-inclusion study of metamorphosed pelitic and carbonate rocks, south-central Maine. *Am. Mineral.* **75**, 59-70.

SMITH, M. (1995): Modeling of fluid evolution on the basis of crush leach analyses of fluid inclusions from the Cligga Head greisen related Sn–W deposit, S.E. England. *In* Abstr. XIII ECROFI Conf. *Bol. Soc. Espan. Mineral.* **18**(1), 237-238.

SMITH, T.E. (1975): Layered granitic rocks at Chebucto Head, Halifax County, Nova Scotia. *Can. J. Earth Sci.* **12**, 456-463.

STERN, L.A., BROWN, G.E., JR., BIRD, D.K., JAHNS, R.H., FOORD, E.E., SHIGLEY, J.E. & SPAULDING, L.B., JR. (1986): Mineralogy and geochemical evolution of the Little Three pegmatite–aplite layered intrusive, Ramona, California. *Am. Mineral.* **71**, 406-427.

STERNER, S.M. & BODNAR, R.J. (1989): Synthetic fluid inclusions in natural quartz. VII. Re-equilibration of fluid inclusions in quartz during laboratory simulated metamorphic burial and uplift. *J. Metamorph. Geol.* **7**, 243-260.

SUZUOKI, T. & EPSTEIN, S. (1976): Hydrogen isotope fractionation between OH-bearing minerals and water. *Geochim. Cosmochim. Acta* **40**, 1229-1240.

TAYLOR, R.G. & POLLARD, P.J. (1988): Pervasive hydrothermal alteration in tin-bearing granites and implications for the evolution of ore-bearing magmatic fluids. *In* Recent Advances in the Geology of Granite-Related Mineral Deposits (R.P. Taylor & D.F. Strong, eds.). *Can. Inst. Mining Metall., Spec. Vol.* **39**, 86-95.

TEERTSTRA, D.K., ČERNÝ, P. & HAWTHORNE, F.C. (1999): Subsolidus rubidium-dominant feldspar from the Morrua pegmatite, Mozambique: paragenesis and composition. *Mineral. Mag.* **63**, 313-320.

TINDLE, A.G., BREAKS, F.W. & SELWAY, J.B. (2002): Tourmaline in petalite-subtype granitic pegmatites: evidence of fractionation and contamination from the Pakeagama Lake and Separation Lake areas of northwestern Ontario, Canada. *Can. Mineral.* **40**, 753-788.

TUTTLE, O.F. & BOWEN, N.L. (1958): Origin of granite in light of experimental studies in the system $NaAlSi_3O_8$–$KAlSi_3O_8$–$SiO_2$–$H_2O$. *Geol. Soc. Am., Mem.* **74**.

VANKO, D.A., BODNAR, R.J. & STERNER, S.M. (1988): Synthetic fluid inclusions. VIII. Vapor-saturated halite solubility in part of the system NaCl–$CaCl_2$–$H_2O$ with application to fluid inclusions from oceanic hydrothermal systems. *Geochim. Cosmochim. Acta* **52**, 2451-2456.

_____, GRIFFITH, J.D. & ERICKSON, C.L. (1992): Calcium-rich brines and other hydrothermal fluids in fluid inclusions from plutonic rocks, Oceanographer Transform, Mid-Atlantic Ridge. *Geochim. Cosmochim. Acta* **56**, 35-47.

VIGNERESSE, J.L., BARBEY, P. & CUNEY, M. (1996): Rheological transitions during partial melting and crystallization with application to felsic magma segregation and transfer. *J. Petrol.* **37**, 1579-1600.

VITYK, O. & BODNAR, R.J. (1995): Textural evolution of synthetic fluid inclusions in quartz during re-equilibration, with application to tectonic reconstruction. *Contrib. Mineral. Petrol.* **121**, 309-323.

WALKER, R.J., HANSON, G.N., PAPIKE, J.J., O'NEIL, J.R. & LAUL, J.C. (1986): Internal evolution of the Tin Mountain pegmatite, Black Hills, South Dakota. *Am. Mineral.* **71**, 440-459.

WATSON, E.B. & HARRISON, T.M. (1983): Zircon saturation revisited: temperature and composition effects in a variety of crustal magma types. *Earth Planet. Sci. Lett.* **64**, 295-304.

WEBBER, K.L., FALSTER, A.U., SIMMONS, W.B. & FOORD, E.E. (1997): The role of diffusion-controlled oscillatory nucleation in the formation of line rock in pegmatite–aplite dikes. *J. Petrol.* **38**, 1777-1791.

_____, SIMMONS, W.B., FALSTER, A.U. & FOORD, E.E. (1999): Cooling rates and crystallization dynamics of shallow level pegmatite–aplite dikes, San Diego County, California. *Am. Mineral.* **84**, 708-717.

WORDEN, R.H., WALKER, D.L., PARSONS, I. & BROWN, W.L. (1990): Development of microporosity, diffusion channels and deuteric coarsening in perthitic alkali feldspars. *Contrib. Mineral. Petrol.* **104**, 507-515.

YAVUZ, F., İSENDEROĞLU, A. & JIANG, SHAO-YONG (1999): Tourmaline compositions from the Salikvan porphyry Cu–Mo deposit and vicinity, northeastern Turkey. *Can. Mineral.* **37**, 1007-1023.

ZANE, A. & RIZZO, G. (1999): The compositional space of muscovite in granitic rocks. *Can. Mineral.* **37**, 1229-1238.

ZHENG, YONG-FEI (1993a): Calculation of oxygen isotope fractionation in anhydrous silicate minerals. *Geochim. Cosmochim. Acta* **57**, 1079-1091.

_____ (1993b): Calculation of oxygen isotope fractionation in hydroxyl-bearing silicates. *Earth Planet. Sci. Lett.* **120**, 247-263.

*Received February 1, 2002, revised manuscript accepted October 2, 2002.*